OSCILLATION PHENOMENA IN ARGON LASER DISCHARGES

John Neil Ross

A Thesis Submitted for the Degree of PhD
at the
University of St Andrews

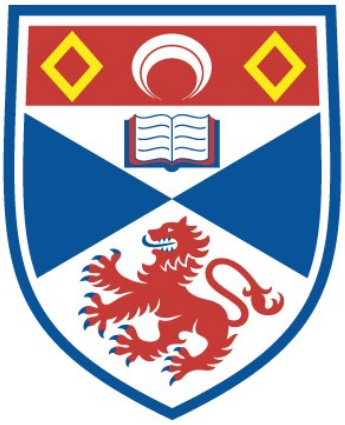

1974

OSCILLATION PHENOMENA IN ARGON LASER DISCHARGES

A thesis

presented by

J.N. Ross, B.Sc.,

to the

University of St. Andrews

in application for the Degree

of Doctor of Philosophy.

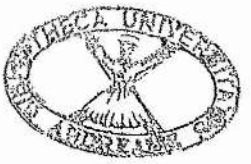

Th 8085

CAREER

The author attended Acklam Hall Grammar School, Middlesbrough before coming up to the University of St. Andrews in 1966. He was awarded the degree of B.Sc. with first class honours in June 1970. From September 1970 until November 1972 he was employed by Laser Associates Ltd., Rugby, and worked on the development of an argon ion laser. This work was undertaken in the Department of Physics of the University of St. Andrews under the supervision of Dr. A. Maitland. From 1972 until the present time he has been employed as a Research Assistant in the Department of Physics of the University of St. Andrews, working on the generation of ultra-violet laser radiation by argon discharges in segmented metal systems.

DECLARATION

I hereby certify that this thesis has been composed by me, and is a record of work done by me, and has not previously been presented for a Higher Degree.

This research was carried out in the Physical Sciences Laboratory of St. Salvator's College, in the University of St. Andrews, under the supervision of Dr. A. Maitland.

J.N. Ross

CERTIFICATE

I certify that J.N. Ross, B.Sc., has spent eight terms (see Senate Minutes 1972-73, No 3, page 83, 8 Dec. 1972) at research work in the Physical Science Laboratory of St. Salvator's College, in the University of St. Andrews, under my direction, that he has fulfilled the conditions of Ordinance No. 12 and resolution of the University Court, 1967, No. 1 and that he is qualified to submit the accompanying thesis in application for the Degree of Doctor of Philosophy.

Research Supervisor

ACKNOWLEDGEMENTS

I gratefully acknowledge the guidance and encouragement I have received from Dr. A. Maitland who has taught me much about lasers and much about the techniques and attitudes of scientific research. I also acknowledge with thanks the helpful discussions I have had with my colleagues, especially Mr. M.H. Dunn, Dr. J.C.L. Cornish and Mr. P.G. Browne. Finally I thank Miss L. McLean for typing this manuscript.

ABSTRACT

In this thesis instabilities which occur in the plasma tube of an argon ion laser are examined. Coherent oscillations in the discharge potential across the plasma tube are found to be a usual feature of an argon laser. The light output of the laser is shown to be modulated by these oscillations only if the discharge current is modulated. It is found that these oscillations are due to instabilities in the anode zone of the gas discharge.

The oscillations occurring within the anode zone of an argon laser have been studied using optical and Langmuir probe techniques. The oscillations are discussed in terms of a phenomenological model due to Pupp. Many of the observed features of the oscillations can be described in terms of this model.

The values of the anode fall that have been observed in the argon laser are substantially less than would be expected on the basis of earlier work on glow discharges in argon. This is discussed and an estimate of the anode fall is made which is closer to the observed value than that predicted by Von Engel's theory of the anode fall. A simple mathematical model of the anode zone is presented and it is shown that under the conditions appropriate to an argon laser the anode fall is not expected to be stable. These instabilities in the anode zone of the plasma tube, while they appear to be a normal feature of the argon laser discharge, do not necessarily modulate the laser light. It is shown that if the power supply for the laser has a high output impedance at the frequency of the oscillations then the modulation of the light may be reduced to a negligible level.

CONTENTS

CHAPTER 1

INTRODUCTION

1.1 The Argon Ion Laser

The argon ion laser is the gas laser which operates with the highest powers of continuous wave radiation in the visible region of the spectrum. It operates in the blue-green region (strongest lines 488 nm and 514.5 nm), where the sensitivity of photo-electric detectors is greatest. This combination of high power and short wavelength makes the argon ion laser a useful source of coherent light for optical scattering experiments (e.g. Raman or Brillouin scattering). To record the small signals which are characteristic of these scattering processes, it is essential to reduce noise to a minimum. In the argon laser discharge there are many sources of noise (1). Amplitude noise takes the form of random fluctuations of power (white noise) often with a coherent modulation superimposed (the frequency of the modulation is usually between 5 and 100 KHz). It is the source of the amplitude noise, especially the coherent modulation, that is the subject of this thesis.

The active medium of an argon ion laser is an electric discharge of high current density (100 - 700 A cm^{-2}) in low pressure argon (0.1 - 0.6 torr). The excitation mechanisms responsible for the laser action and the properties of the discharge have been the subject of many investigations. An excellent review by Kitaeva et al (2) discusses most of what is known about the argon laser. More recent studies of the spontaneous light emitted by the discharge (3) have provided new information about the electron density and electron temperature in the discharge, but this unfortunately disagrees with the results of other measurements both in magnitude and in the way in which the parameters vary (2). There is as yet no altogether satisfactory understanding of the argon laser discharge.

The large power dissipation in an argon laser discharge (100 - 500 W per cm length of discharge capillary) make the construction of

a suitable discharge tube difficult. Fused silica and beryllia are two electrically insulating materials with good thermal conductivity that have been used successfully. Alternatively, a conducting material may be used if the tube is divided into segments insulated from one another. Graphite and various metals have been used in segmented laser tubes (4). The laser tube used in the investigations reported here was of all metal construction (see Appendix A1), some features of such lasers have been described by Cornish and Maitland (5).

1.2 Amplitude Noise in Gas Lasers

The fundamental lower limit on the amplitude noise of a single mode laser is determined by spontaneous emission. The semi-classical model of the laser predicts that the noise spectrum of a laser due to spontaneous emission decreases in amplitude and increases in bandwidth as the laser power is increased (6 pp 288-292). Provided the laser is operating far above threshold so that the coherent power radiated into the cavity mode by stimulated emission is much greater than the incoherent power radiated spontaneously into the mode, then the noise due to spontaneous emission is very small. Although spontaneous emission noise has been detected near threshold (7,8) it is generally negligible when compared with other sources of noise in a practical laser.

In order to measure the noise spectrum of a laser the radiation is detected with a photo-detector (usually a photomultiplier or a photo-diode). The shot noise of the detector is the lowest noise level that may be observed. Any noise above the shot noise is referred to as the excess noise of the laser (7).

Excess noise has been studied in He Ne and argon ion lasers, but is usually much greater for argon lasers (1). The noise takes the form of a continuous random noise spectrum superimposed on which there may be peaks of noise at discrete frequencies (9,10,11).

The coherent oscillations that produce noise at discrete frequencies in He Ne lasers have been attributed to moving striations in the positive column of the discharge (9) and to oscillations associated with the negative slope of the voltage current characteristic of the discharge (10). In argon ion lasers the discrete frequency components of the laser noise have been attributed to oscillations in the anode region of the discharge (11,12).

It has been shown that for a He Ne laser there is a correlation between the discharge current noise and the laser light noise which extends over a wide range of noise frequency (1 - 100 KHz) (7). The discharge current noise is independent of whether or not the laser is oscillating, so that it appears that the noise on the laser light is a result of the discharge current noise, although it has not been demonstrated that stabilizing the discharge current reduces the noise of the laser output.

Suzuki (12) has shown that for an argon ion laser the relation between the coherent oscillations of the discharge voltage and the modulation of the laser light is consistent with the assumption that the modulation of the light is due to modulation of the discharge current. It is shown in the present work (chapter 2) that if the discharge current is held constant anode oscillations of the type observed by Suzuki (12) and Galehouse et al (11) do not modulate the laser light, even though the discharge voltage is modulated with a peak to peak amplitude of 10 - 15 V.

1.3 Anode Oscillations

It is shown in chapters 2 and 3 that the oscillations that occur in the plasma tube of an argon laser (described in Appendix A1) are due to oscillations in the anode fall of the discharge. This is consistent with the observations of Suzuki (12) and Galehouse et al (11). The mechanism of such anode oscillations is not clearly understood

although they have been observed in a wide variety of different gas discharges.

One of the earliest studies of anode oscillations was by Pupp (13), who observed oscillations of the anode fall in discharges in argon at a pressure of around 1 torr, and with a discharge current of around 1 A. Since then anode oscillations have been observed in gas discharges over quite wide ranges of pressure and current (0.1 - 50 torr, 1 mA-100 A), and in a number of gases (Ar, Ne, He, and Hg) (13, 14, 15). The oscillations are usually linked with "glow balls" that appear on the anode (13, 14). These are small highly luminous spots which emit light in pulses with a repetition frequency equal to the frequency of the oscillations (15). Sometimes, there may be more than one "glow ball", in which case they emit light alternately (15),(16).

The "glow balls" often appear to be linked with moving striations (17, 18). However, moving striations have been observed in the positive column when the anode fall is stable (19), and oscillating "glow balls" may occur without moving striations (17). The apparent link between the "glow balls" and the striations may be a secondary effect, as the latest studies of moving striations (20) do not link them in any way with processes occurring at the anode.

There is no satisfactory theory of anode oscillations. Pupp (13) proposed a phenomenological model which describes the main features of the oscillations. In chapter 3 this model is discussed in relation to the oscillations observed in the argon ion laser. The weakness of the model is that it does not provide any indication of the conditions under which the anode fall will be unstable.

An alternative theory of anode oscillations associated with "glow balls" has been given by Grossu (21). He attributes the oscillations to standing ionic sound waves within the "glow ball". The theory is based on the observation that the product of the

frequency of the oscillation and the diameter of the glow ball is approximately constant. This theory can not be applied to the oscillations observed in an argon ion laser since, in most cases the expected wavelength of ionic sound waves at the frequency of the oscillations is large compared with the dimensions of the discharge tube. It is also difficult to see how this theory can explain the high intensity pulses of light observed by Ogwa (15), or the observations of the light emitted from the anode glow which are described in chapter 3.

In chapter 5 a new model for the anode fall is discussed, and it is shown that the model predicts that the anode fall should be unstable with discharge conditions appropriate to an argon laser.

1.4 Excess Noise Associated with the Optical Cavity of a Laser

A significant contribution to the noise of a laser is often due to mechanical vibrations of the optical components within the laser cavity. This produces frequency jitter by varying the optical path length within the cavity, and may also produce amplitude noise by varying the cavity losses (e.g. by misaligning the mirrors). In an argon ion laser, the high flow rate of the cooling water round the laser capillary is a source of vibration which is difficult to eliminate. In the plasma jet laser (22), used in the experiments discussed here, the large rotary vacuum pump is an additional source of low frequency vibrations.

A more fundamental noise source associated with multi-mode optical cavities is mode competition. In a multi-mode laser there are two distinct operating conditions. The modes may be locked in phase, so that they have a definite phase relation between one another, in which case the laser is said to be mode locked. Alternatively, the modes may be unlocked, in which case the phase relation between the modes is not stable and changes randomly with time. If the modes are

locked, then they have a stable spectrum in the frequency domain, each mode having a stable amplitude. If the modes are unlocked, then the mode spectrum is unstable, and modes increase and decrease in amplitude in a random manner. This is due to competition between the modes for the same population of excited states; first one mode is favoured and dominates then another (23).

Both axial modes and transverse modes may be phase locked (24), but it is usual to suppress all but the fundamental T.E.M.$_{oo}$ transverse mode (by the use of an apperture if necessary). If the higher order transverse modes are suppressed, then a dramatic reduction of low frequency noise (20 dB) is obtained by phase locking the axial modes (23, 25).

The modes may lock spontaneously (26, 27), although it is in general more reliable to use one of the mode locking techniques that have been devised. One method, that has been widely used to induce mode locking, is to modulate the cavity internally at the mode spacing frequency (either phase or loss modulation may be used). Another, common method is to include a saturable absorber in the cavity. Mode locking techniques have been reviewed by Smith (24).

The low frequency noise of a mode locked laser is less than that of a free running laser, but the output is usually a train of pulses whose repetition frequency is a multiple of the mode spacing frequency. However there is one exception, and that is the so-called F.M. laser, in which the cavity is internally phase-modulated at a frequency slightly detuned from the cavity mode spacing. The output of such a laser is a frequency-modulated (F.M.) wave of constant amplitude. The operation of an F.M. laser has been demonstrated by Harris and Targ (28). The theory of F.M. mode locking has been discussed by Harris and McDuff (29) using Lamb's semi-classical theory of the laser (30). Lamb's theory expands the electric field in the optical cavity as a set of standing waves. An alternative treatment of F.M.

modes in a passive cavity has been given by the author (31), in which the electric field is treated as two phase-modulated travelling waves; both two mirror and ring cavities are considered. A copy of this paper is included in appendix A6.

CHAPTER 2

DISCHARGE CURRENT NOISE IN AN ARGON LASER

2.1 The Effect of the External Circuit

Coherent oscillations have been found to occur within the plasma tube of a metal clad argon laser (described in appendix A1) and these oscillations often contribute to the amplitude noise of the laser light. The oscillations have their origin in the plasma within the discharge tube. There is however an interaction between the oscillations and the external circuit. This interaction is important in understanding the modulation of the laser light by the oscillations and will be considered first.

The oscillations modulate the discharge voltage and the discharge current. (The effect of the oscillations on the light output of the laser is considered in section 2.3). The relation between the discharge voltage modulation $V(\omega)$, and the discharge current $I(\omega)$ at a frequency ω is determined by the output impedance of the discharge power supply $Z(\omega)$. The current modulation is given by,

$$I(\omega) = - V(\omega)/Z(\omega).$$

The negative sign arises since the convention is used that I and V are taken as positive when the modulation voltage and current are in the same direction as the steady state voltage and current.

The modulation current is observed on an oscilloscope connected across a low value (0.2 Ω) resistor in series with the discharge tube. With the discharge tube connected directly to the motor generator power supply, without a series inductor, (Appendix A1), both voltage and current oscillations are observed. The voltage and current waveform are not the same (fig. 2.1). The discharge current appears to 'ring' at about 100 KHz. The frequency at which the ringing occurs is independent of the fundamental frequency of the voltage oscillations. This suggests that it is due to a resonance

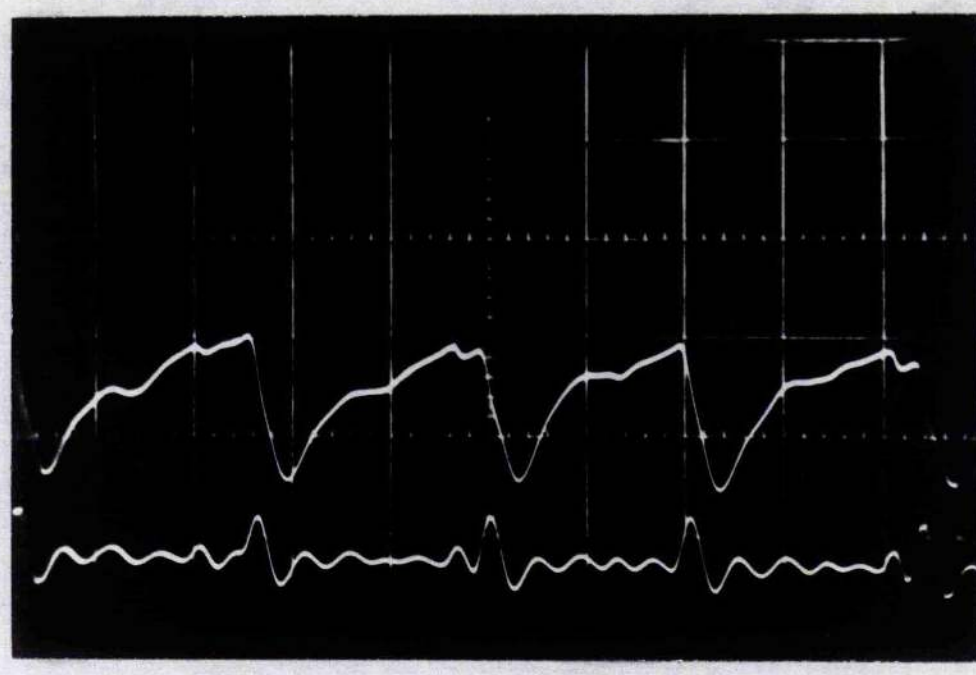

fig 2.1 Upper trace, discharge voltage (8 V/div.)
Lower trace, discharge current (2 A/div.)
Horizontal scale 20 μsec/div.

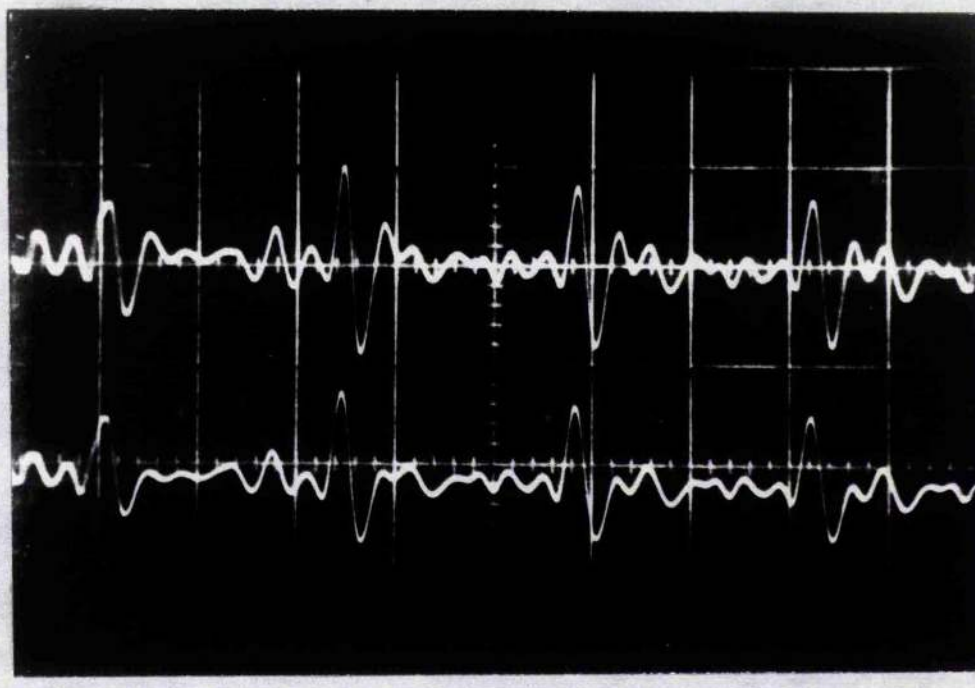

fig 2.2 Upper trace, discharge current (2 A/div.)
Lower trace, voltage between adjacent segments (0·3 V/div.)
Horizontal scale 20 μsec/div.

in the external circuit. If the ringing frequency is a low order harmonic of the fundamental oscillation frequency, then the current is strongly modulated (greater than 2 A peak to peak). It seems that the output impedance of the motor generator has a resonance at a frequency of 100 KHz, and goes through a minimum.

If the oscillation frequency is the same as the external resonance frequency, the oscillations become very stable. In this case the frequency of the oscillations may remain constant as the discharge current and system pressure are varied. This behaviour is very different from that when an inductor is included in series with the tube to keep the current constant (see chapter 3 fig. 3).

2.2 The Localization of the Oscillations

Suzuki (12) and Galehouse et al (11) attribute the oscillations they observed in their argon lasers to instabilities in the anode region of the discharge. The segmented metal tube provides a convenient method of locating the oscillations, to see if they occur in the capillary region, or the anode or cathode regions. The segments are used as probes to measure fluctuations in space potential, averaged over the length of the segment. The use of segments as probes for studying discharge parameters has been discussed by Maitland and Cornish (32).

The voltage oscillations between segments have been measured using an oscilloscope with a differential amplifier. The voltage modulation between adjacent segments is the same along the length of the tube, and follows the current oscillations (fig. 2.2). The voltage oscillations across all 8 segments have a peak to peak amplitude of about 2 V. A careful check of the phase relation between the current and voltage between segments ruled out the possibility of travelling waves or moving striations within the laser capillary.

The voltage oscillations between the anode and the segment nearest to it are of large amplitude (13 V) and the waveform closely approximates that across the whole tube. The voltage between the cathode and the segment nearest to it is almost the same as that between the segments.

If an inductor of 20 mH is connected in series with the laser discharge the current modulation is reduced to a level which can not be detected (less than 100 mA peak to peak), and oscillations are not observed in the voltage between segments. There are however strong oscillations (13 V) between the anode and the segment nearest to it. When the differential amplifier is connected between the anode and the copper cylinder which confines the plasma in the anode region of the laser (Appendix A1), these strong oscillations are still observed.

From these observations, it is concluded that the observed oscillations occur in a region of the discharge close to the anode, and not in the laser capillary. The oscillations only interact with the plasma in the laser capillary if the discharge current is modulated.

2.3 Modulation of the Laser Output Power

The modulation of the laser power has been detected with a fast photo-diode (Hewlett Packard type hpa 42033). The response time of the detector is limited by the time constant of the load resistor and stray capacity. A load resistor of 3.3 KΩ is used as this enables a satisfactory signal to be obtained without dissipating excessive laser power in the diode. A single transistor voltage follower is used to match the 3.3 KΩ load resistor to the 70 ohm co-axial cable to the oscilloscope, and reduce the stray capacity across the load resistor (fig. 2.3). The rise time of the voltage follower is better than 0.5 μsec. The response of the photo-diode is much faster than the voltage follower.

When the inductor is connected in series with the laser tube no modulation of the light can be detected at the frequency of the

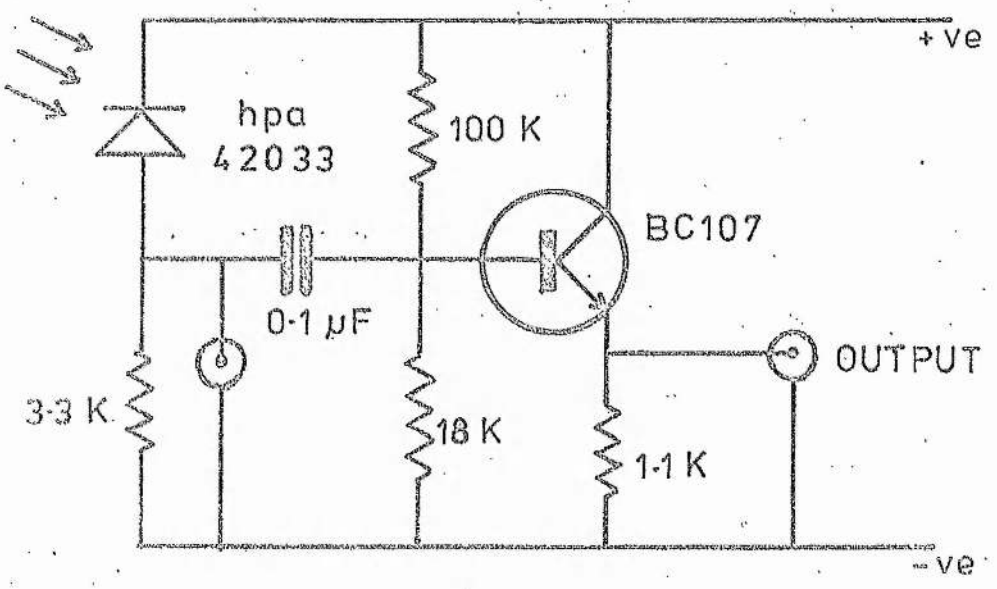

fig 2.3 Fast Detector for Laser Light

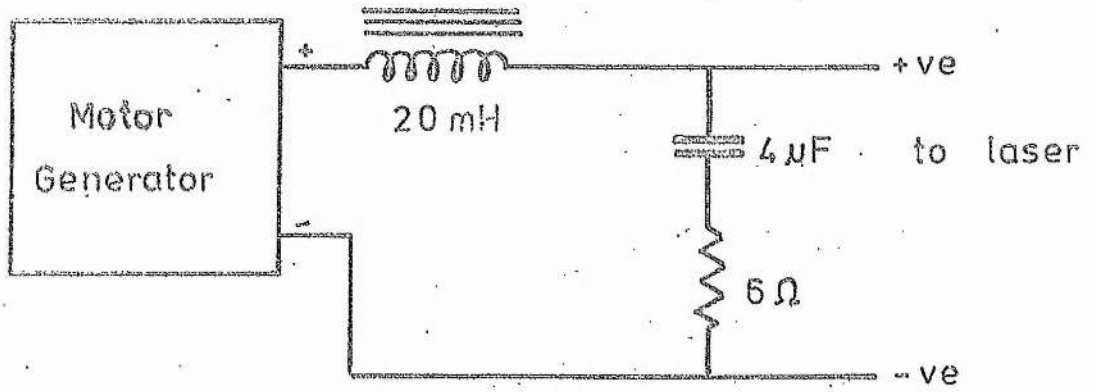

fig 2.4 Circuit for Simulating a Low Impedance Power Supply

oscillations. The dominant sources of noise are the low frequency ripple from the motor generator, and the vibration of the optical cavity. This shows that the oscillations only modulate the laser light if they are allowed to modulate the discharge current.

With the laser connected directly to the motor generator, some modulation is observed, and the light waveform follows the current. The depth of the current and light modulation depend on the frequency and are only strong if the frequency is close to the 'resonance' discussed in section 2.1. In order to observe more readily the relation between the current and light modulation the circuit shown in fig. 2.4 was used to simulate a power supply with a low output impedance. Provided the frequency of the oscillations is much greater than the resonant frequency of the L.C. circuit (3.5 KHz) the laser 'sees' a source impedance equal to that of the resistor and capacitor. This is very close to 6 ohms at the frequencies of interest here. The value was chosen to be of the same order as the value of the ballast resistor used with simple laser power supplies.

The amplitude of the current modulation ΔI is calculated from the voltage across the 6 ohm resistor. The peak-to-peak amplitude of the current modulation is found to be 0.8 A and independent of the average discharge current for the 3 m.m. laser. The light modulation follows that of the current (fig. 2.5). The peak-to-peak amplitude of the light modulation is measured as a fraction of the average power. This is found to be 11% at a current of 20 A and 5.8% at a current of 30 A for the 3 m.m. laser. The percentage modulation of the current was 4% and 3.2% respectively.

The ratio of the modulation depth of the laser power $\Delta P/P$ to the modulation depth of the current $\Delta I/I$ for an argon laser has been examined by Suzuki (12), who found a ratio of 2 at low frequencies, which decreased with increasing frequency. The low frequency value depends on the relation between the power P and the current I.

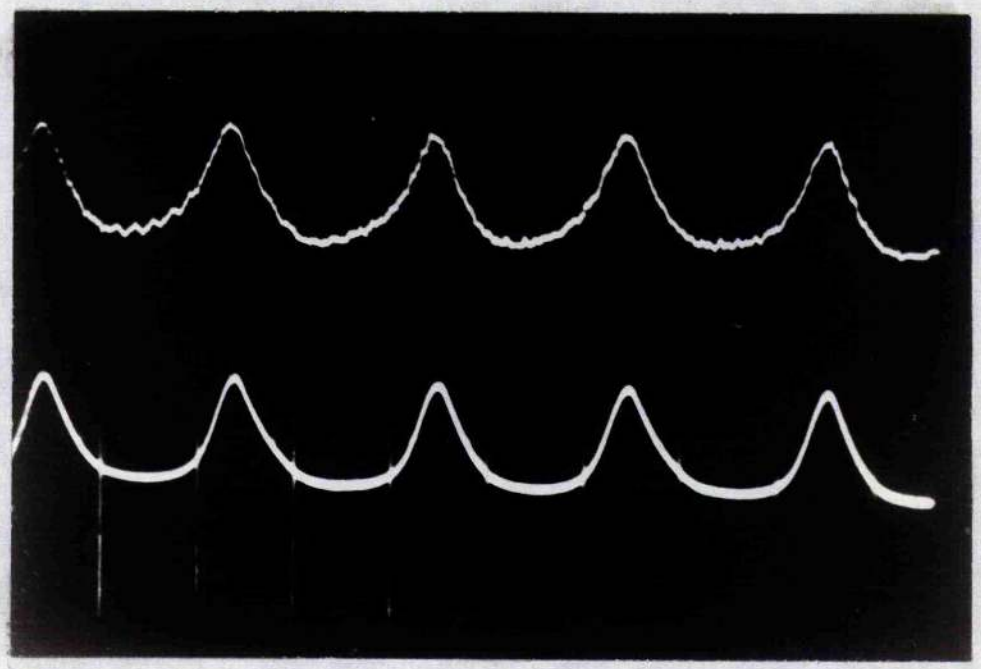

fig 2.5 Upper trace discharge current (1·2 A/div.)
Lower trace laser light
Horizontal scale 10 μ sec./div.

In appendix A2.1 it is shown that for the 3 m.m. laser the low frequency value of the ratio should range from 4.5 at 20 A to 2 at 40 A. The ratio was 2.8 at 20 A (53 KHz) and 1.8 at 30 A (77 KHz). These values are substantially less than the predicted low frequency values.

If this lower value of the ratio of $\Delta P/P$ to $\Delta I/I$ is due to the lifetime of the excited states and the lifetime of the radiation in the cavity as discussed by Suzuki (12) then the phase of the light modulation should be retarded with respect to the current modulation. No such effect could be observed.

CHAPTER 3

TRANSIENT PHENOMENA IN THE ANODE REGION

In chapter 2 experiments are described which indicate that the coherent oscillations which modulate the discharge voltage, and under certain circumstances the laser light, are due to instabilities in the anode zone of the laser discharge. This chapter takes the form of a paper which describes experiments that have been performed to investigate these oscillations, and discusses a phenomenological model for the oscillations.

J. Phys. D: Appl. Phys., Vol. 6, 1973. Printed in Great Britain.

Transient phenomena in the anode region of a metal-clad argon laser

J N Ross
School of Physical Sciences, University of St Andrews, North Haugh, St Andrews, Fife

Received 19 March 1973, in final form 19 June 1973

Abstract. Coherent anode oscillations occuring in an argon ion laser are examined. Time-resolved spectra of the light emission from the anode zone are compared with the voltage oscillations. A simple model for anode oscillations is compared with the experimental data.

1. Introduction

The voltage across an argon ion laser discharge tube is frequently found to be modulated by coherent oscillations with an amplitude of between 10 and 15 V. These oscillations are usually in the frequency range 1 to 100 kHz. Such oscillations have been studied by Galehouse *et al* (1971) and by Suzuki (1971). Suzuki showed that the laser light was modulated by these oscillations, and that the amplitude of the modulation of the light decreased as the ballast resistor in series with the discharge tube was increased. From this he concluded that the modulation of the laser light was due to modulation of the discharge current.

Both Suzuki and Galehouse attributed the oscillations to instabilites in the anode fall region, although they did not investigate the mechanism by which the oscillations were produced. Oscillations produced in the anode region of a gas discharge have been studied by Pupp (1933) and by later workers, usually in low current discharges (<1 A) and frequently in connection with moving striations (Coulter *et al* 1961).

The mechanism by which the oscillations are generated is not clear. A qualitative description of what may happen has been given by Pupp (1933), when the oscillations originate from a well-defined 'anode spot'. However, in the present work oscillations have been obtained both with small well-defined anode spots of very high luminosity and with what appears to be a uniform glow over the anode surface.

The present paper is concerned with anode oscillations that occur in an argon laser using a plasma jet cathode (Maitland 1969) and a segmented metal discharge tube. Tubes of different capillary diameter have been used, ranging from 3 to 6 mm, but with the same anode structure. The character of the oscillations was the same for all the tubes. The discharge currents ranged from 5 to 90 A. Thus the current densities at the anode and elsewhere are about a factor of 10 greater than in previous studies.

2. The experimental arrangement for studying anode oscillations

The geometry of the anode and the discharge envelope of the laser is illustrated in figure 1. The anode is made from two concentric copper cylinders cooled by water flowing between them. Two anodes have been used in this investigation: the first has an external diameter of 28·6 mm and an internal diameter of 12·5 mm; the second anode has an

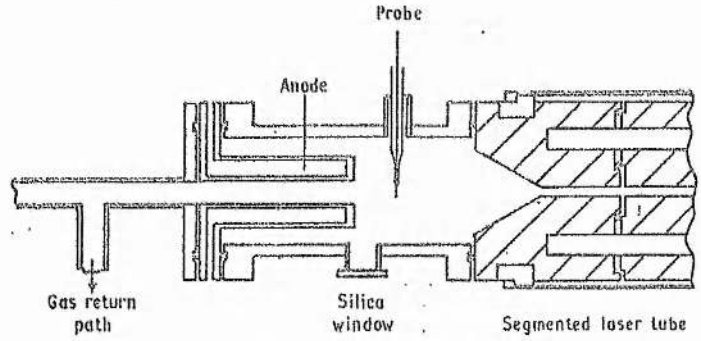

Figure 1. Geometry of the anode and the discharge envelope.

external diameter of 16 mm and an internal diameter of 6·3 mm. Both anodes are the same length (75 mm) but the discharge confines itself to the last 15 mm of the surface at the end of the anode nearest the cathode. The silica window in the metal wall of the discharge tube enables the discharge near the anode to be examined visually or with a photoelectric spectrometer. An electric probe can be immersed in the plasma at a distance of 1 cm from the end of the anode. This probe is a tungsten rod 0·5 mm in diameter, insulated with a thin layer of fused silica apart from the final 4 mm. The second electrode used in the probe circuit is not the discharge anode as is usual, but the discharge cathode, since the oscillations studied are produced between the probe and the discharge anode. The probe is used to measure the electron density and the electron temperature in the anode region of the discharge. It is also used to measure the peak anode fall.

Light emitted from the anode region is collected by a lens, and the image plane is scanned with a pinhole so that modulation of the light from the different parts of the region can be recorded. The light passing through the pinhole is focused on to the slit of a photoelectric spectrometer. The modulated output of the photomultiplier is averaged with a boxcar integrator and displayed on an XY recorder. The reference signal is provided by the anode voltage oscillations. The response time of the circuit is limited by the gate width of the boxcar integrator (1 μs). This response time is compatible with the events studied.

3. The characteristics of anode oscillations

3.1. Surface effects and gas impurities

Before examining the oscillations in detail it is necessary to make some brief comments about the conditions under which oscillations occur. The same anode structure operating under the same conditions of pressure and current has on different occasions given oscillations and been completely quiet. The oscillations seem to occur if the discharge

does not run uniformly to the anode with at least approximately axial symmetry. The area of the anode to which the discharge has been running becomes covered with a fine black powder, which microscopic examination shows is probably finely divided copper. Thus the active area of the anode is easily seen and quite well defined. The region to which the discharge runs seems to be quite stable, unless the tube is left unused for a week or so, or dismantled and the anode cleaned. The anodes were originally cleaned by sand blasting. After this treatment, strong oscillations were observed. When however the anodes were cleaned in dilute nitric acid, oscillations only occurred at low currents (<15 A). It seems that particular 'sensitive' areas of quite small extent may be produced by surface treatments of various kinds. If these areas become too small, the current density at the site becomes greater than a critical value and oscillations result. The change in behaviour with different surface treatments may be due to secondary electron emission or perhaps to the release of gas from the surface by electron bombardment.

The effect of adding various gaseous impurities has been investigated. Nitrogen or water vapour have the effect of making the oscillations irregular. Sometimes they suppress the oscillations altogether. There is always some hydrogen present as an impurity, which appears to come from either the discharge tube walls or the electrodes; the effect of this residual hydrogen is difficult to ascertain. Small quantities of helium added to the gas have little or no effect on the oscillations.

3.2. The frequency of the oscillations

The oscillations observed usually have well-defined frequency and are often the resultant of two or more oscillations from separate regions near the anode surface. The frequency is reduced by increasing the pressure (figure 2). The effect of current on frequency is quite complex. At low currents (<15 A) the frequency always increases continuously with current: at higher currents the frequency sometimes increases and sometimes remains constant with increasing current. The frequency has never decreased with increase of

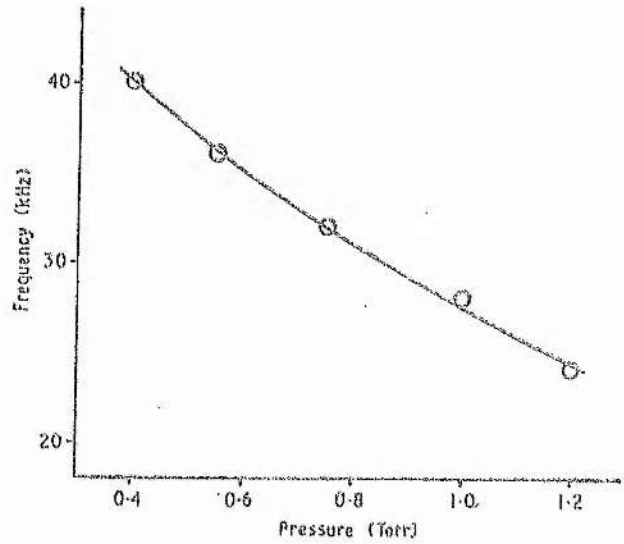

Figure 2. Variation of frequency of anode oscillations with system gas pressure at constant laser discharge current.

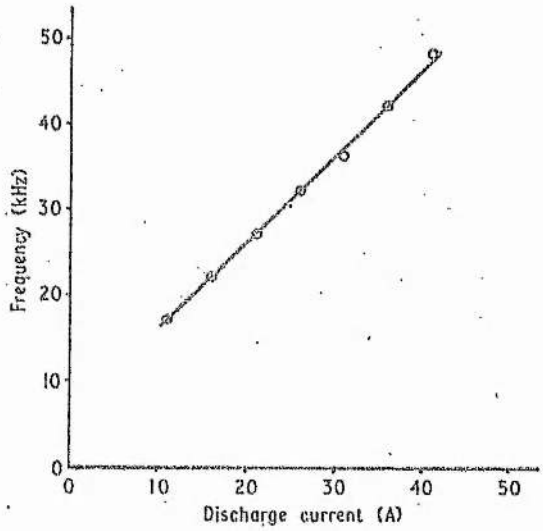

Figure 3. Variation of frequency of anode oscillations with laser discharge current at constant system gas pressure

current. The situation is further complicated when the geometry of the discharge changes. The frequency may then jump to a higher value at a particular current which is reproducible in both directions. A typical variation of frequency with current is shown in figure 3. Such curves as are shown in figures 2 and 3 are quite reproducible over a period of several hours of continuous operation, but, if the system is switched off and left for a while, a different set of reproducible curves may be obtained.

The waveform of the discharge voltage oscillations has two characteristic shapes. The first is characteristic of the oscillations when there are small intensely luminous spots on the anode producing oscillations of the form shown in figure 4. The peak-to-peak amplitude of these oscillations is about 12–14 V superimposed on a steady potential of about 250 V. Sometimes these spots are referred to as glow balls (Ogwa 1959). These will be called anode spots, and the oscillations associated with them, spot oscillations.

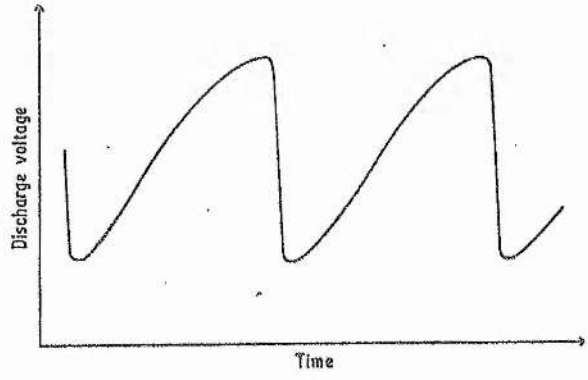

Figure 4. General shape of anode oscillations associated with anode spots (glow balls). These are usually of frequency 1–10 kHz.

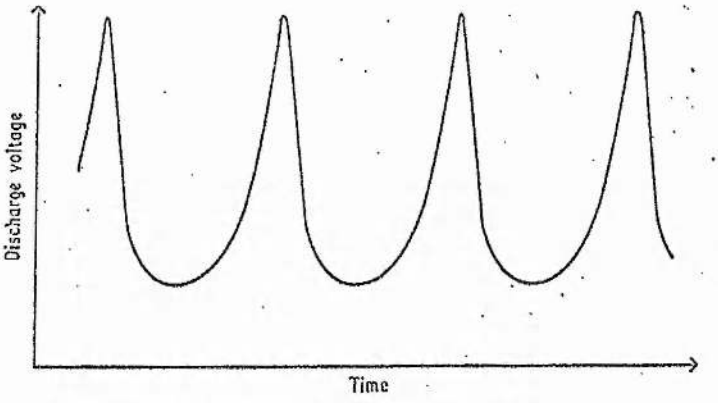

Figure 5. General shape of anode oscillations associated with a diffuse glow over the anode surface (no spots). These are usually of frequency 20–100 kHz.

The voltage waveform is triangular and at the sharp edge where the voltage falls a strong pulse of light of the ArII spectrum is emitted from the spot giving it a characteristic blue colour. The second waveform is shown in figure 5, and again the peak-to-peak amplitude is about 12–14 V. These oscillations will be called glow oscillations. This waveform appears to be associated with oscillations produced in a more diffuse region. There is no blue spot in this case. The light from regions near the anode is still modulated, but the ArI lines are much stronger than ArII lines. Each 'pulse' of light is short and correlated with the falling edge of a voltage 'pulse'. *

4. Probe measurements of the anode fall

The usual method of measuring the space potential with an electric probe is to find the voltage at which a logarithmic plot of the electron current drawn by the probe deviates from a straight line, as the probe current saturates. This technique could not be used, since even for currents as high as 1 A there was no indication of the electron current saturating. The current could not be increased further without risk of overheating the probe. The probe current did however saturate for probe potentials sufficiently below the space potential. The saturation ion current increased only very slowly as the voltage was reduced, indicating that a thin sheath was formed.

The electron temperature and density were found in the usual way. The results indicate that a Maxwell–Boltzmann distribution of electron energy is appropriate, at least as a first approximation. The plasma potential V_p was found by measuring the floating potential V_f of the probe, at which potential I_e and I_p are equal. The plasma potential V_p is calculated from

$$V_p = V_f + (kT_e/2e) \ln (2M/\pi m).$$

In the absence of oscillations, V_p was found to be slightly less than the anode potential. The difference (the anode fall) varied between 0 and 5 V. This is much less than that predicted by von Engel's theory of the anode fall (von Engel 1941). This theory predicts an anode fall of about the value of the ionization potential (15·5 V). The probe is believed to be outside the high-field region since observation of the light intensity near the anode indicated that the anode fall region extends only 3 to 5 mm from the anode.

*Some typical discharge voltage waveforms are shown in fig. 3.1 (a) - (d).

Typical values of electron density and temperature are $n_e = 1{\cdot}5 \times 10^{13}$ electrons cm^{-3} and $T_e = 18\,000$ K, at a current of 35 A and a pressure of 0·4 Torr. The anode fall in this case is 5 V. The values of electron density increase with current and pressure, whereas the values of electron temperature tend to decrease. The anode fall voltage remains constant as the current and pressure are varied.

When oscillations are present the probe measurements need to be interpreted with care. When an oscilloscope is coupled between the probe and the cathode it is found that the probe voltage is modulated slightly. With the probe biased into the region where the electron current is varying rapidly, the voltage modulation on the probe is less than 2 V peak-to-peak. With the probe biased to ion saturation this increases to about 4 or 5 V peak-to-peak.

The effect of imposed fluctuations on a probe characteristic has been considered by Garscadden and Emeleus (1962) and Crawford (1963). The effect of modulations of probe potential, or space potential when the probe is negative with respect to the plasma, is to shift the whole characteristic to a lower potential. The values of n_e and T_e are not altered, but the floating potential V_f is reduced. Theory shows that if n_e alone is modulated, the floating potential is not modulated. However, experimentally it is found that the floating probe potential V_f is modulated. The space potential or the electron energy must therefore be modulated. That n_e is also modulated is indicated by the strong modulation of the probe voltage when the saturation ion current is drawn by the probe.

However, ignoring these complications, a value for V_p may be calculated as before. When this is compared with the peak anode voltage it is found that the peak anode fall is increased to between 5 and 16 V. The peak-to-peak amplitude of the anode oscillations is within 2 V of the peak anode fall in each case.

The minimum anode fall is sometimes negative by as much as 2 V. This is outside the possible experimental error, so that the effect is believed to be real. The anode fall can be negative if the random electron current to the anode exceeds the discharge current. Negative anode falls are well known in low-voltage arcs where the electron density is high.

It is possible to estimate the random electron current I_r to the anode using the usual equation from probe theory:

$$I_r = n_e e c a/4$$

where a is the area of the anode and c is the average random velocity. If the energy distribution is maxwellian with temperature T_e, then c is given by

$$c = (8kT_e/\pi m)^{1/2}.$$

Assuming that T_e is 10^4 K and that the discharge current density at the anode surface is 20 A cm^{-2}, then the random current density is equal to the discharge current density when n_e is about 6×10^{12} cm^{-3}. This value is slightly less than the electron density of the plasma away from the anode fall region. It is therefore quite possible that the peak ionization during the anode oscillations is sufficient to produce a negative sheath at the anode surface.

5. Modulation of the light emitted from the anode region

The average waveform of the light emitted from the anode region is recorded with the aid of a boxcar integrator. The stability is such that recordings of successive waves may

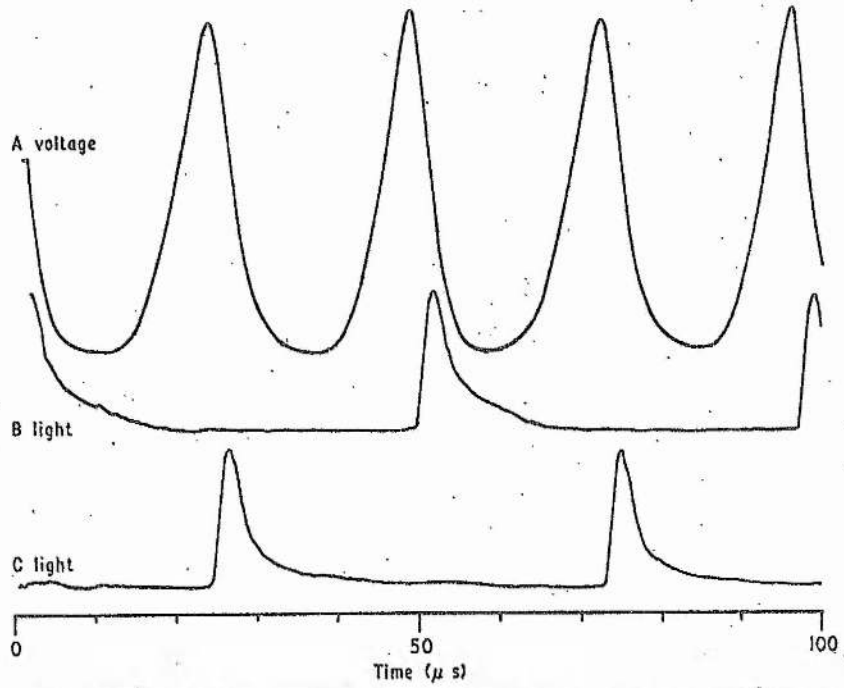

Figure 6. Correlation between voltage oscillations A, and light emitted from different parts of the anode glow.

be made from different areas of the anode region without any change in the triggering signal derived from the voltage oscillations. Each scan of the waveform requires several minutes, so that the oscillations must be stable for periods of half an hour or more. Light emitted from different regions near the anode is compared. Comparison is also made between light pulses emitted at different times relative to the voltage oscillations.

The voltage oscillations are compared with the light emission at 4702 Å (Ar I) from two different areas of the anode in figure 6. The two areas from which the light was collected were on opposite sides of the anode and about 0·2 mm in front of the end of the anode, but there were no visible anode spots. The light was 100% modulated, the zero having been shifted between the two traces for clarity. The light intensity started to rise a short time after the anode voltage started to fall. The rise time of the light pulse was limited by the resolution of the boxcar integrator. After rising to a maximum the light intensity fell rapidly.

As the region from which the light was collected was moved further from the anode surface, the time at which the maximum emission occurred was delayed, and the width of the light pulse increased. Figure 7 shows the emission profile of the 4702 Å Ar I line for 4 different distances from the anode surface. As the sampling region is moved further from the anode, the background intensity increases and the maximum light intensity is reduced.

When the light emitted by the ions is compared with that emitted by the neutral atoms (figure 8) it is found that the width of the pulse of light from the ions near the anode is narrower than that from the netural atoms. The intensity of the ion lines decreases rapidly as the distance from the anode is increased, so that it is only possible to observe the modulation close to the anode. No difference in behaviour could be

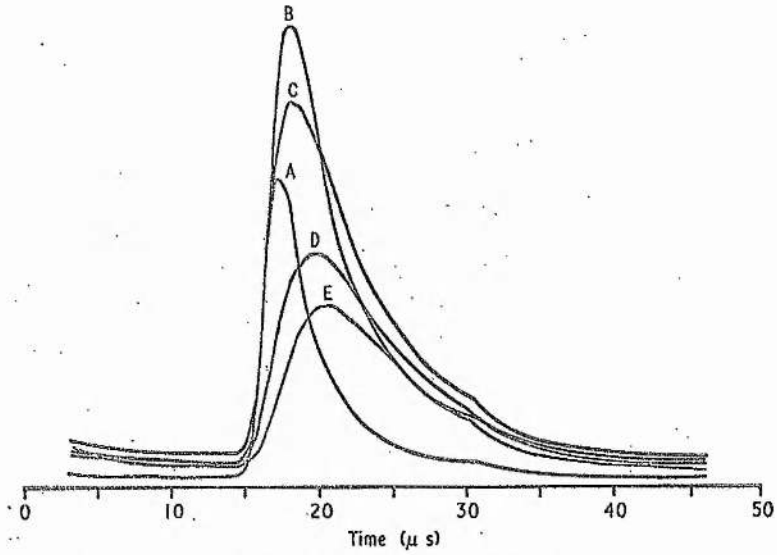

Figure 7. Light emitted from regions at different axial distances from the anode surface: A, 0·1 mm; B, 0·8 mm; C, 1·6 mm; D, 2·0 mm, E, 2·4 mm.

detected between different lines originating from the same state of ionization. This is to be expected since the time resolution (1 μs) is slow compared with the lifetimes of most excited atomic states. The upper energy levels of ArI, II etc are fairly close in energy, so that the changes of electron energy with time effect all such levels to much the same extent.

There is always a fairly strong background continuum to the argon spectrum. This becomes a nuisance when looking for the weaker ArII lines. The continuum shows no distinguishable features but is presumed to be due to molecular impurities. It is quite different from the C_2 and CN bands that appear if oil vapour from the rotary pump or other organic vapour has diffused into the tube. The intensity of the continuum is

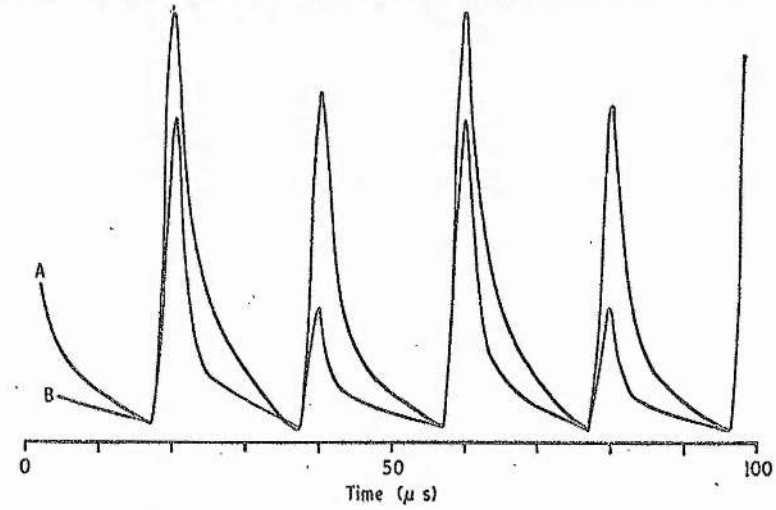

Figure 8. Correlation between light emitted from neutral species A, and ionic species B.

modulated quite strongly by the oscillations, but its response time is slower than that of the ArI and ArII lines. The rise time for an ArII line close to the anode was about 2 μs and that of the continuum 5 μs. The decay time for the continuum is likewise much greater, decaying almost linearly until the next cycle of the oscillation.

6. A model for anode oscillations

The probe and light emission studies indicate that the oscillations are produced very close to the anode, and that the oscillations in discharge voltage are due to oscillations in the anode fall. The model that has been most widely used to describe such oscillations is that due to Pupp (1933). It has been used to describe oscillations in mercury and in the noble gases (Ogwa 1959, Yosimoto 1953). The predictions of this model will be compared with the experimental observations.

The model proposed by Pupp is that initially the ionization rate near the anode is not sufficiently high to supply the ion current to the positive column of the discharge. A negative space charge accumulates near the anode and produces a large axial electric field between the anode and the rather ill-defined end of the positive column. The voltage across this region is the anode fall. The anode fall increases until the electrons accelerated towards the anode have sufficient energy to produce ion pairs by collision. Pupp proposed that when the anode fall exceeds a critical potential, the ionization rate increases very rapidly to produce an excess of ions. The anode fall, then, is reduced to zero and the rate of production of ions becomes zero. The ions then drift away from the anode and the anode fall increases once more.

The model was proposed to describe the spot-type oscillations with a 'saw tooth' waveform (figure 4). The light emission studies described herein indicate that the second type of oscillation with a spiky waveform (figure 5) and no distinct anode spot may be produced by the same mechanism. When spot-type oscillations occur, it is found that there are usually two spots, and sometimes more, which emit light alternately. Each time a spot emits light the anode fall decreases sharply (Ogwa 1959).

In this study it has been found that there are always two 'active regions' of the anode when oscillations are present in our laser tubes. Light is emitted alternately from these regions as shown in figure 6. Sometimes it is possible to distinguish visually between the two regions which may appear as well-defined blue spots on the anode, but often the glow round the anode looks quite uniform to the eye.

From these observations it is concluded that ionization occurs alternately at two regions of the anode. Once ionization has occurred at one of the active regions, the high electron density in this region will produce a low-impedance path for the discharge current to flow to the anode, while the low electron density at the other active region will provide a high-impedance path. The discharge current will therefore flow to the low-impedance region. The impedance of this region will rise as the ion density falls and the anode fall will increase. When the anode fall is sufficiently large for ions to be produced once more another burst of ions will be produced but this time at the other region. The current will therefore switch to this other region.

7. The emission of light from the anode zone

The light emission studies may be interpreted in terms of this model. The rapid rise of light intensity near the anode (figure 7, curves A and B) indicates that there is a rapid rise in

excitation due to the current switching to this region and the rapid rise in electron density as ions are produced. The anode fall is initially large, so that the electrons gain sufficient energy from the electric field to excite both neutral and ionic species (figure 8). The light from the ionic species decays rapidly as the electric field falls. The light from the neutral species decays more slowly as first the electric field falls to a low value and then the electron density falls.

Further away from the anode the intensity of the light emission increases more slowly (figure 7, curves D and E). The electrons have not gained much energy in the anode fall at this distance from the anode and are unable to produce ion pairs. The electron density can only increase as ions and electrons drift from the region in which they are created (close to the anode surface) to the region under consideration (about 2 mm from the anode). The delay of 3 or 4 μs shown in figure 7 between the maxima is due to the small drift velocities of the positive ions.

The delay in the increase of ionization in this region of the anode zone is important for the oscillation mechanism. The anode fall can only be reduced to a low value if the ion density is large throughout the whole anode zone. The transit time of the ions across the anode zone means that the anode fall is unable to respond instantaneously to changes in the ionization rate at the anode surface. It is this delay in the response of the anode fall to changes in ionization rate that makes it possible for an excess of ions to be created before the anode fall has had time to respond.

8. The frequency of the oscillations

With this model the frequency of the oscillations depends on how long it takes for the ions produced in the burst of ionization either to move away from the anode as ion conduction current or to diffuse to the tube walls. Since details of the processes occurring are not known, the frequency cannot be determined; however, it is of interest to see if it is possible to predict the variation of frequency with pressure and current.

Experimentally it is found that the time during which light is emitted from the region close to the anode is independent of current and pressure, as is the rate at which the anode fall collapses. From this it is concluded that the time during which ionization occurs is at least to a first approximation independent of pressure and current.

The total number of ions produced in each burst of ionization depends on the discharge current I, the ionization cross section σ, the number density of the Ar atoms, N, and the time during which ionization occurs. The number n of ions produced per pulse may be written

$$n=(I/e)N\langle\sigma\rangle x\Delta t \qquad (1)$$

where $\langle\ \rangle$ denotes an average over the pulse time, x is the effective depth of the region over which ionization occurs, and e is the electronic charge.

This expression only applies if $N\langle\sigma\rangle x \ll 1$, and if the ionization is by single electron collision. If the ionization occurs by a two-step process with excitation of an argon atom to a metastable state by electron collision and then ionization of the metastable by a second electron collision, then n will be proportional to I^2. The frequency of the oscillations is the average ion loss rate divided by n. If the dominant process by which ions are lost from the anode zone is the ion conduction current, which increases linearly with I, then this model predicts that the oscillation frequency should be independent of current.

Experimentally this is not so: the frequency always increases with current. A possible explanation of this disagreement is that the average ionization rate is not linear with current as assumed in (1), but that it saturates with current. One way in which this could occur is if the destruction of ions by electron collision becomes important. This requires a three-body collision between an electron, an ion and a third body to conserve momentum. While the ionization rate depends only on the number of incident electrons (and their energy), the three-body recombination depends also on the ion density, and thus becomes more important as the ion density rises. This may provide a limit to the number of ions created in a burst of ionization, since the number of ions will increase until the loss rate is equal to the creation rate and then can rise no further. In this case a linear relation between the oscillation frequency and the current would be expected.

The observed change of oscillation frequency with pressure is in better agreement with that predicted by the model. The model predicts that the frequency should be proportional to p^{-1}. It is found that the frequency always decreases with pressure, although less rapidly than p^{-1}.

9. Estimation of ionization rate

It is of interest to try to estimate the number of ions produced per burst of ionization, n, and the average cross section $\langle\sigma\rangle$ calculated from equation (1). From figure 6 the pulse width Δt is about 4 μs and the time between pulses 25 μs. The discharge current when figure 6 was recorded was 16 A and the gas pressure 0·7 Torr. An estimate of the average ion current is used to calculate n. Outside the high-field region of the anode zone the ratio of the ion current to the electron current is v_+/v_e, where v_+ is the ion drift velocity and v_e the electron drift velocity. The value of this ratio is dependent on X/p_0, where X is the axial electric field and p_0 the gas pressure reduced to 0 °C. The temperature of the gas has been estimated in these studies to be 1800–2000 K by measuring the line width of the 4702 Å and 5188 Å ArI lines in the anode zone using a scanning Fabry–Perot interferometer. This high temperature is probably due to the effect of high current density in the constricted plasma between the anode and the capillary together with the hot ionized gas which is squirted into the anode region by the well-known gas pumping processes which operate in the capillary region of the discharge (3000–4000 K at the current densities of the investigation). The gas pressure reduced to 0 °C is therefore about 0·1 Torr. The axial field is estimated to be about 0·1 V cm^{-1}. The mobility of Ar^+ ions in argon at 1 Torr is 1200 cm^2 s^{-1} V^{-1} (McDaniel 1964, p 470). The electron drift velocity is 5×10^5 cm s^{-1} (McDaniel 1964, p 541). The ratio of ion current to electron current is therefore $1{\cdot}2\times10^3/5\times10^5$, and the estimated ion current is $2{\cdot}4\times10^{17}$ ions s^{-1}. Each burst of ionization must therefore create at least 6×10^{12} ion pairs, and the average ionization rate $n/\Delta t$ must be at least $1{\cdot}5\times10^{18}$ ions s^{-1}.

To estimate the average ionization cross section $\langle\sigma\rangle$ it is necessary to assume a value for x. The light emission studies suggest that a value of 1 mm may be appropriate. At a temperature of 2000 K and a pressure of 0·7 Torr, the gas number density is about 4×10^{15} cm^{-3}. Using these values of $n/\Delta t$, x and N together with $I=16$ in (1) gives the value of the average ionization cross section of 4×10^{-17} cm^2.

This value of the cross section is averaged over the energy distribution of the electrons after they have been accelerated through the anode fall. The value is too large for the ionization to be predominantly due to the high-energy tail of the energy distribution, and

so the average energy must be at least of the order of the ionization energy. If the random energy of the electrons is ignored, then the above cross section would require the anode fall to be about 18·5 V (using the cross section data of Rapp and Englander-Golden 1965). The random energy of the electrons is about 2 eV, so that the peak anode fall might be expected to be within the range 15–18 V. Anode falls as large as this have been measured when strong oscillations are present (peak-to-peak amplitude 13–15 V). Frequently, however, the peak value of the anode fall is much less, often only 10 V and sometimes as small as 6 V. The oscillations have a peak-to-peak amplitude of the same magnitude as the anode fall in each case.

These very low values of the peak anode fall could not provide sufficiently high ionization rates for this model. The ionization may occur in a much larger volume (which does not seem likely in view of the observed light emission) or multistage ionization through metastable levels of argon ($3p^5\,4s\,{}^3P_2$, $3p^5\,4s\,{}^3P_0$) may be an important mechanism. The lowest metastable potential $3p^5\,4s\,{}^3P_2$ of Ar is 11·55 V, so that values of anode fall of around 11 V are expected if most of the ionization occurs via the metastable levels. This is in fair agreement with the usual experimental values of 10–12 V.

Acknowledgments

The author would like to thank Dr A Maitland for helpful discussions and the SRC for financial support.

References

Coulter J R M, Armstrong N H K and Emeleus K G 1961 *Proc. Phys. Soc.* 77 476–82
Crawford F W 1963 *J. appl. Phys.* 34 1897–902
von Engel A 1941 *Phil. Mag.* 32 417–26
Galehouse D C, Ingard U, Ryan T J and Ezekiel S 1971 *Appl. Phys. Lett.* 18 13–5
Garscadden A and Emeleus K G 1962 *Proc. Phys. Soc.* 79 535–41
McDaniel E W 1964 *Collision Phenomena in Ionized Gases* (New York, London, Sydney: Wiley)
Maitland A 1969 *J. Phys.* D: *Appl. Phys.* 2 535–9
Ogwa K 1959 *J. Phys. Soc. Japan* 14 1746–51
Pupp W 1933 *Z. Phys.* 34 756–61
Rapp D and Englander-Golden P 1965 *J. chem. Phys.* 43 1464–79
Suzuki T 1971 *Jap. J. appl. Phys.* 10 1419–24
Yosimoto H 1953 *J. Phys. Soc. Japan* 8 69–76

fig 3.1 Discharge Voltage Oscillations

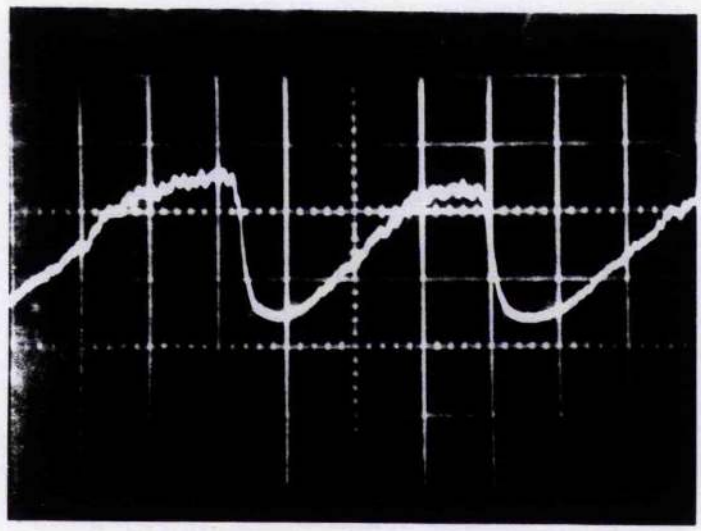

(a) Spot oscillations : vertical scale = 5 V/div.
horizontal scale = 2 μsec./div
discharge current = 40 A , system pressure = 0·6 torr.

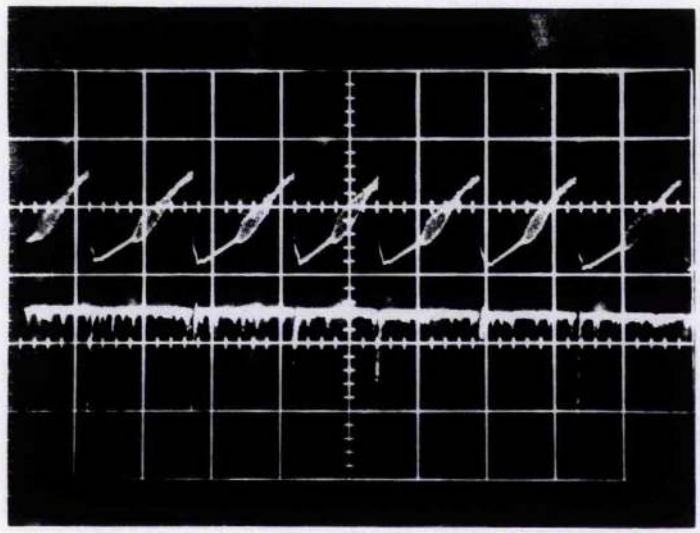

(b) Spot oscillations : upper trace ; discharge voltage (5 V/div.), lower trace ; light emission from the anode spot (increasing in -ve direction) at 472·7 n.m. horizontal scale = 20 μsec./div.
discharge current = 10 A, system pressure = 1 torr.

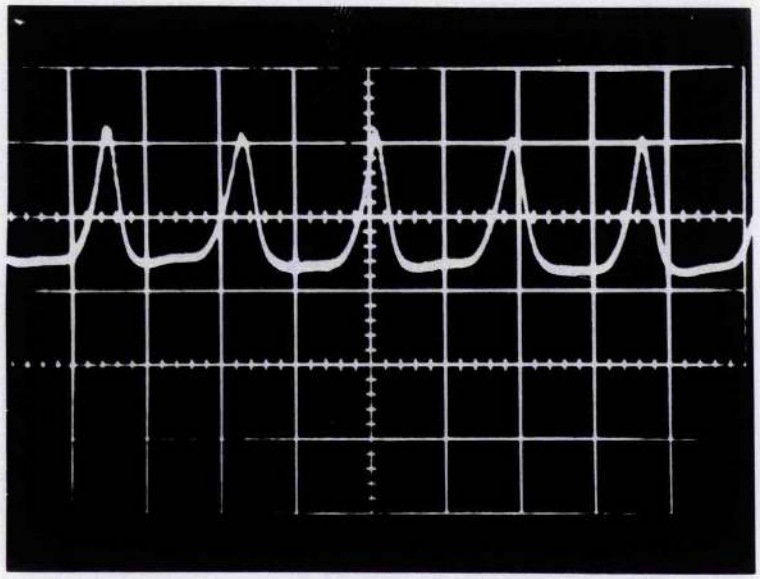

(c) Two coupled glow oscillations of almost equal amplitude : vertical scale = 5 V/div., horizontal scale = 10 μsec/div., peak anode fall = 11·7 V, discharge current = 25 A, system pressure = 0·6 torr.

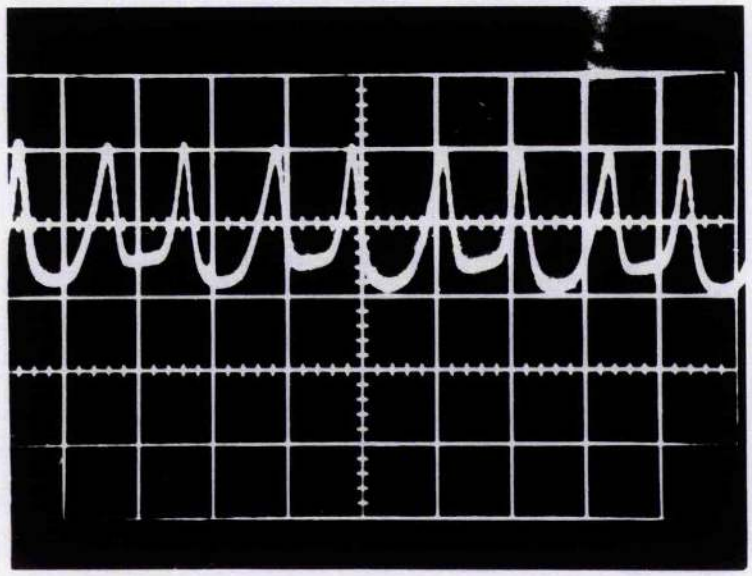

(d) Two coupled glow oscillations of unequal amplitude : vertical scale = 5 V/div., horizontal scale = 20 usec./div., peak anode fall = 10·9 V discharge current = 15 A, system pressure = 0·6 torr.

Comments on "Transient Phenomena in the Anode Region"

The experiments discussed above are all concerned with an argon laser discharge. Oscillations have also been observed in the same laser tube filled with krypton in place of the argon. Only a few experiments have been performed (because of the high cost of krypton) but a few general features emerge. The frequency of the oscillations is always greater in krypton, at the same pressure and discharge current (by a factor of 1.5 to 2). The oscillations are less stable in krypton than argon, but this may be due to gas pumping problems arising from the residual argon in the discharge. The amplitude of the oscillations in krypton is slightly less than in argon (9 or 10 V for Kr; 10 or 12 for A). The variation of frequency with pressure and current follows the same pattern as in argon.

The laser normally operates with an axial magnetic field produced by a solenoid round the capillary region of the discharge. The anode is in the fringe field of this solenoid. The effect of the magnetic field is complicated and somewhat unpredictable. Usually the magnetic field increases the frequency of the oscillations. If the discharge is quiet in the absence of a magnetic field (i.e. no oscillations are present) then applying a magnetic field will sometimes induce oscillations, which reproduceably appear and disappear as the solenoid is turned on and off. Such behaviour is shown in fig. 3.2 for a discharge in argon. The magnetic field quoted is the field in the central region of the solenoid. At the anode the magnitude of the field is about 1/6 this value.

It has also been observed that the magnetic field may suppress oscillations that are present in the absence of the field, although this behaviour is not usual. The most probable explanation of the effect of the magnetic field is that it alters the discharge path and the current density in the anode zone. It is noted that when the magnetic field changes the oscillations, the distribution of glowing

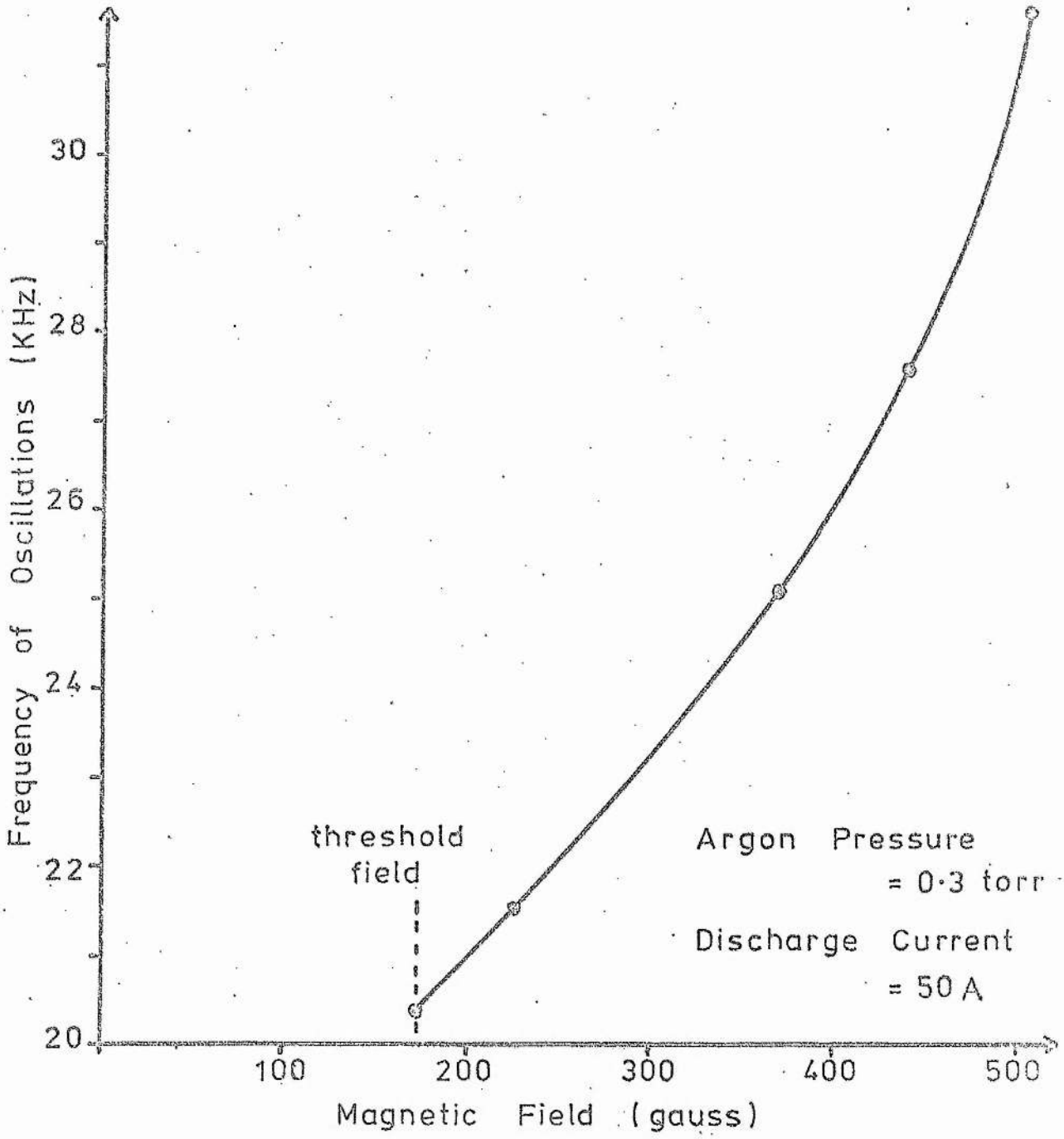

fig 3.2 Variation of Oscillation Frequency with Magnetic Field

plasma round the anode is changed.

Finally it should be pointed out that the discharge current was kept constant during all these experiments by including a 20 mH choke in series with the discharge. This is especially important for the probe measurements where the modulation of current would introduce oscillations in the plasma potential in the region of the probe. For further details of the probe measurements, see appendix A3.

CHAPTER 4

THE ANODE ZONE

4.1 The Origin of the Anode Fall

It has been shown that the oscillations are produced in a region very close to the anode. The processes occurring in the anode zone in the absence of oscillations will be considered in more detail before considering a model for the anode zone which includes temporal variations of the anode fall (chapter 5).

At the anode surface the discharge current is carried only by the electrons. Between the positive column of the discharge and the anode there is a region in which ions are produced at a rate which is sufficient to maintain charge neutrality in the positive column. The field of the anode fall is necessary to accelerate the electrons so that near the anode they have sufficient energy to produce ions at the required rate. This explanation was first suggested by Pupp (13).

The region of large electric field across which the anode fall is produced is referred to as the anode zone. The anode zone is a difficult region to treat theoretically because of the complicated interrelations between space charge, electric field and ion and electron currents. The only attempt to produce a mathematical model of the anode zone appears to be that of Von Engel (33). Von Engel's theory assumes a parabolic variation of electric field in the anode zone, based on the experimental observations of Günterschulze, Bär and Betz (34). A prediction of Von Engel's theory is that the anode fall should be almost equal to the ionization potential of the gas (15.5 V for A). In the argon ion laser the anode fall (when stable) has been found to be much less than this (usually between 3 and 5 V). In section 4.5 the ionization rate is estimated assuming the parabolic variation of electric field used by Von Engel, but a different approach to the ionization rate is used in order to consider the case when the anode fall is less than the ionization potential.

4.2 Spectroscopic Studies of the Anode Zone

The intensity of the light emission from the stable anode zone has been investigated as the axial distance of the sampling region from the anode is varied, in a similar manner to the light emission studies discussed in chapter 3, but in this case the intensity is independent of time. The variation of intensities of the AI and AII lines are quite different. A typical variation is shown in fig. 4.1. The intensity of the AII lines increases rapidly close to the anode while that of the AI lines decreases. The total width of the anode zone appears to be 5 or 6 m.m.

Hydrogen lines are always visible in the spectrum of the light emitted from the anode region of the discharge. (The hydrogen is probably evolved from the walls of the aluminium discharge tube). The intensity ratio I_β/I_α of the H_β and H_α lines should increase as the electron energy increases. The ratio I_β/I_α is shown in fig. 4.2. The ratio at first increases as the anode is approached, but falls sharply very close to the anode. The anode fall (measured using the Langmuir probe) was 5 V when fig. 4.1 and fig. 4.2 were recorded at a discharge current of 30 A and a system gas pressure of 0.2 torr.

The rapid rise of intensity of the AII lines close to the anode indicates that there must be a rapid rise of ion density in this region. The rapid decrease of the AI lines and the decrease in the ratio I_β/I_α indicates that the rise in ion density is accompanied by a fall in electron energy.

4.3 Probe Measurements in the Anode Region

A Langmuir probe is used to study the plasma in the region of the anode, and to measure the anode fall. The probe is inserted into the plasma perpendicular to the discharge axis, at an axial distance of about 10 m.m. from the anode (for details of the probe and its use see Appendix A3). The probe is not moved closer to the anode as the

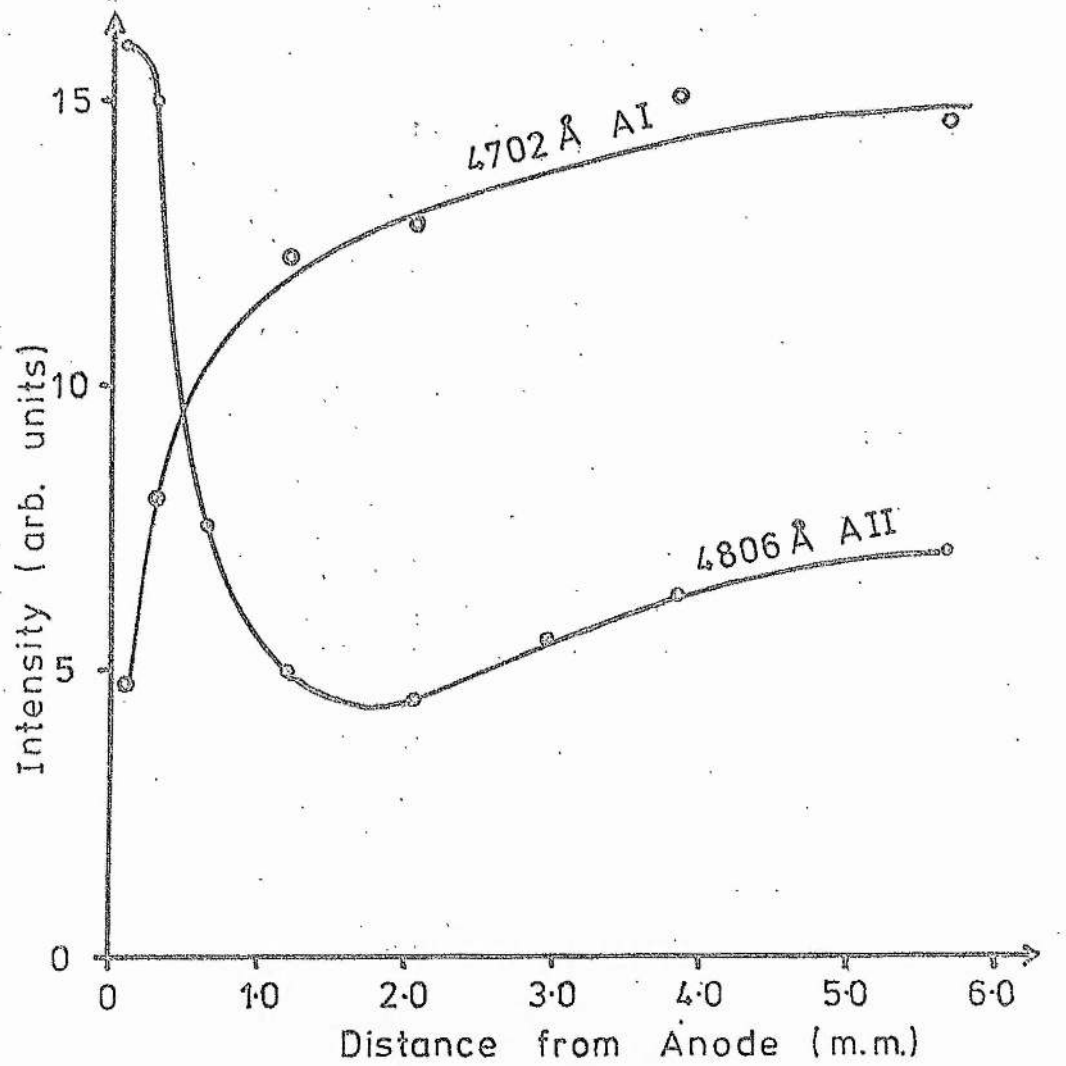

fig 4.1 Variation of Light Intensity with Axial Distance from the Anode

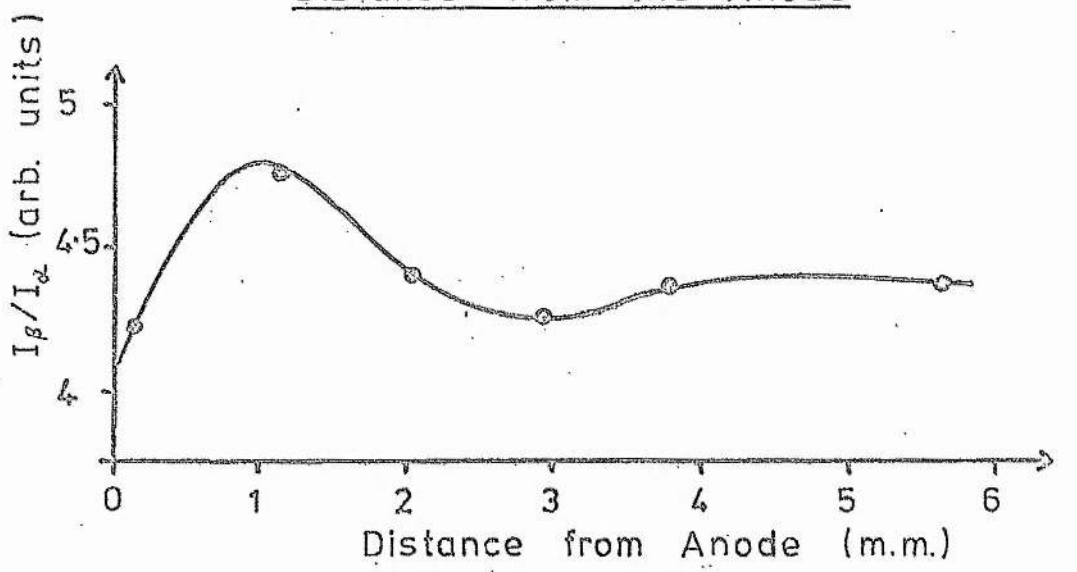

fig 4.2 Variation of I_β / I_α with Axial Distance from the Anode

characteristics of Langmuir probes can only be interpreted in a plasma (and even then interpretation is often not easy), little work has been done on probes in regions of space charge.

The electron temperatures found from the probe measurements varied from day to day but are usually in the range 18,000 - 23,000 K. The electron temperature decreases slowly as the gas pressure is increased (fig. 4.3) and varies slowly with discharge current (fig. 4.4).

The electron density n_e is calculated from the positive ion saturation current of the probe. The electron density increases with pressure (fig. 4.5) and with current (fig. 4.6). The absolute values of n_e are somewhat uncertain because of the well known problems associated with the interpretation of probe characteristics concerning the collection of positive ions by a negative probe. The electron density has been calculated from equation (A7) of Appendix A3. The relative magnitude of n_e at different pressures and currents should be more reliable.

The space potential of the plasma near the probe is measured using the method described in Appendix A3. If oscillations are present the peak anode voltage is measured using a digital voltmeter in the circuit shown in fig. A3.1. The peak value of the anode fall is then found from the probe space potential. The instantaneous value of the anode fall may be found from the peak value and an oscilloscope photograph of the anode voltage oscillations.

In the absence of oscillations the measured values of the anode fall range from 2 to 5 V. When oscillations are present the peak anode fall is usually between 10 and 15 volts and often increases slowly with discharge current (fig. 4.7). The anode fall is about 2 V greater than the peak to peak amplitude of the oscillations.

Random noise and fluctuations in discharge voltage contribute an uncertainty of ± 0.5 V in the anode fall measurements. The limitations of the theory of positive ion collection introduce an

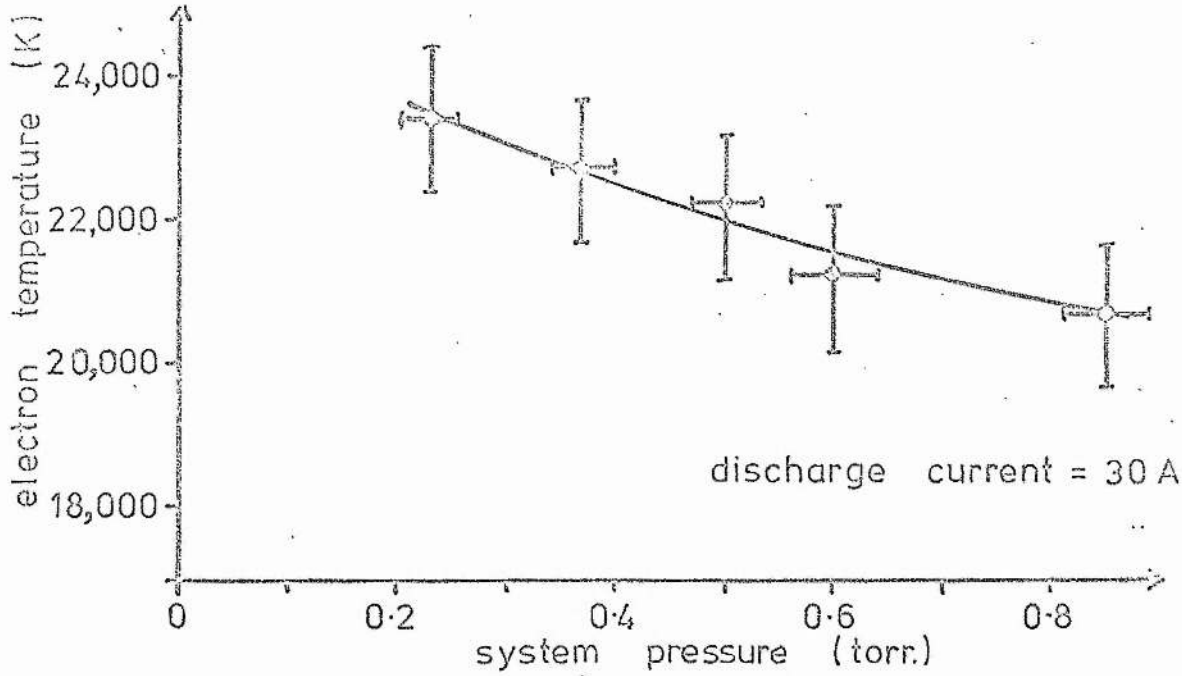

fig. 4.3 The Variation of Electron Temperature with System Pressure

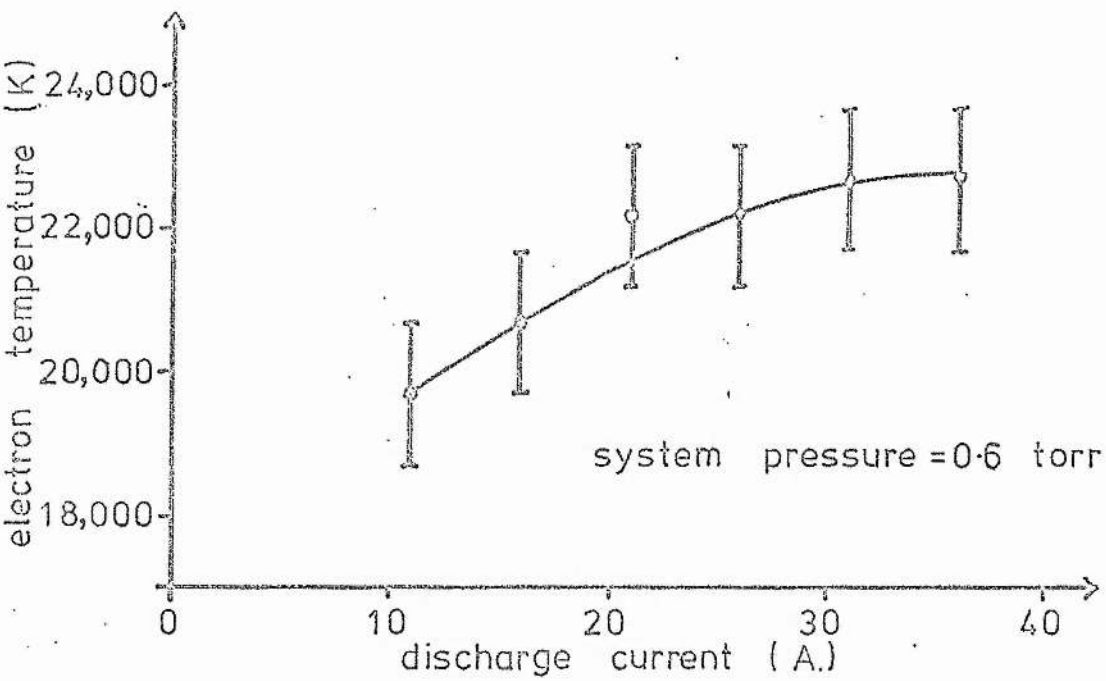

fig. 4.4 The Variation of Electron Temperature with Discharge Current

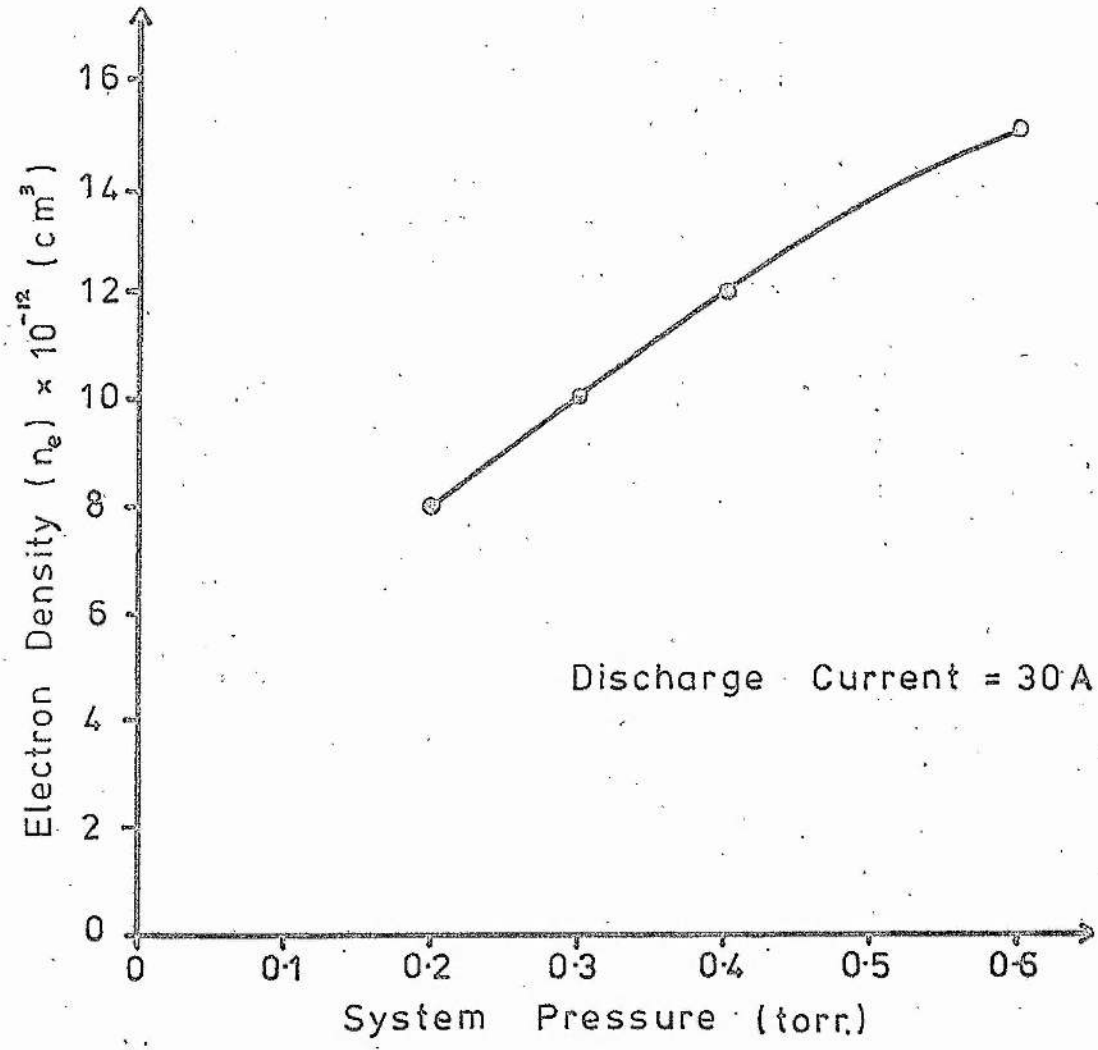

fig. 4.5 Variation of n_e with Pressure at Constant Current

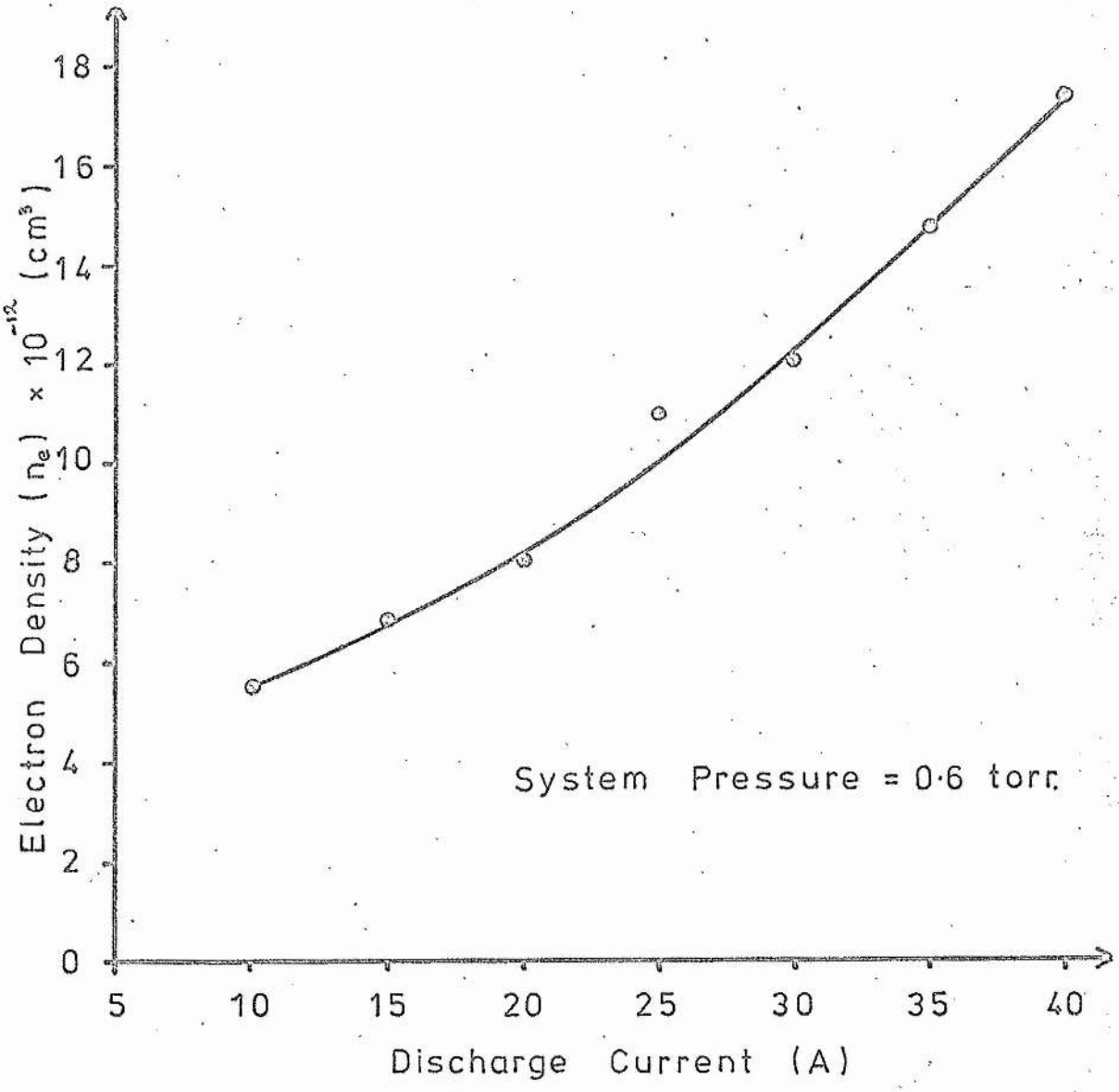

fig. 4.6 Variation of n_e with Current at Constant Pressure

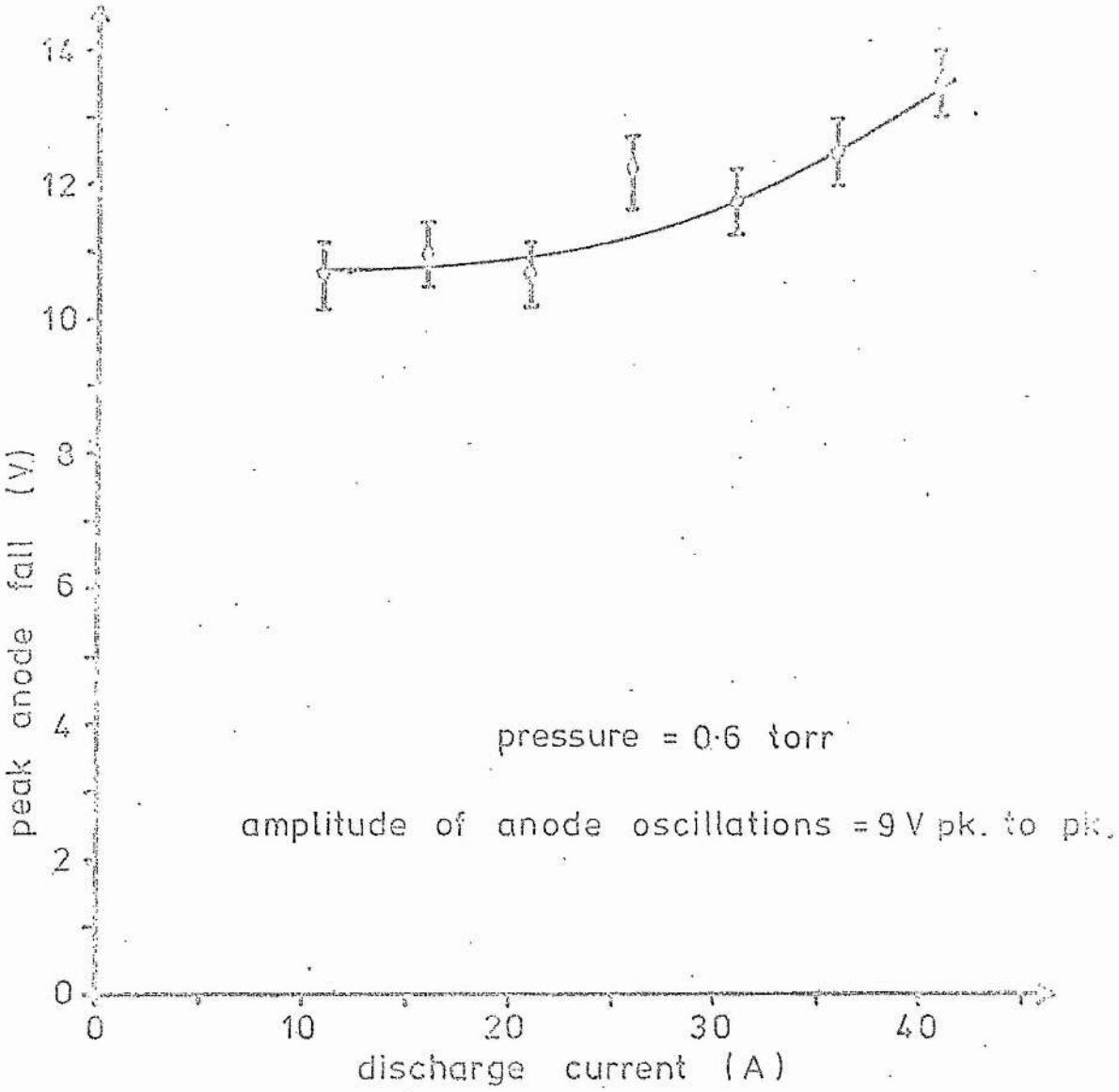

fig. 4.7 The Variation of the Anode Fall with Discharge Current

uncertainty in n_e of perhaps a factor of 2. This corresponds to an uncertainty of about 1.5 V in the anode fall. (Appendix A3 equations A6, A7). The total uncertainty in the value of the anode fall is therefore ± 2 V.

4.4 Line Width Measurements

The broadening of the AI lines is predominantly due to the thermal motion of the argon atoms. The Doppler broadened profile of a spectral line due to the thermal motion of the atoms is Gaussian with a half width given by

$$\Delta\lambda = \left(\frac{8kT \ln 2}{Mc^2}\right)^{\frac{1}{2}} \lambda_o$$

where λ_o is the centre wavelength, M is the mass of the atoms and T is the temperature. The gas temperature T may be found by measuring $\Delta\lambda$ provided the homogeneous line width is much smaller than the Doppler line width. The homogeneous line width includes contributions from pressure broadening, Stark broadening and the natural line width.

The hydrogen lines experience an appreciable Stark broadening due to the interaction of hydrogen atoms with ions and electrons. The data of Griem (35 page 448) suggests that the Stark broadening of the H_β line may be detectable if the electron density is of the order of 10^{13} cm^{-3} as given by the probe measurements (at an electron density of 10^{13} cm^{-3} the Stark width of the H_β line is about 9×10^{-3} n.m.) The H_α line is broadened much less than the H_β line and so may be used to measure the 'temperature' of the hydrogen. The plasma is not in thermal equilibrium and the hydrogen being lighter than the argon will gain energy more rapidly from the electrons and thus will reach a steady state with a higher average energy.

The line widths are measured using a piezo-electrically scanned Fabry-Perot interferometer. The technique is described in appendix A7.

The ratio of the width of the H_α line to the width of the H_β line is found to be 1.35 to within the experimental error (about 5%). This is the ratio of the wavelengths of the H_α and H_β lines (656.3 n.m. and 486.1 n.m.) and is the value expected if the broadening is due only to the motion of the atoms (thermal or otherwise). No extra broadening of the H_β line could be detected in these experiments. Typical widths of the H_α and H_β lines are 0.0350 n.m. and 0.0256 n.m. respectively at a discharge current of 40 A and a system pressure of 0.3 torr. The temperature of the hydrogen obtained from these line widths is 5,500 K. This very high temperature would certainly mask the Stark broadening.

A few measurements have been made of the line widths of the 470.2 n.m. and 518.8 n.m. of AI and 480.6 n.m. line of AII (see Appendix A7). These measurements give a temperature of 1,800 K for the neutral argon atoms under the same discharge conditions as above. The temperature of the positive ions is about 2,400 K. It is assumed that the broadening of the spectral lines is due only to the thermal motion of the atoms and ions. Stark broadening should not be significant, at least for the 470.2 n.m. line, for which information about the Stark width is available (35 page 493). Other broadening processes such as pressure broadening and self absorption are not expected to be significant. This is confirmed in as much as the temperatures calculated from the two AI lines are the same.

The large differences between the argon temperature and the hydrogen temperature is somewhat surprising and is discussed in more detail in Appendix A4.

4.5 The Ionization Rate in the Anode Zone

Von Engel's theory of the anode fall predicts that the anode fall (V_a) is of the same order as the ionization potential (V_i). The

magnitude of the anode fall in the argon laser is found to be much less than this (when the fall is stable). Von Engel's calculation of the ionization rate is, however, only appropriate if the anode fall is greater than the ionization potential. In this section the ionization rate is estimated with the assumption that the anode fall is less than the ionization potential. This will be used to estimate the anode fall in the steady state, and when oscillations are present, to estimate the peak ionization rate assuming the phenomenological model discussed in chapter 3.

The ionization rate is given by

$$z = \int_0^\infty \sigma(E)\, N\, nv\, f(E)\, dE \qquad (1)$$

where $\sigma(E)$ is the ionization cross section, N is the neutral atom density, n is the electron density, v is the velocity of an electron with energy E, and f(E) is the electron energy distribution function.

The mean free path of electrons is greater than the width of the anode zone under the conditions of the experiments and the energy gained by an electron in traversing the anode zone is greater than the random energy of electrons outside the anode zone. In this case the electrons can not be treated as having a random isotropic velocity distribution with a small superimposed drift motion. A more appropriate model is to consider a beam of electrons all falling freely towards the anode, the electrons having a small spread of energy. This second model will be adopted.

If the angular spread of this beam of electrons is small then equation (1) may be written in the form,

$$z = \int_0^\infty \sigma(E)\, Nj(E)\, dE \qquad (2)$$

where $j(E)\, dE = vn\, f(E)\, dE$ is the component of the electron current crossing unit area with an energy between E and E + dE; j(E) is normalized so that

$$\int_0^\infty j(E)\, dE = J \qquad (3)$$

where J is the total electron current density (which is approximately equal to the total current density), and is expressed in terms of the number of electrons per second.

It is clear that j must be a function of position, through its dependence on the energy gained in moving through the anode zone. If V(x) is the voltage between the point x and the junction of the positive column and the anode zone, then j will be a function of E and V, i.e. $j \equiv j(E,V)$. The mean free path of the electrons is long, so that collisions may be ignored (to a first approximation). Between two points along the discharge axis differing in potential by ΔV, the energy of all the electrons must increase by ΔV (energy is measured in eV). It follows that

$$j(E,V) = j(E + \Delta V,\ V + \Delta V) \qquad (4)$$

Equation (4) is satisfied if j is a function of E - V. Since the electrons are moving towards the anode in order to enter the anode zone the electrons at x have an energy greater than V(x) (i.e. $j(E,V) = 0$ if $E \leq V$). A form must be assumed for j(E,V) that satisfies the above conditions and also tends to zero for large values of E. The rate at which it tends to zero depends on the random energy with which the electrons enter the anode zone from the positive column. The form chosen for j(E,V), which satisfies the above requirements is,

$$j(E,V) \propto (E - V) \exp - \frac{e(E-V)}{kT_e} \qquad (5)$$

where T_e is the electron temperature in the positive column.

The ionization cross section data of Rapp and Englander-Golden (36) for argon may be represented by the equation

$$\sigma(E) = a(E - E_i) \tag{6}$$

where E_i is the ionization potential, provided $E - E_i$ is not too large (say less than 50 eV). The value of a is found to be 1.66×10^{-17} cm^2 eV^{-1} when E and E_i are in eV.

The ionization rate per unit volume (z(x)) at a point x in the anode zone where the space potential is V is obtained from (2), (3), (5) and (6) and is given by,

$$z(x) = \frac{aJN \int_V^\infty (E-E_i)(E-V)\exp\{-\frac{E-V}{V_e}\}\, dE}{\int_V^\infty (E-V)\exp\{-\frac{E-V}{V_e}\}\, dE} \tag{7a}$$

if $V > E_i$,

$$z(x) = \frac{aJN \int_{E_i}^\infty (E-E_i)(E-V)\exp\{-\frac{E-V}{V_e}\}\, dE}{\int_V^\infty (E-V)\exp\{-\frac{E-V}{V_e}\}\, dE} \tag{7b}$$

if $V < E_i$,

where $V_e = kT_e/e$.

Equations (7a) and (7b) may be integrated to give

$$z(x) = JNa(V + 2V_e - E_i) \qquad V \geq E_i \tag{8a}$$

$$z(x) = JNa(E_i + 2V_e - V)\exp\frac{V-E_i}{V_e} \qquad V < E_i \tag{8b}$$

The total number of ions created per unit cross section of the discharge (Z) is given by,

$$Z = \int_o^d z(x)\, dx \tag{9}$$

where x is the distance along the axis of the discharge measured from the junction of the positive column and the anode zone, and d is the

total width of the anode zone.

Since the variation of potential with distance is not known, the form used by Von Engel (33) in his theory of the anode zone is assumed. This may be written

$$V(x) = 3V_a \left(\frac{x}{d}\right)^2 (1 - x/d) \tag{10}$$

The ionization rate per unit cross section Z is found by substituting (8a), (8b) and (10) into (9) and integrating, and may be expressed in the form

$$Z = JNa\ d\ F(V_a, V_e) \tag{11}$$

The function $F(V_a, V_e)$ has been found by numerical integration and is plotted in fig. 4.5 as a function of V_a for several values of V_e.

In the steady state the positive ion current J_+ must be less than or equal to the ionization rate Z. The equality will hold if no ions are lost by diffusion or recombination. Assuming that J_+ is equal to Z the equilibrium value of $F(V_a, V_e)$ is given by

$$F(V_a, V_e) = \frac{J_+}{JNa\ d} \tag{12}$$

In chapter 3 section 9 the ratio J_+/J is estimated to be $1.2 \times 10^3 / 5 \times 10^5$, this value is expected to be independent of discharge current. Typical values of N and d are 4×10^{15} cm^{-3} and 0.5 cm (d is obtained from the variation of light emission with axial distance from the anode). Substituting these values into (12) gives a value of 0.073 for $F(V_a, V_e)$. The probe measurements give a value of 2 V for V_e, so that the steady state value of the anode fall is found from fig. 4.8 to be about 7.5 V. This value will be independent of the discharge current (provided V_e, d etc. do not vary with current).

The value of the anode fall predicted in this way is substantially less than the value predicted by the theory of Von Engel (about 15 V), but is larger than the observed value (about 5 V). One possible

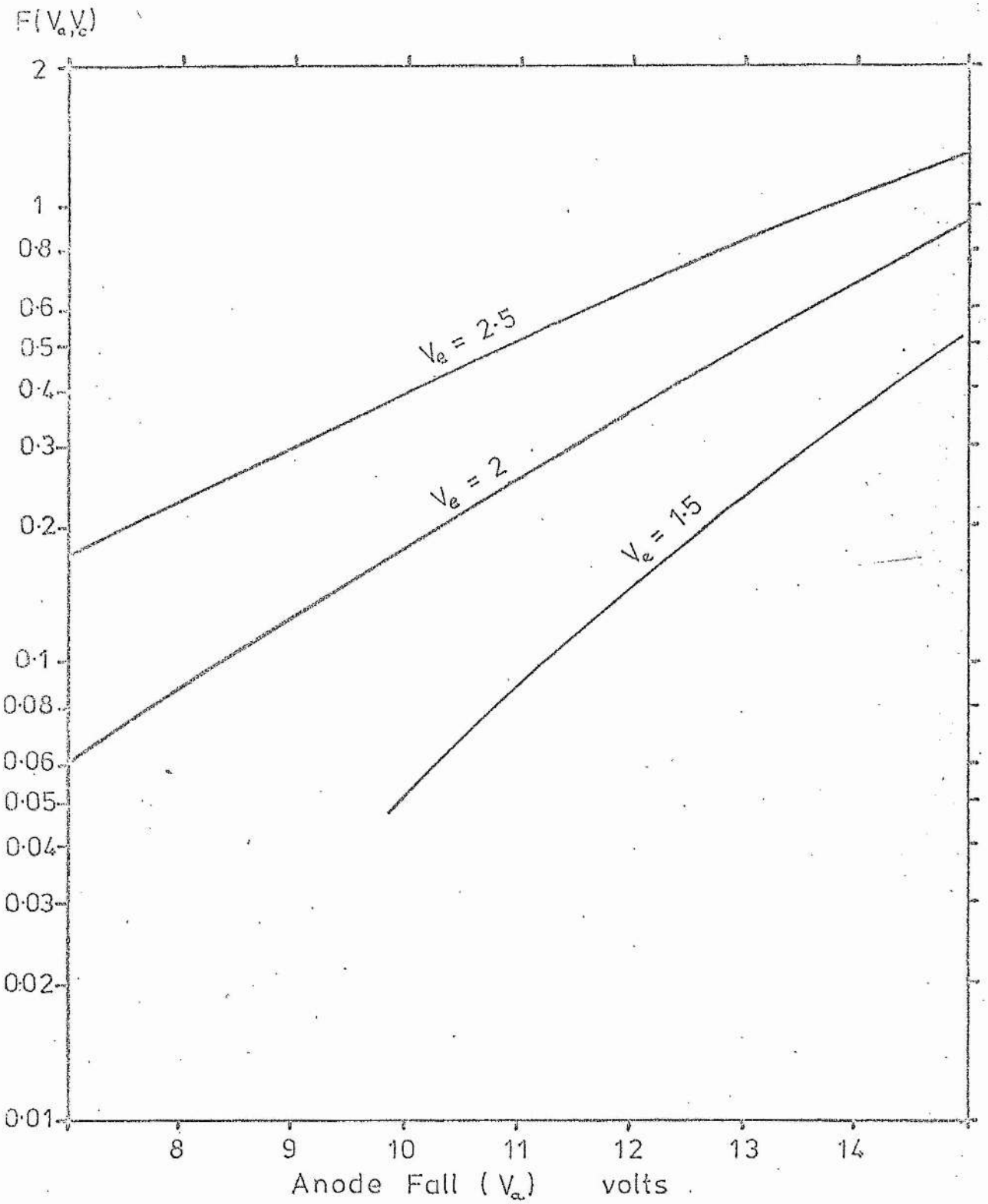

fig. 4.8 F(Va,Ve) as a Function of Va with Ve as a Parameter

explanation of this discrepancy is that the ionization also occurs by a two-step process, in which a neutral argon atom is first excited to a long lived excited state by a first electron collision and then ionized by a second collision. The two metastable states most likely to be involved are the $3p^5 4s\ ^3P_2$ and $3p^5 4s\ ^3P_0$ states, but the cross sections for excitation and ionization of these states by electron collision have not been measured (although the cross section for ionization has been calculated (37)). It is not possible therefore to estimate the ionization rate by this two step process.

In this chapter the discussion has centred on the anode zone in its stable state. If anode oscillations are present the above calculation of ionization rate may be applied to estimate the peak value of the anode fall. In chapter 3 the value of the ionization rate during the bursts of ionization was estimated (assuming Pupp's model of anode oscillations) to be 1.5×10^{18} ions s^{-1} at a discharge current of 16 amps (10^{20} electrons s^{-1}). The appropriate value of $F(V_a, V_e)$ is found from (11) to be 0.45 (assuming $N = 4 \times 10^{15}$, $d = 0.5$). The value of the anode fall necessary to produce this value of $F(V_a, V_e)$ is about 13 V (with $V_e = 2$ V), this is in good agreement with the measured values of the peak anode fall when oscillations are present (the measured value of the peak anode fall is usually between 12 and 14 V).

CHAPTER 5

THE STABILITY OF THE ANODE FALL

5.1 A Simple Model for the Anode Zone

In chapter 3 the anode oscillations were discussed in terms of Pupp's phenomenological theory of the anode fall. This theory assumes that it is possible for ions to be produced, for a short time, at a rate exceeding that required to maintain charge neutrality and that during this time an excess of ions is produced. This is only possible if the space charge which controls the anode fall does not respond instantaneously to changes in the ionization rate, otherwise once the ionization rate reaches the equilibrium value the anode fall will stabilize at the steady state value (V_o). The length of time that the ionization rate may exceed the steady state value will be determined by the rate at which the anode fall responds to changes in the ionization rate.

In this chapter a simple model of the anode fall is presented, and its response to changes in ionization rate determined. It is shown that under certain conditions the model predicts that the anode fall will be unstable.

The processes occurring within the anode zone are very complex and can not easily be analysed, especially if the distribution of space charge, electric field and electron and ion currents are all allowed to vary with time. In order to examine the conditions necessary for the anode fall to be stable, a simple model of the anode zone will be introduced and its stability examined.

The variation of potential in the anode zone is assumed to be as illustrated in fig. 5.1. The discharge is considered in one dimension for simplicity. To the left of $x = o$ is the positive column and between $x = o$ and $x = d$ is the anode zone. Between $x = \ell$ and $x = d$ it is assumed that the electric field is constant. The space charge is concentrated between $x = o$ and $x = \ell$, where the field

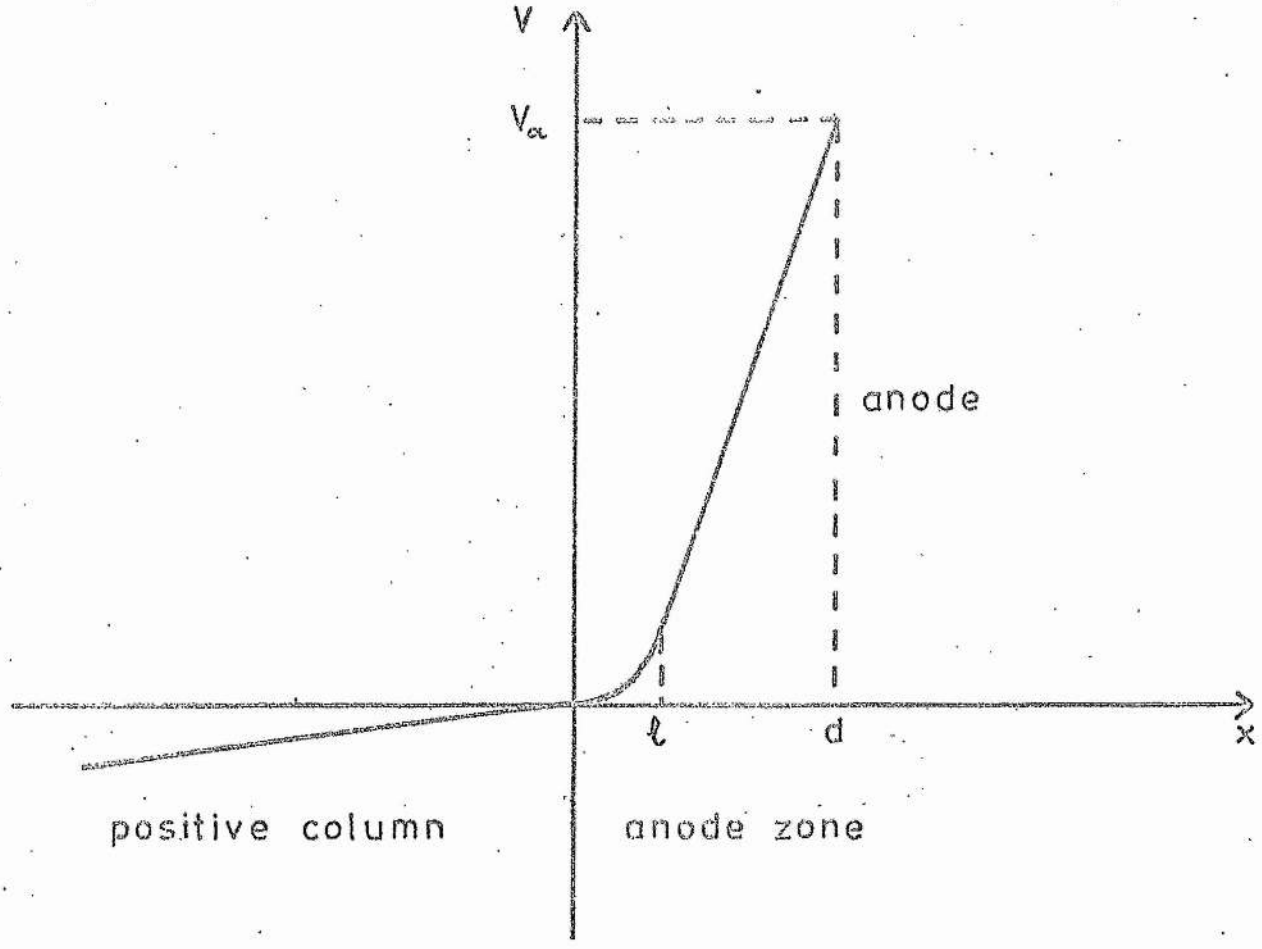

fig 5.1 The Assumed Variation of Potential with Position in the Anode Zone

changes from the low value in the positive column to the high value in the anode zone. It is also assumed that in the region $o \leq x \leq \ell$ the space charge is uniform.

The relation between the electric field in the positive column and the electric field in the anode zone may be found using Poisson's equation,

$$\frac{dE}{dx} = \frac{\rho}{\varepsilon_o} \tag{13}$$

where ρ is the space charge density.

If ρ is constant in the region $o \leq x \leq \ell$ and if the electric field in the positive column is $-E_o$, (13) may be integrated to give

$$E = \frac{\rho x}{\varepsilon_o} - E_o , \qquad o \leq x \leq \ell , \tag{14}$$

and (14) may be integrated again to give the voltage

$$V(x) = -\frac{\rho_o x^2}{2\varepsilon_o} + E_o x . \tag{15}$$

In the region $\ell \leq x \leq d$ the space charge is zero and the voltage is given by

$$V(x) = \frac{\rho \ell}{\varepsilon_o} (x - \tfrac{1}{2}\ell) + E_o x , \tag{16}$$

so that the anode fall is given by

$$V_a = -\frac{\rho \ell}{\varepsilon_o} (d - \tfrac{1}{2}\ell) + E_o d . \tag{17}$$

It is assumed ℓ is much less than d and that $E_o d$ is much less than $\frac{\rho \ell d}{\varepsilon_o}$ so that (17) may be approximated to give

$$V_a \simeq -\frac{\rho \ell d}{\varepsilon_o} . \tag{18}$$

The space charge ρ will vary according to the rate at which ions and electrons enter the region of space charge. The positive ion current J_+ in the positive column is constant if the discharge current is held constant. The ion current entering the space charge region

however is dependent on the rate at which ions are created in the anode zone. This ionization rate depends on the anode fall V_a. The ion current entering the space charge region at a time t is $eb\ Z(t-\tau)$ where $Z(t)$ is the rate at which ions are created by electrons accelerated through the anode fall at a time t, per unit cross section of the discharge. The transit time for ions to cross the anode zone is τ and b is the fraction of the ions which take part in the conduction current and are not lost by diffusion to the walls, or by recombination. The ions are created close to the anode so that the ion current entering the space charge region is delayed by a time τ.

The electrons enter the space charge zone at a rate determined by the plasma in the positive column and which is independent of what happens in the anode zone. The electrons have a mean free path which is several times greater than the width of the anode zone, d, so that they may be assumed to free fall through the anode zone. Since the electron current is constant the electron density is inversely proportional to the electron drift velocity. The voltage across the space charge region is small if $\ell << d$ so that the electrons are not accelerated greatly in this region and their drift velocity is determined by the velocity with which they enter the zone. Thus the electron density in the space charge zone is independent of the anode fall.

With the above assumptions about the way in which the space charge varies, the rate of change of space charge is given by

$$\ell \frac{d\rho}{dt} = eb\ Z(t-\tau) - J_+ . \tag{19}$$

Substituting (18) into (19) to eliminate ρ gives

$$-\frac{\varepsilon_o}{d} \frac{d\ V_a}{dt} = eb\ Z(t-\tau) - J_+ . \tag{20}$$

In equilibrium the ionization rate is Z_o where Z_o is given by

$$Z_o = \frac{J_+}{eb} \quad . \tag{21}$$

Since Z is a function of the anode fall, equation (21) determines the equilibrium anode fall V_o. If the anode fall is given by $V_a = V_o + v(t)$ where $v << V_o$ then (20) becomes, after cancelling the constant terms,

$$\frac{dv}{dt} = - \frac{edb}{\varepsilon_o} \left.\frac{dZ}{dV_a}\right|_{V_o} v(t-\tau) \tag{22}$$

where $\left.\frac{dZ}{dV_a}\right|_{V_o}$ is the rate of change of ionization rate with voltage evaluated at the equilibrium voltage. The behaviour of equation (22) determines the stability, or otherwise, of the anode fall. This will be considered in the next section.

5.2 The Stability of the Anode Fall

In section 5.1 a model of the anode zone has been discussed culminating in equation (22) which describes the temporal behaviour of the anode fall close to equilibrium. The condition for the anode fall to be stable is that $V_a(t)$ tends to its equilibrium value V_o as t tends to infinity (i.e. v(t) tends to zero as t tends to infinity).

The solution of (22) is of the form

$$v(t) = \sum_i \alpha_i e^{p_i t} \tag{23}$$

where the values of the constants p_i are the solutions of the equation

$$p + \frac{ebd}{\varepsilon_o} \left.\frac{dZ}{dV_a}\right|_{V_o} e^{-p\tau} = 0 \tag{24}$$

and the α_i are constants.

For v(t) to tend to zero as t tends to infinity all the p_i of (24) must have negative real parts. It is shown in Appendix A5

that this condition requires that

$$c = \frac{edb\tau}{\varepsilon_o} \left.\frac{dZ}{dV_a}\right|_{V_o} < \pi/2 \ . \qquad (25)$$

The value of dZ/dV_a can be estimated using the theory of section 4.5. In order to be consistent it is necessary to assume a linear variation of voltage in the anode zone rather than the cubic form used in section 4.5. (This has the added advantage that it gives Z as a fairly simple function which may be differentiated).

The voltage in the anode zone is assumed to be given by

$$V = V_a \, x/d \ . \qquad (26)$$

If the electron energy distribution is as assumed in section 4.5 then the theory may be followed through as before with (26) replacing (10) for the voltage distribution. The ionization rate is given by

$$Z(V_a) = JNa \; d \; G(V_a, V_e) \qquad (27)$$

where

$$G(V_a, V_e) = \exp\left(-\frac{E_i}{V_e}\right)\left[\left\{\frac{(E_i+3V_e-V_a)V_e}{V_a}\right\} \exp\frac{V_a}{V_e} - \frac{(E_i+3V_e)V_e}{V_a}\right] \qquad (28)$$

Since (25) requires the value of dZ/dV_a, (28) must be differentiated to give

$$\frac{dG}{dV_a} = \exp\left(-\frac{E_i}{V_e}\right)\left[\frac{E_i+3V_e-V_a}{V_a} \exp\frac{V_a}{V_e} - \left(\exp\frac{V_a}{V_e} - 1\right)\frac{(E_i+3V_e)V_e}{V_a^2}\right] \qquad (29)$$

In fig. 5.2 G and dG/dV_a are plotted as functions of V_a with $V_e = 2$ (a typical value).

This theory is applied to the example considered in chapter 3 section 9. The average positive ion current is estimated in chapter 3 to be 2.4×10^{17} sec^{-1} with an electron current of 10^{20} sec^{-1}. The active area of the anode is about 1 cm^2, the gas number density 4×10^{15} cm^{-3} and the width of the anode zone about 0.5 cm. Using

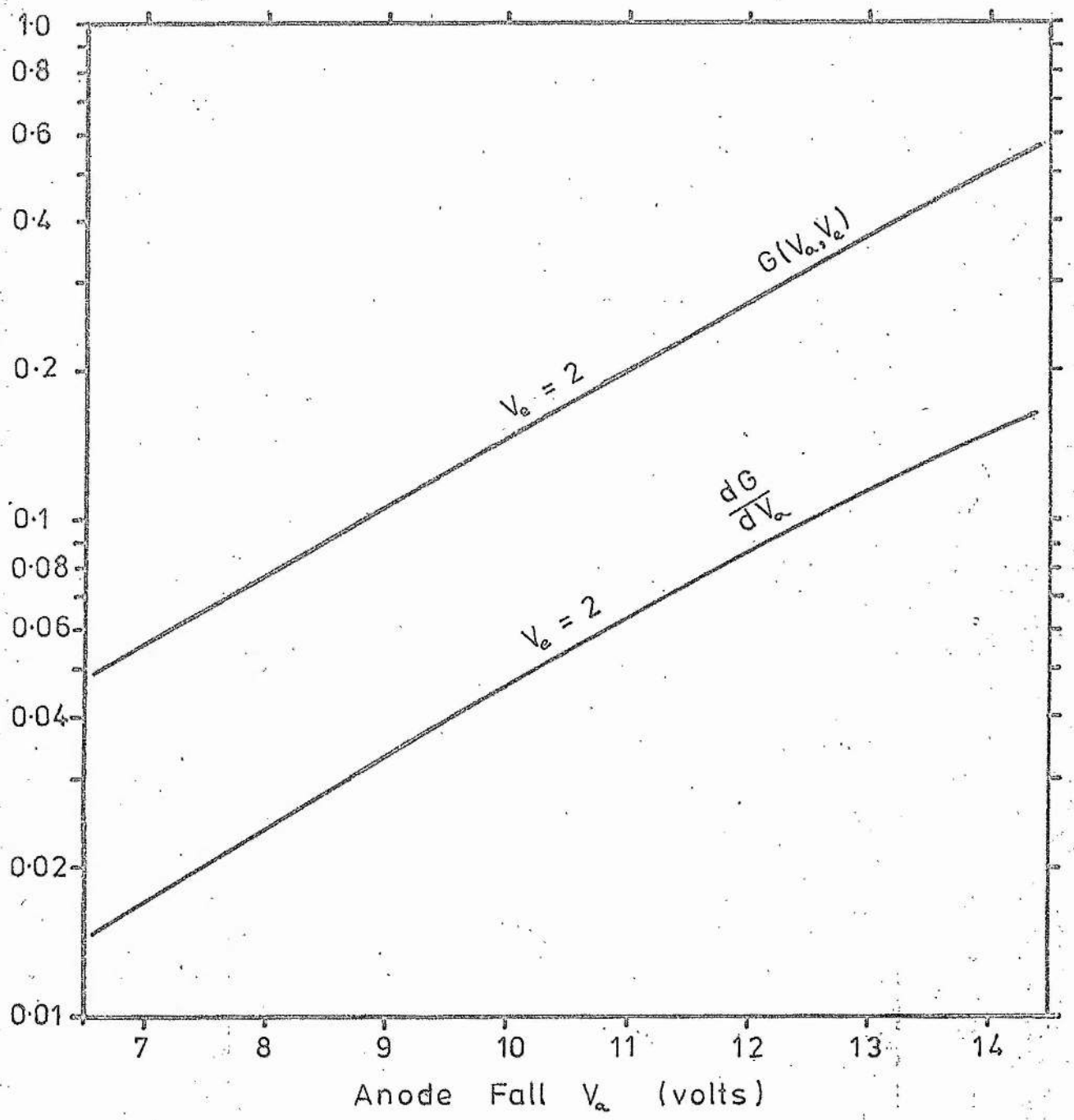

fig 5.2 Semi-log Plot of G and dG/dV_a against V_a

this data in equations (21) and (27) gives $G(V_a, V_e)$ equal to 0.072, assuming b = 1 (i.e. all the ions created take part in the ion current). If V_e is taken to be 2 then V_o, the equilibrium value of the anode fall may be found from fig. 5.2 and is about 8V.

Before the constant c (defined in (25)) can be calculated it is necessary to estimate the ion transit time τ. Since the ions fall freely through the anode zone, τ is given by

$$\tau = d \left(\frac{2M}{eV_a}\right)^{\frac{1}{2}} \qquad (30)$$

where M is the mass of the ions. With V_a equal to 8 volts τ is 1.6×10^{-6} sec.

The value of dG/dV_a at $V_a = 8$ may be found from fig. 5.2 and is 0.024 so that c may be calculated from the definition in (25) and is 1.16×10^5. Clearly this value is much greater than $\pi/2$! The model predicts therefore, that the anode fall should be very unstable. This was evidently the case since large amplitude oscillations occurred under the above conditions. Since the value of c given by the model is so large, the anode fall will be unstable for all the likely values of J, N, d, τ and V_e in an argon laser.

It has been found that the anode fall is normally unstable in the argon ion laser used in the experiments reported here. It is most unstable (the oscillations have largest amplitude) when the anode forms 'spots' and the discharge current is concentrated onto a small area of the anode. When anode spots are present the anode fall is never stable. This model predicts that c increases, and the anode fall becomes more unstable as the discharge current density increases (dZ/dV_a is proportional to the current density). Thus the anode fall is expected to be most unstable when anode spots are present.

Occasionally the anode fall has been found to be stable. This is contrary to the predictions of this model. There are two main reasons why the model may over-estimate the instability of the anode fall. Firstly it is observed that when the anode fall is stable its

value is small (3 - 5 volts). At low values of the anode fall the estimation of ionization rate fails since the assumption made in section 4.5 that the random electron energy should be much less than the anode fall fails. With such low values of the anode fall the ionization rate will depend strongly on the electron random energy, but only weakly on the value of the anode fall. The second reason that the model over-estimates the instability is that it has been assumed that all the ions are created very close to the anode. This is not so, ionization occurs throughout the anode zone. The shorter the distance from the point at which the ion is created to the region of space charge, the shorter its transit time. This will tend to reduce the instability of the anode zone as the anode fall will respond more rapidly to changes in the ionization rate.

It is not possible to predict the frequency of the oscillations that will occur when the anode fall is unstable as the amplitude of the oscillations will grow until they are limited by non-linearities. This contradicts the assumptions made in deriving (22) from (20). However a more fundamental limitation is that if the fluctuations in anode fall are not very much smaller than the mean value of the anode fall the transit time τ can not be considered to be a constant which is independent of the fluctuations in the anode fall.

CHAPTER 6

REDUCTION OF ANODE MODULATION NOISE IN THE LASER OUTPUT AND CONCLUSIONS

6.1 Suppression of the Anode Oscillations

It has been found that anode oscillations may modulate the laser light to a depth of several percent (section 2.3). The most obvious way of preventing this source of excess noise on the laser output is to suppress the anode oscillations, possibly by suitable design of the discharge tube. Sometimes a stable anode fall has been observed in the plasma jet laser used in the experiments reported here. Such behaviour only occurs over restricted ranges of operating parameters (i.e. pressure, current, and magnetic field). A stable anode fall has only been observed at currents above about 15 Amps and usually only at pressures between 0.2 and 0.4 torr. (This is also the region in which the laser usually operates). However it has been found that it is not possible to obtain reliable quiet operation (i.e. no oscillations) especially when the laser is operated with an axial magnetic field.

The experiments of Suzuki (12) suggest that the stability of the anode zone is affected by the geometry of the anode region of the plasma tube and that operation free from oscillations may be obtained with a cylindrical anode co-axial with the axis of the discharge tube if the anode is close to the end of the laser capillary (within about 1 cm). Such behaviour has been sought in the laser used here, but it has not been observed. The distance between the end of the anode and the laser capillary has been varied between 1 and 5 cm but no significant difference in the stability of the anode fall has been observed.

There is some indication that the condition of the surface of the anode may influence the stability of the anode fall. If the surface of the anode is not cleaned before use (for example by sand blasting) then 'anode spots' are liable to form. Such anode spots

are associated with anode oscillations of large amplitude (chapter 3). The quietest operation has been obtained when the anode has been cleaned in dilute nitric acid.

A reliable method of preventing anode oscillations was devised by Pupp (19,13) who placed a thermionic cathode close to the anode and a subsidiary discharge was run between this cathode and the anode. The effects of this cathode were to reduce the anode fall of the main discharge to a low value (13), and to suppress the oscillations. Galehouse, et al (11) have used this method in an argon ion laser.

6.2 Stabilization of the Discharge Current

It appears that the use of an auxiliary cathode close to the anode of the main discharge is the most reliable way of suppressing anode oscillations. However it is not necessary to eliminate the oscillations in order to prevent them from modulating the laser light. If the laser discharge current is stabilized so that the oscillations do not modulate the discharge current then the laser light is not modulated (section 2.3). The stabilization is readily achieved by including an inductor in series with the laser tube so that the impedance of the discharge circuit is large at the frequency of the oscillations (section 2.2).

The value of the inductor necessary to reduce the modulation of the laser power below a predetermined fraction F of the average power is readily estimated. It is assumed that the impedance of the gas discharge and the output impedance of the power supply are much less than the impedance of the inductor at the frequency of the oscillations (f). The relation between the modulation of the discharge current and the modulation of the laser power is discussed in appendix A2. If the laser is operating sufficiently far above threshold so that the laser power does not drop to zero during part of the cycle of the oscillations, then $\Delta P/P$ is given by $C(I)\ \Delta I/I$ where I is the discharge current, ΔI is the amplitude of the current modulation, P and ΔP are

the average output power and the amplitude of the modulation of the output power, and C(I) is defined in appendix A2.

The required condition is

$$\frac{\Delta P}{P} < F , \tag{31}$$

which may be written

$$\frac{\Delta I}{I} < \frac{F}{C(I)} . \tag{32}$$

If the amplitude of the oscillations in the anode fall is ΔV then ΔI is given by

$$\Delta I = \Delta V/(2\pi f L) , \tag{33}$$

where L is the inductance of the choke.

Hence the minimum inductance for the required stability is given by

$$L_{min} = \frac{\Delta V}{2\pi f} \frac{C(I)}{IF} . \tag{34}$$

Typical values of the parameters are $\Delta V = 12$ V (peak to peak), $f = 20$ KHz, $I = 40$ A and $C(I) = 2$. If it is desired to reduce the peak-to-peak power modulation to less than 1% then the minimum value of the inductor is 4.8 mH. In commercial argon ion lasers it is usual to use an electronically stabilized power supply. A simplified diagram of such a supply is shown in fig. 6.1. The discharge current is regulated by a bank of transistors connected in parallel in a common collector circuit. The output impedance of such a power supply is determined by the value of the emitter resistances R_e and the gain of the transistors. With suitable transistors the output impedance will remain large up to high frequencies so that the anode oscillations will not modulate the discharge current.

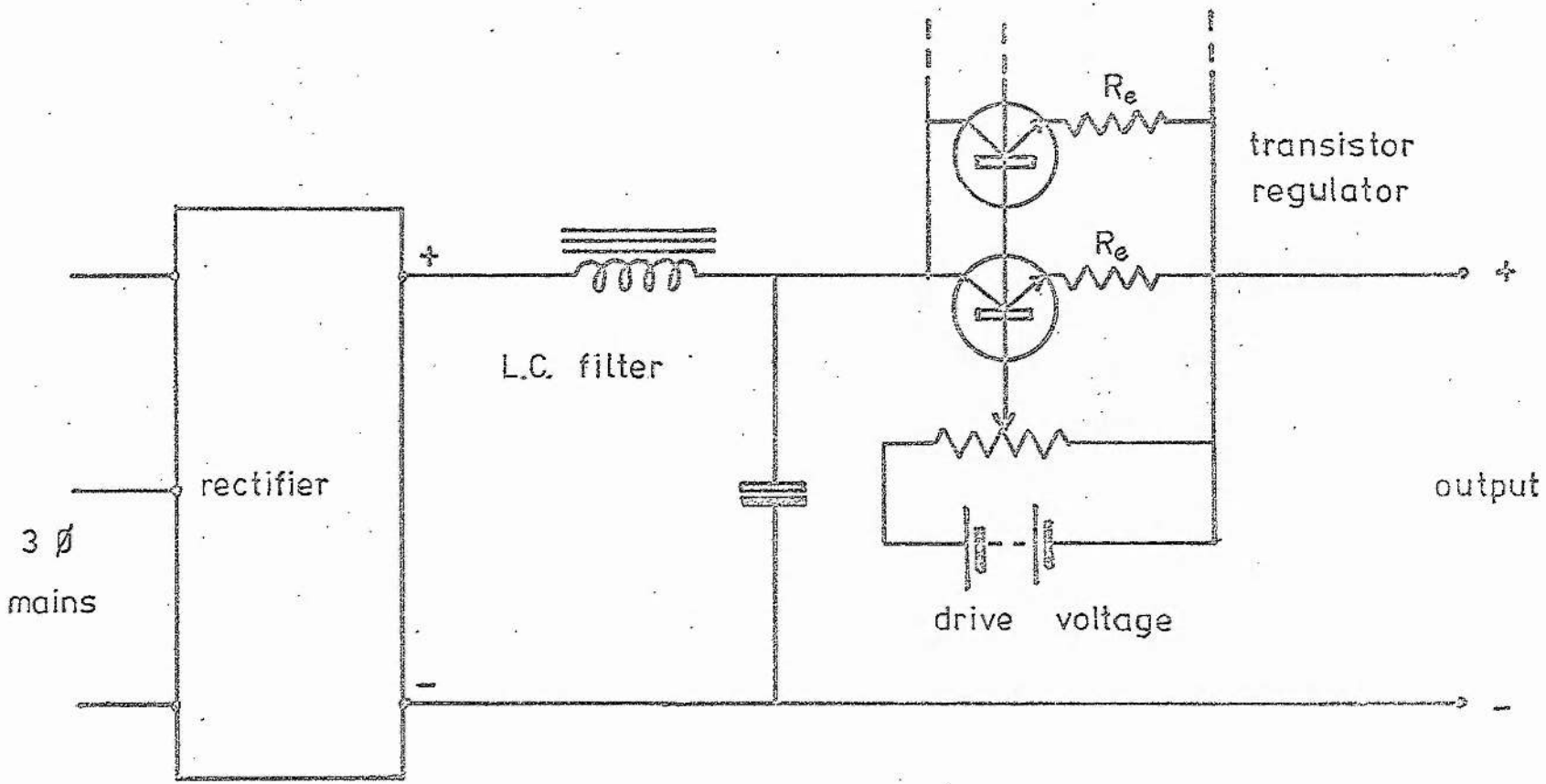

fig 6.1 Simplified diagram of electronically stabilized power supply

6.3 Conclusions

It has been demonstrated that anode oscillations are frequently a feature of the argon laser discharge. Langmuir probe measurements and studies of the light emitted from the anode region of the discharge show that oscillations are produced in the anode zone, and these observations can be understood in terms of Pupp's phenomenological theory of anode oscillations (13). The simple model of the anode fall discussed in chapter 5 enables the stability of the anode fall to be examined and this model predicts that the anode fall will be unstable for all values of the discharge parameters appropriate to an argon laser, and so agrees with experimental findings.

The inherent instability of the anode fall need not be a source of excess noise in the laser output as it has been demonstrated that the oscillations in the anode fall only modulate the light if they are allowed to modulate the discharge current. If the discharge current is stabilized then the anode oscillations have no effect on the output of the laser.

APPENDIX A1

THE PLASMA JET LASER WITH A SEGMENTED METAL TUBE

A1.1 The Laser Tube

All the experiments discussed involve an argon ion laser with a segmented metal tube and a plasma jet cathode. The design of the laser is unconventional in that all the sections of the plasma tube are metal. This provides a robust structure that is fully demountable, a feature that proved very useful when studying the anode oscillations.

A plasma jet cathode for an argon laser has been described by Maitland (22). A simplified diagram of the cathode region of the laser is shown in fig. A1.1. Argon enters the cathode discharge chamber through a nozzle and flows through a small orifice in the plasma jet anode from the cathode discharge chamber into the plume expansion chamber. The pressure in the plume expansion chamber is maintained at a value appropriate to the laser discharge (usually between 0.2 and 1 torr). The pressure in the cathode discharge chamber is between 30 and 100 torr. A direct current arc of about 80 amps between the tungsten rod and the plasma jet anode heats the tungsten rod to incandescence and provides a copious source of electrons. The ionized gas emerges from the orifice as a luminous plume reminiscent of a flame. The main discharge is established between this plume of ionized gas and the laser anode.

The laser tube consists of aluminium segments insulated from one another and vacuum sealed with neoprene 'O' rings (fig. A1.2). The segments are cooled by water flowing through a series of holes around the central bore. The tube must be segmented and the segments insulated from one another to ensure that the discharge runs through the capillary and does not form arcs at the ends of the tube. During the course of the investigation tubes of different bore and segment length have been used. The bores range from 3 mm to 6 mm diameter. For tubes of bore 4,5 and 6 mm a segment length of 75 mm

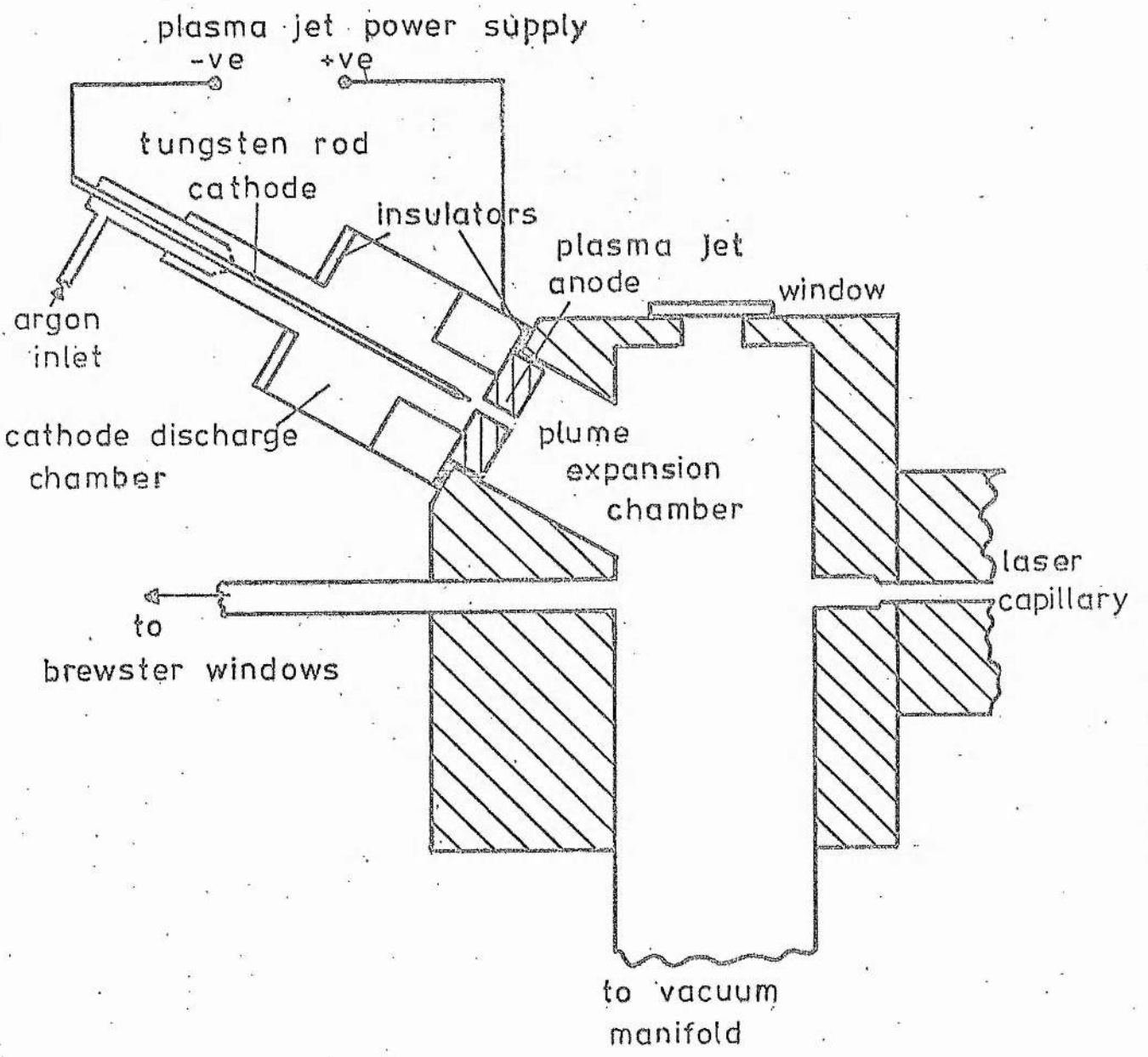

fig A1.1 Plasma Jet Cathode Assembly

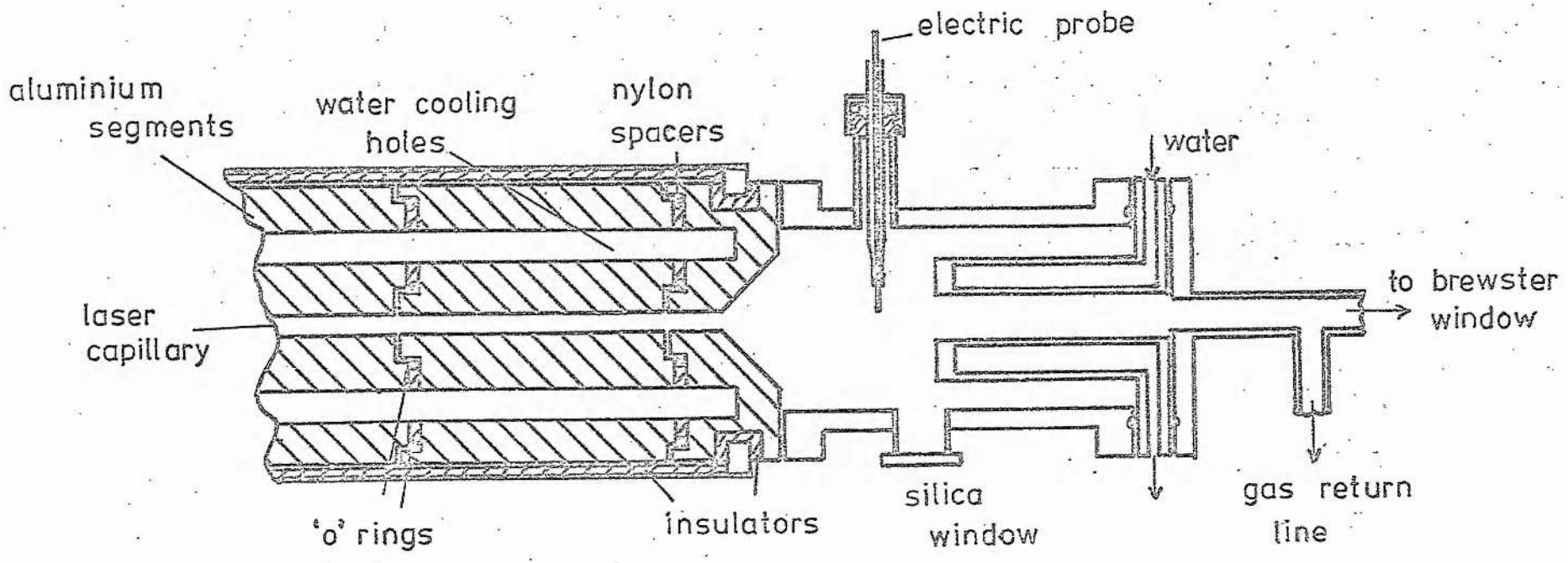

fig A1.2 The Segmented Laser Tube and Anode Assembly

was used. For the 3 mm bore tube the segment length was reduced to 15 mm.

The smaller the bore the shorter the maximum usable segment length that can be used. Of the tubes that have been used, the 4 mm tube had segments which were rather too long at 75 mm. The consequence of this is that the range over which the operating parameters can be varied is reduced and arcing between segments occurs when the range is exceeded. The inter-segment arcs burnt the 'O' rings and let water into the tube, extinguishing the discharge.

The anode region of the discharge was bounded by a water cooled copper cylinder. The anode itself was constructed from two concentric copper cylinders with water flowing between them fig. A1.2 The cylinders were concentric with the laser axis. Two anodes of different diameter have been used: 75 mm x 28 mm od x 13 mm id and 75 mm x 16 mm od x 6 mm id. Although both anodes have a length of 75 mm, the discharge never spreads back more than 20 mm from the end of the anode nearest the capillary.

A gas return path is provided between the anode and the plume expansion chamber. This is necessary to prevent gas pumping increasing the pressure at the anode end of the tube. The 3 mm tube has local gas return paths produced by drilling two 2 mm holes through each segment parallel to the axis and just inside the inner 'O' ring. The holes in successive segments are offset so that the gas return path forms a labyrinth and the discharge does not run through the return path. The gas pressure is measured at the anode end of the tube with a McLeod gauge isolated from the system by a liquid nitrogen cold trap.

A fused silica window in the wall of the tube enables light from the discharge near the anode to be observed. The effective diameter of this window is only about 12 mm, limiting the region from which light can be collected.

Figure A1.2 shows the location of the Langmuir probe used to study the anode plasma.

The laser tube is surrounded by a solenoid to provide an axial magnetic field. The solenoid is a single layer of water cooled copper tubing wound on a former at 1 turn per cm. The solenoid operates at currents of up to about 500 Amps. The magnetic field thus reaches a value of about 600 gauss in the central region but declines to about half this value at the ends of the solenoid. The fringing fields are still sufficiently strong near the anode for the magnetic field to alter the frequency and amplitude of the anode oscillations.

A1.2 Power Supplies

The voltage across an argon ion laser changes only slowly as the current is varied between quite wide limits (see appendix A2 fig. A2.1). It will be shown in appendix 2 that the power supply must have a high output impedance if a stable discharge current is to be maintained with such a load. This may be achieved either by including a large ballast resistor in series with the power supply, which is very wasteful of power, or by some system of electronic current stabilization. The requirements are further complicated by the need to supply the full range of current over a wide range of discharge voltages, since the voltage across the discharge tube varies with pressure and magnetic field.

The power supply used in this investigation was a Newport Instruments motor generator magnet power supply type C4b. This unit supplies currents of up to 90 amps at a voltage of up to 250 V. The current is stabilized to 1 part in 10^4 when connected to a resistive or inductive load. The stability may be somewhat poorer with a gas discharge load.

The most serious limitation of the C4b is that its maximum load voltage (250 V) is rather low. The range of available operating voltages has been extended by using a subsidiary unstabilized power supply in series with the generator. The circuit of the power supply

used for the 3 mm tube is shown in fig. A1.3. The subsidiary supply is a 3 phase half wave rectifier whose voltage is controlled by a 3 phase auto-transformer. The subsidiary supply has a rather inadequate LC filter for smoothing. The ripple current is however greatly reduced by the motor generator.

The diode D1 protects the power supply when a large voltage (about 1.5 KV) is applied across the tube to initiate the discharge. The high voltage is obtained from a separate starter supply (not shown) capable of supplying 2 KV at 1 amp. The 50 ohm resistor in parallel with the generator and the 3 ohm series resistor ensure smooth starting. Once the discharge is drawing a few amps from the motor generator S1 may be closed and the 3 ohm resistor shorted out.

The diode D2 and the capacitor C suppress voltage spikes that occur if the discharge current is interupted. The diode charges C to the operating voltage and then effectively isolates C from the generator. If the discharge current is broken the inductance of the generator windings produces a positive voltage spike which forward biases D2 and the energy is absorbed by C without the voltage reaching an excessive value. The diode D2 is necessary as the feedback network of the generator may become unstable with a capacative load.

The inductor L ensures that the supply has a high A.C. impedance so that the voltage oscillations do not modulate the current.

A1.3 The Initiation of the Discharge in a Metal Laser Tube

The initiation of a discharge in a conducting wall tube may present some difficulty. In the absence of a conducting gas in the tube with its associated 'wall sheaths' an electric field can penetrate only a short distance into the capillary. The electric field falls to about 1 - 10% of its value between the segments at a distance d into the segment, where d is the diameter of the capillary (45). Applying a high voltage across the tube to initiate the discharge may therefore establish a series of arcs between the segments rather than a discharge through the capillary.

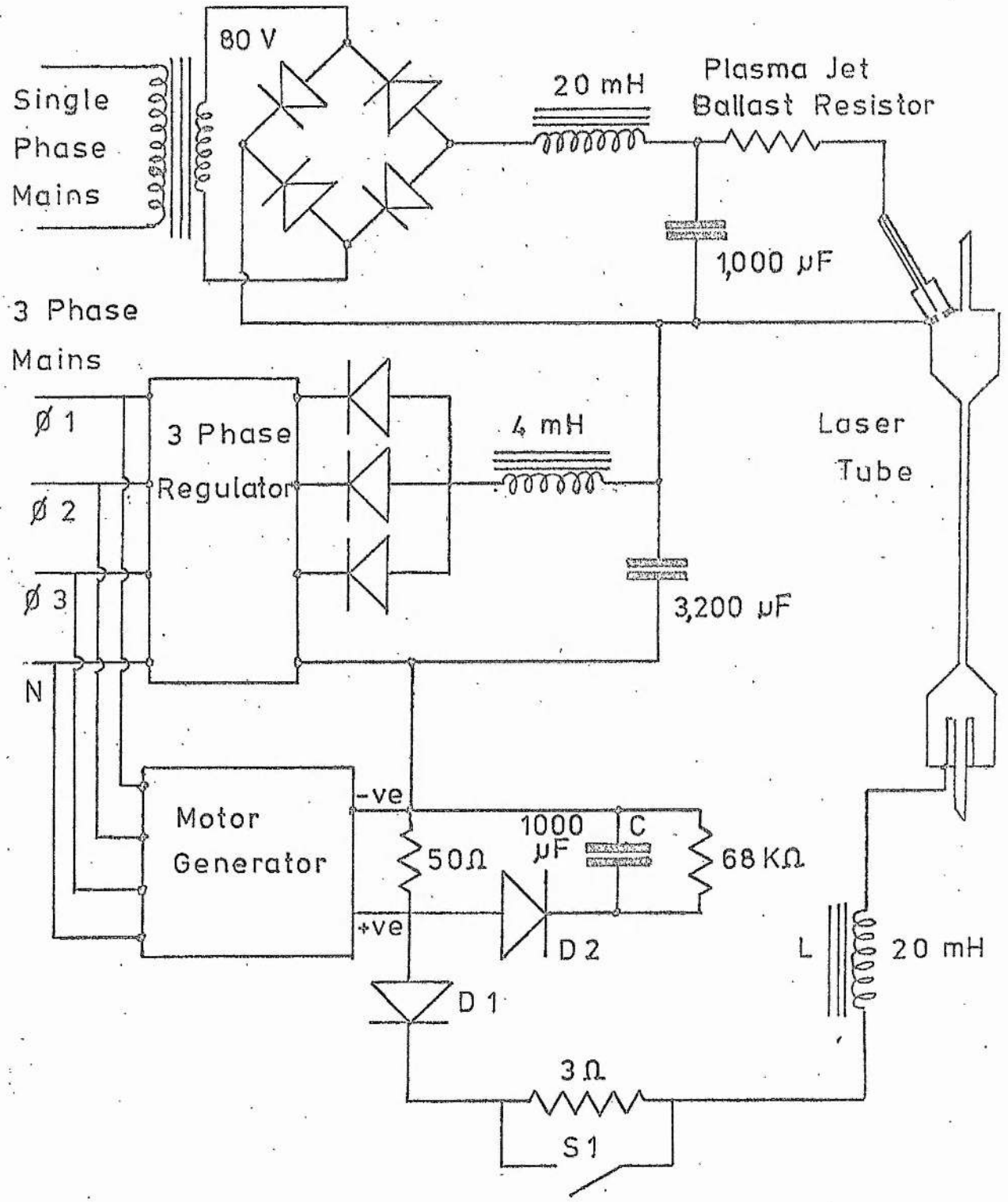

fig A 1.3 Laser Power Supply

It has been found that a discharge may be established in a segmented laser by applying a high voltage across the tube, provided certain precautions are taken. The high voltage is provided by a continuously variable starter supply with its current limited to one amp by a large value ballast resistor.

The laser discharge is initiated at a pressure of about 2 to 3 torr. The voltage is increased slowly until the discharge 'strikes' and the voltage across the tube falls to about 200 V. If the tube has not been used before, or has been exposed to the air for some time then the voltage is increased very slowly in steps allowing time for the current to stabilize after each step, before increasing the voltage further. The current at this stage is of the order of tens of milliamps. When the current reaches about 100 mA the discharge starts to go over to the low voltage mode. The current increases to about 1 amp when the voltage falls but the high current discharge is rapidly extinguished as gas and vapours are released from the walls. After a minute or so when the vapours have been pumped away the discharge strikes again. This continues until the tube is clean and a stable low voltage discharge is established. Attempts to rush this procedure usually result in intersegment arcs which destroy the 'O' rings.

A tube which is in regular use can be started by applying the high voltage immediately and a stable high current discharge is formed. Exposure of the tube to the air for short periods (say 10 mins.) does not contaminate the tube significantly and restarting the discharge presents no difficulty.

A1.4 The Performance of the Segmented Metal Tube Laser

The four different laser tubes used in this investigation all behaved in an essentially similar manner. The performance of two of them will be described as they represent two different approaches to argon laser design. The first is the 6 mm bore tube. This is

a large capillary size and seems to be suitable for generating high powers with good electrical efficiency. The second tube to be described is the 3 mm bore laser which is more representative of present practice in argon laser design. The small bore laser operated at high current density provides moderate powers at somewhat lower efficiency than the large bore system but has the advantage that a greater fraction of the maximum power is available in the TEM_{oo} mode. The small bore laser is also capable of generating U.V. radiation from the Ar III spectrum without excessively high discharge currents.

The 6 mm laser had an active length of 650 mm and could be operated at currents of up to 90 amps. The output power of the laser is shown in fig. A1.4 as a function of current. The power is in 5 lines, predominantly the 4880 Å and 5145 Å lines. Two 6 m radius mirrors spaced 1.8 m apart with a 5% output coupling formed the cavity. No attempt was made to optimise the mirror radius or output coupling. The power is divided between many transverse and longitudinal modes.

The maximum power that has been obtained from this laser is 14 W at a current of 85 amps, a pressure of 0.38 torr and a magnetic field of 500 gauss. The efficiency of a laser is usually defined as the ratio of the output power to the power dissipated in the discharge tube, ignoring the power dissipated in the solenoid etc. Using this definition the efficiency of the 6 mm bore laser was 0.075% in the above case, and the power per unit volume of active medium was 0.8 W/cc.

The output power of the 3 mm laser is shown as a function of current in fig. A1.5. The power is again the all lines multi-mode power. The cavity was formed by a 2 m radius maximum reflectivity mirror and a 6 m 5% transmission mirror spaced at 1.2 m. In this case there are signs that the power is beginning to saturate at a current of around 50 amps, although it is possible that

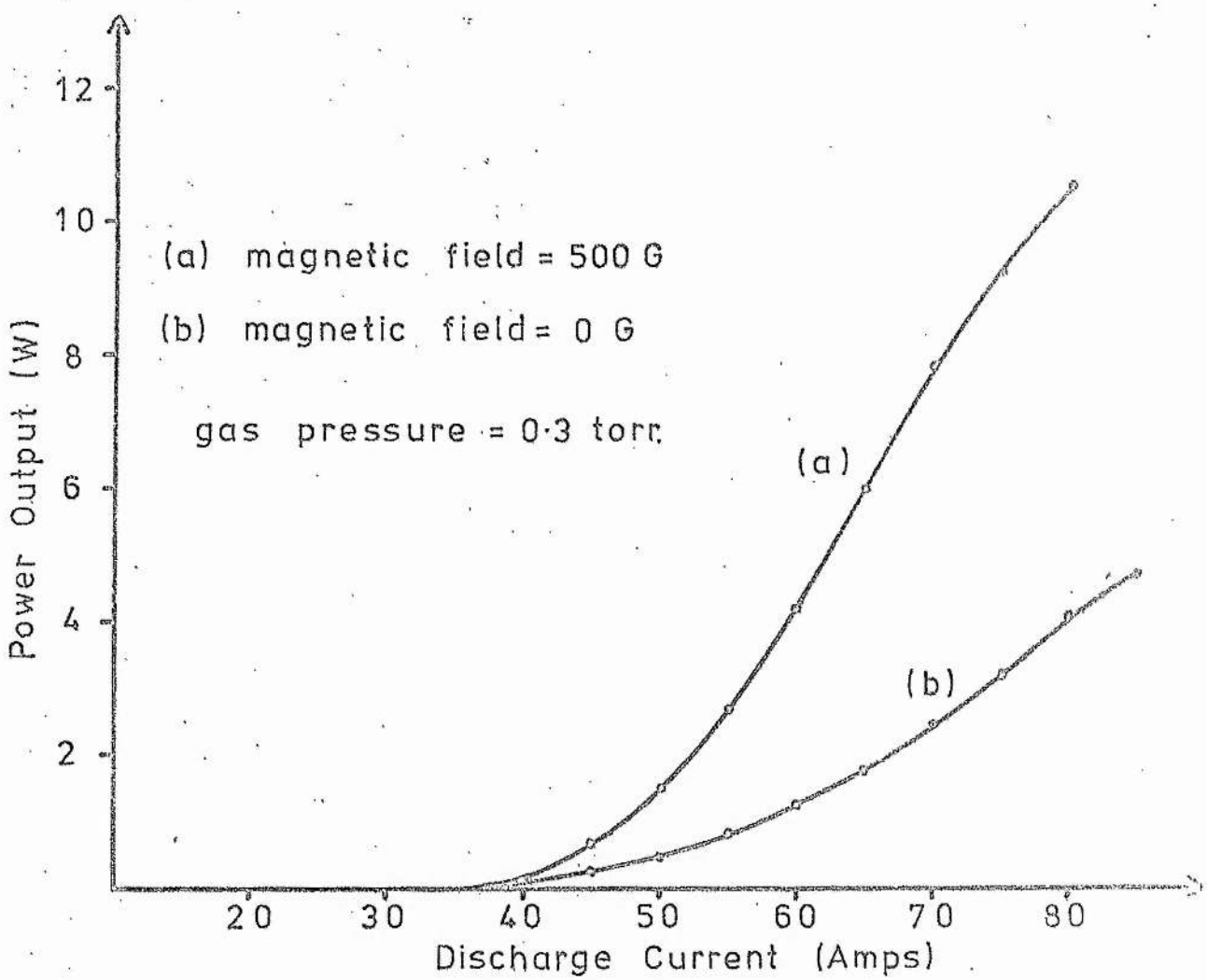

fig A1.4 Output Power of 6 m.m. Laser

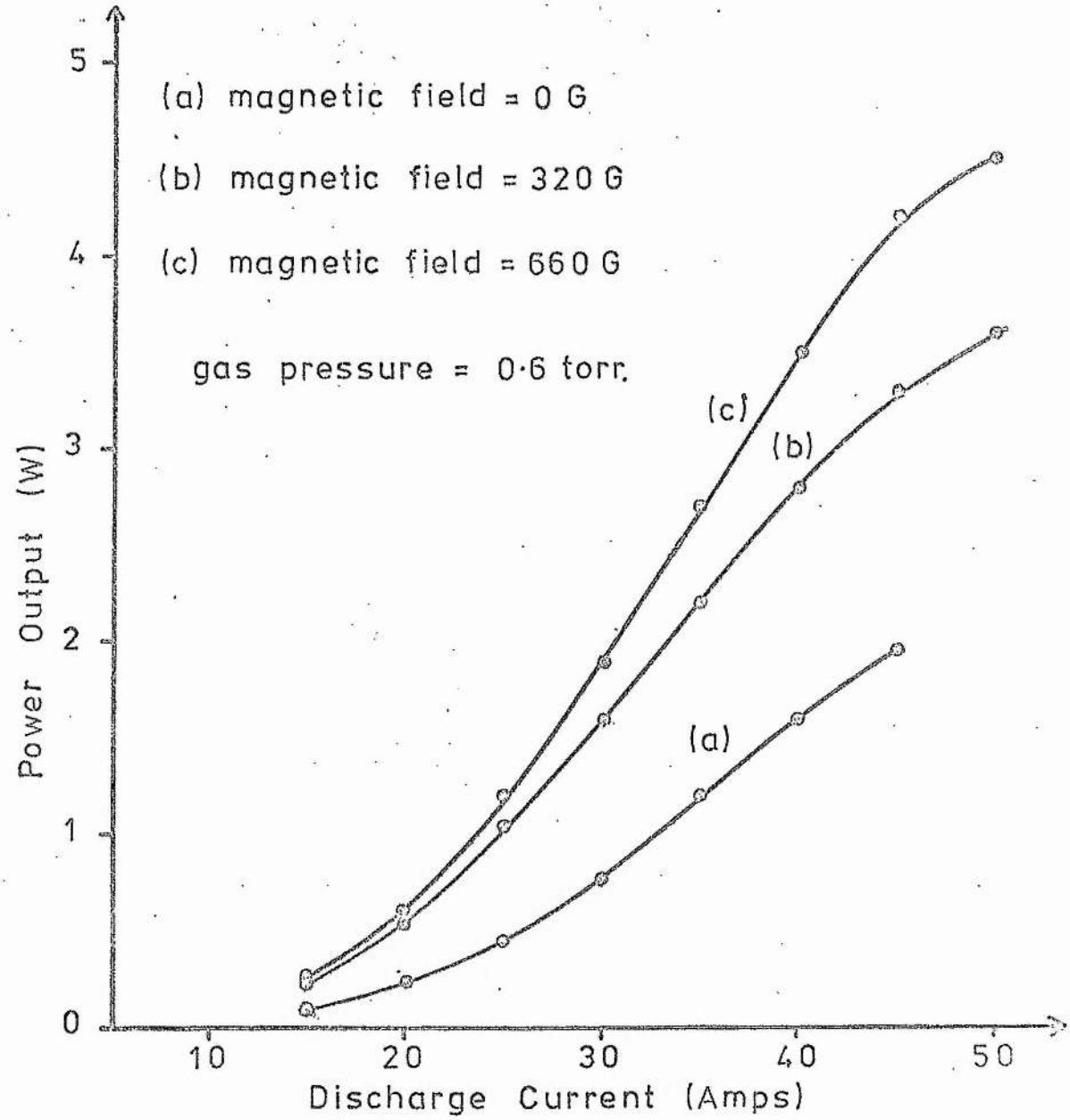

fig A1.5 Output Power of 3m.m. Laser

this may be due to window effects to be discussed below. The maximum efficiency obtained from this laser was 0.035% which occurred not at the highest current but at 45 A. Above this current the voltage across the discharge tube rises steeply whereas the power increases less rapidly and the efficiency is reduced. It is of interest to note that the threshold for U.V. generation is about 45 amps just where the characteristics of the discharge start to change. The power per unit volume of active medium was about 1.8 W/cc.

Herziger and Seelig (38) have predicted that large bore systems should be more suitable for the generation of high power from an argon laser. This seems to be borne out by these findings. The efficiency of the large bore laser is substantially better than that of the small bore system. The greater power per unit volume obtained from the small bore laser is probably due, at least in part, to its higher operating pressure.

A1.5 Power Limitation by Brewster Angle Windows

The powers shown in figs. A1.4 and A1.5 were obtained when the brewster angle windows had just been cleaned. After about 3 hours running at high currents a deposit on the anode end window starts to absorb a significant amount of power. When this happens the inside surface of the window heats up and distorts misaligning the cavity. This causes large fluctuations in the power and eventually the power stabilizes at about 2 W. This effect has been discussed by De Mars et al (39).

The nature of the deposit is not clear, but is probably metallic. It may be due to spluttering from the capillary walls or possibly tungsten from the cathode. The material, whatever its origin, is swept past the anode and deposited on the window. The window at the cathode end is effected much less. Various methods have been tried to prevent the material being deposited on the window. Transverse magnetic fields and subsidiary discharges both transverse and

along the axis of the laser between the window and the anode were ineffective. Some improvement has been obtained by flowing fresh gas into the tube near the window and removing it through the gas return path near the anode. The flow of gas away from the window towards the anode will tend to sweep the unwanted atoms or ions away from the window. This accumulation of an absorbing deposit on the window near the anode is not peculiar to the metal tube plasma jet laser but has been observed in quartz systems also (39). It is probably the most serious problem with high power argon lasers. Sealed systems with beryllia tubes seem capable of quite long life (1000 hrs.) at power levels of around 2 W. However it remains to be seen if continuous power levels of around 10 W can be achieved with long life. The advantage of the plasma jet laser is that when a deposit accumulates on the windows they may readily be removed for cleaning.

APPENDIX A2

THE STABILITY OF THE CURRENT IN AN ARC OR GAS DISCHARGE

Arcs and gas discharges do not have a linear relation between the current and the voltage. A voltage current characteristic of the main laser discharge is shown in fig. A2.1 and a characteristic of the plasma jet in fig. A2.2. The laser discharge shows a positive slope resistance ($r = dV/dI$) while the plasma jet shows a negative slope resistance.

The usual method of controlling the current in an arc or gas discharge is to include a large ballast resistor in series with the discharge. A series resistor is wasteful of power so for the high current discharges associated with argon lasers it is preferable to use some form of electronic current control in the power supply to provide an effective high impedance source for the discharge current. From the point of view of the current stability the large output impedance is equivalent to the series ballast resistor.

A2.1 The Load Line

If the arc or discharge power supply is a constant voltage source with a series ballast resistor then the operating current may be found from the characteristic by means of the load line. If E is the source voltage and R is the resistance of the ballast resistor the load line has the equation

$$V = E - IR$$

The point at which the load line cuts the discharge characteristic gives the operating current and voltage.

The procedure is illustrated in fig. A2.1. With $E = 270$ V, $R = 1$ ohm (line AB), the operating point is B at $I = 53$ A. If E is reduced by 1 percent to 267 V the load line becomes CD and the operating current is reduced to 51 A. The current has changed by 4% for a 1% change in source voltage.

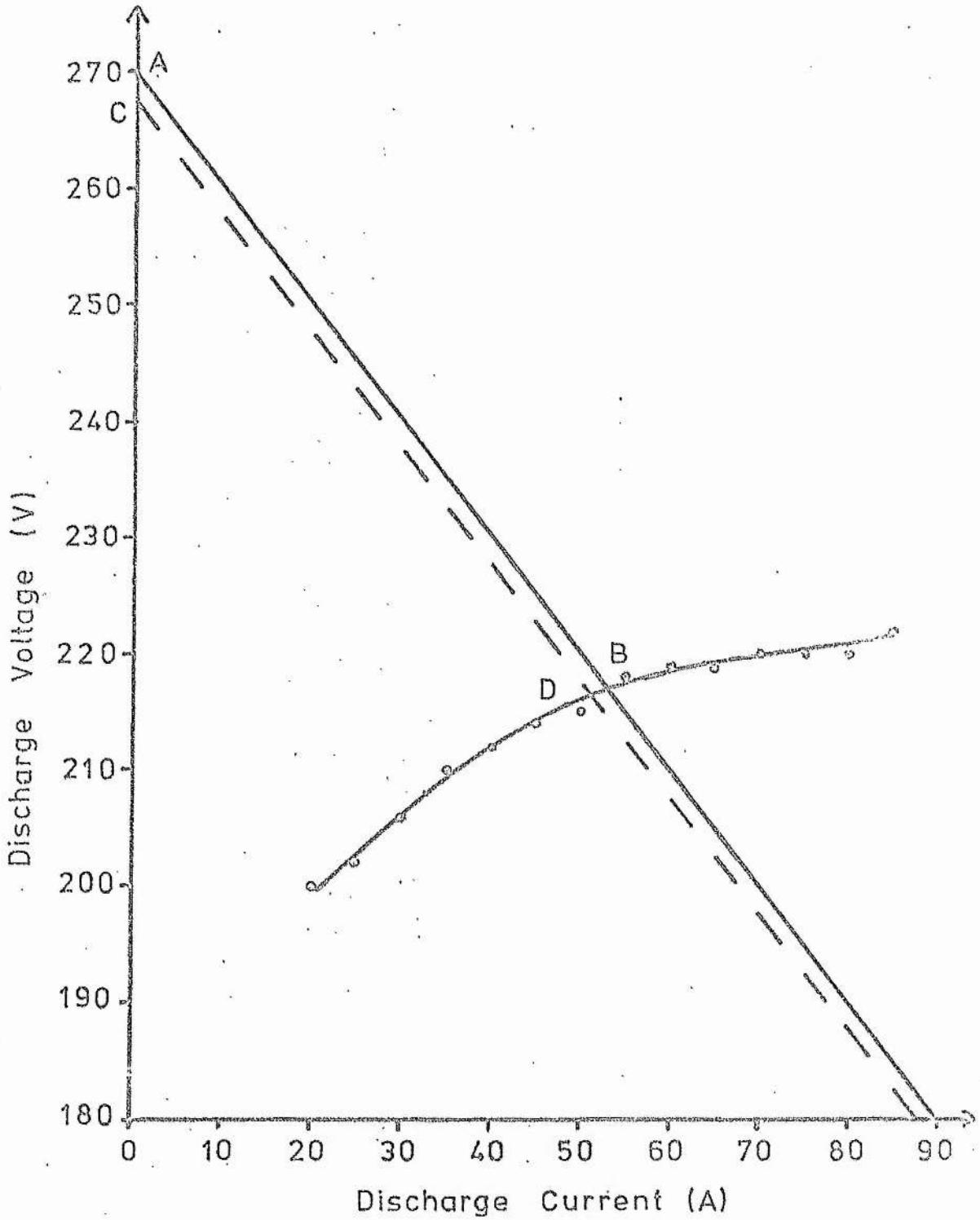

fig. A 2.1 Discharge Voltage-Current Characteristic of the 6 mm Laser Tube

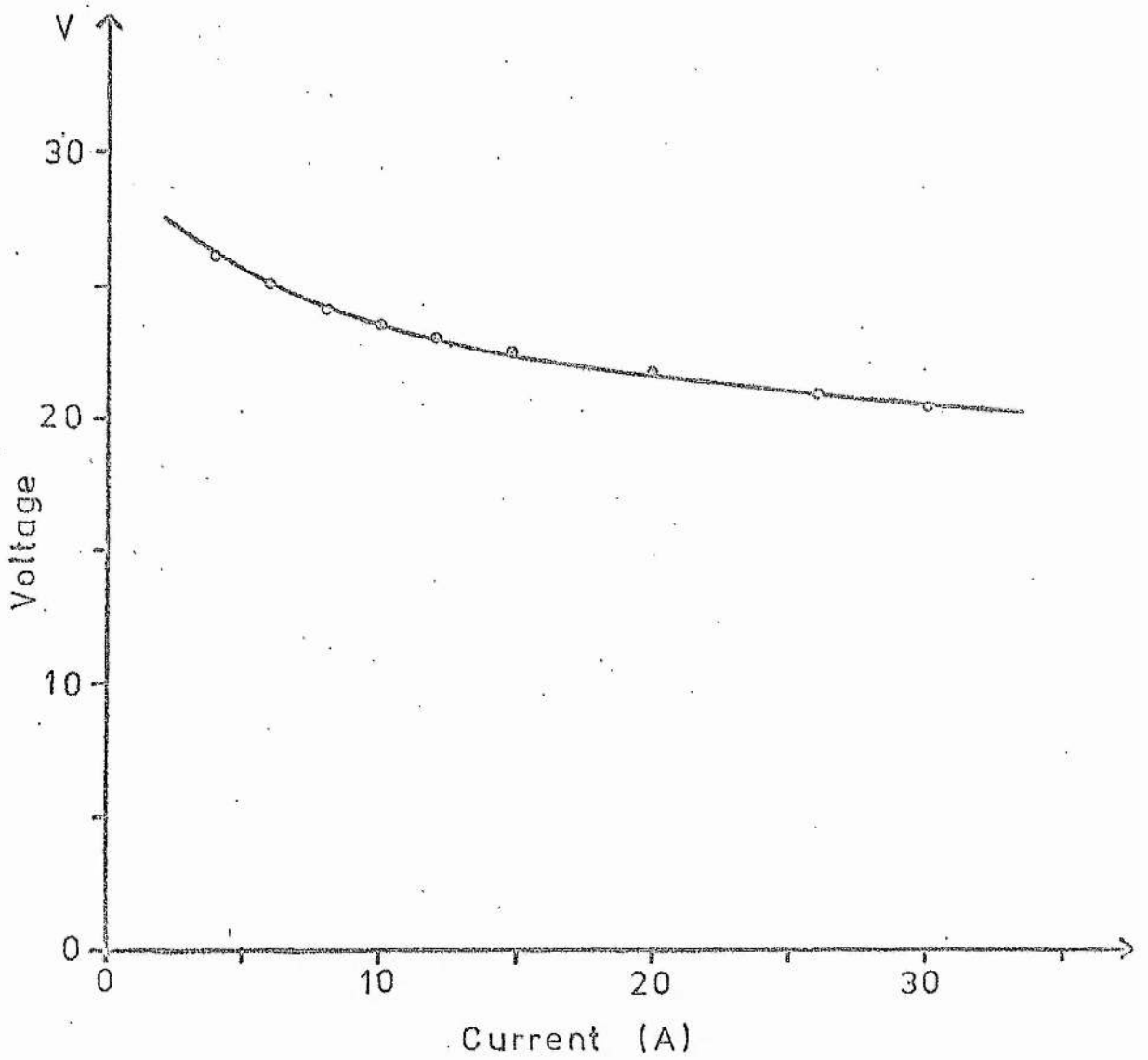

fig A 2.2 Voltage - Current Characteristic of the Plasma Jet

This illustrates the difficulty in maintaining a stable discharge current and hence stable output power from the laser. Increasing the value of the ballast resistor improves the stability of the current but is wasteful of power.

A2.2 The Stability of the Current

The current fluctuations that occur as a result of fluctuations in discharge voltage or supply voltage may readily be calculated for the simple case of the discharge stabilized with a ballast resistor. The relation between E,R, the discharge current I and the voltage V_d is

$$(E-V_d) = IR \qquad (A1)$$

If E and V_d have small time varying components they may be written

$$\begin{aligned} E &= E_o + e(t) && (a) \\ V_d &= V_o + v(t) + Ir && (b) \end{aligned} \qquad (A2)$$

where r is the slope resistance given by the characteristic at I_o and both E_o and V_o are constants. Substituting (A2a) and (A2b) into (A1) and separating the constant and time dependent parts gives

$$I_o = \frac{E_o - V_o}{R+r} \qquad (A3)$$

$$i(t) = \frac{e(t) - v(t)}{R+r} \qquad (A4)$$

where the current is given by $I = I_o + i(t)$.

If e(t) and v(t) are independent, then we have

$$\langle i^2(t)\rangle = \frac{\langle e^2(t)\rangle + \langle v^2(t)\rangle}{(R+r)^2} \qquad (A5)$$

where $\langle\ \rangle$ denotes an average over time.

Equation (A5) shows that for good current stability R+r must be as large as possible. If r is negative R+r may tend to zero in which case $\langle i^2(t)\rangle$ will tend to infinity and a stable discharge will be impossible. If R+r is negative this analysis fails. This can be

seen by taking $v(t) \equiv 0$, then if $e(t) > 0$, $i(t) < 0$ (equation (A4)). This is not consistent with equation (1). A stable discharge is not possible in this case and an analysis of the transient behaviour requires consideration of the inductance and capacitance of the circuit and the transient behaviour of the discharge.

A2.3 The Relation between Fluctuations in Discharge Current and Fluctuations in Laser Power

If the fractional change in the discharge current of the laser is $\Delta I/I$ then the fractional change in the output power is given by

$$\frac{\Delta P}{P} = \frac{d(\ln P)}{d(\ln I)} \frac{\Delta I}{I} = C(I) \frac{\Delta I}{I} ,$$

where ΔP and ΔI are assumed to be small. The value of $C(I)$ may be found from the gradient of a graph of log P against log I. Typical plots of log P against log I for an argon laser are shown in fig.A2.3. For the 3 mm laser $C(I)$ varies from 4.5 at 20 amps to 2 at 40 amps, and for the 6 mm laser $C(I)$ varies from 10 at 40 amps to 2 at 80 amps. The difference between the two low current values of $C(I)$ is that at a power of 100 mW the 3 mm laser is operating further above its threshold current than the 6 mm laser.

It is apparent that close to threshold a small change in discharge current may produce a large change in power output. Even well above threshold the fractional change $\Delta P/P$ in the power is of the order of twice the fractional change in discharge current ($\Delta I/I$). Taking the example considered in A2.1 a 1% change in supply voltage produces a 4% change in discharge current. This will produce a change in output power of 8% or even more depending on how close the laser is to its threshold current.

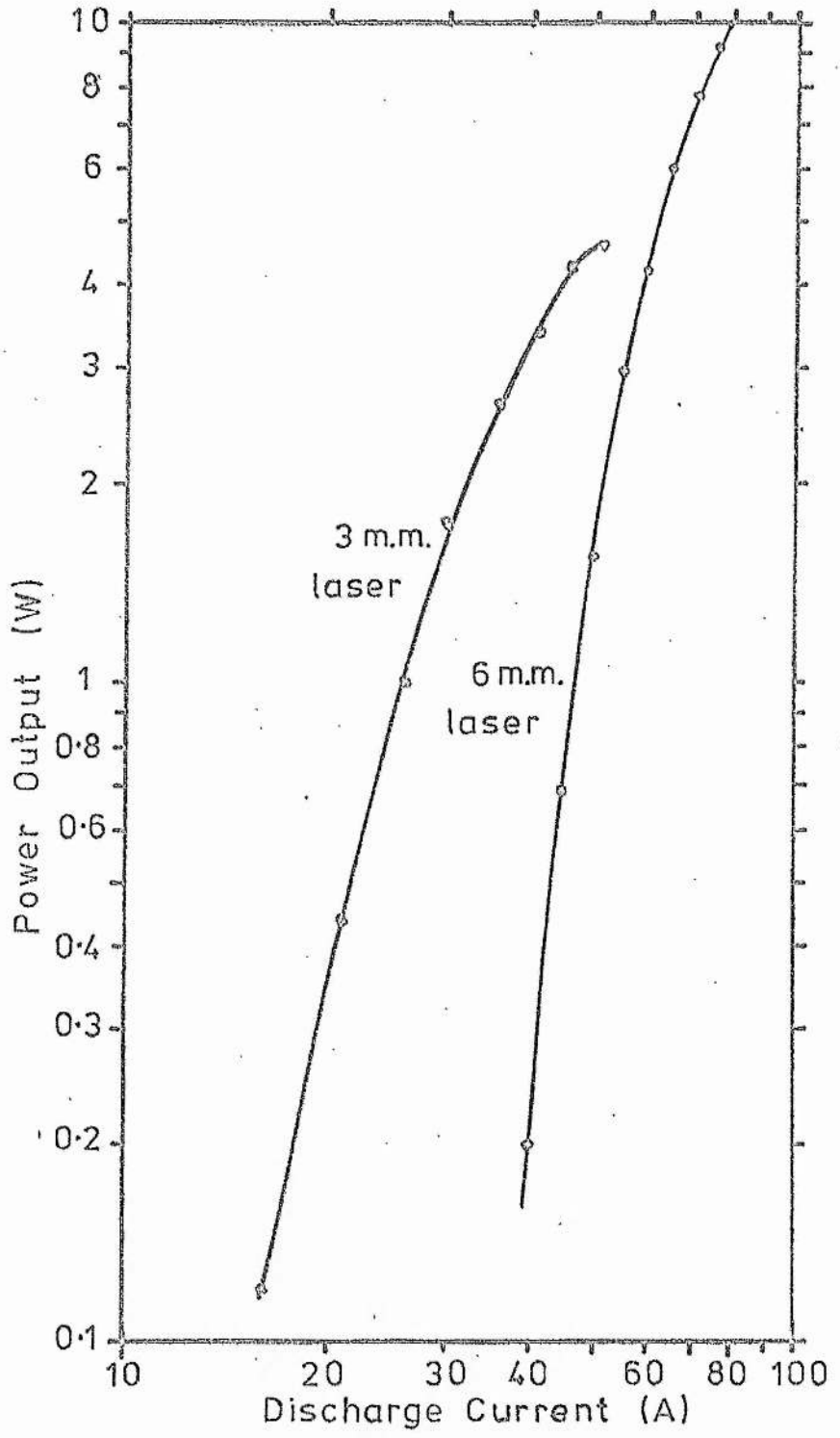

fig A 2.3 Plot of log P against log I

APPENDIX A3

PROBE MEASUREMENTS IN THE ANODE REGION

The plasma in the anode region of the laser (that region between the capillary and the anode) has been studied with a Langmuir probe to obtain information about the electron temperature, electron density and the anode fall. The probe is a length of tungsten wire 0.5 mm in diameter shielded from the plasma by a fused silica sheath except for the final 4 mm. The probe is inserted into the discharge at a distance of 10 mm from the anode with its axis perpendicular to the axis of the laser (fig. A1.2). Measurements of light intensity indicate that the probe is outside the region of high field (and space charge) near the anode. The probe was not moved into the high field region as the interpretation of probe measurements in regions of large space charge is very uncertain.

The properties of the plasma are found from the variation of probe current with voltage (the probe characteristic). The probe characteristics are recorded on an XY plotter using the circuit shown in fig. A3.1. The second electrode used in the probe circuit is not the discharge anode as is usual but the discharge cathode. This is necessary because of the large voltage oscillations between the probe and the anode. The stabilized power supply provides an adjustable offset voltage for the XY plotter. The peak anode voltage is measured with the digital voltmeter using a peak measuring circuit (D1 and C). The digital voltmeter is used to calibrate the scale of the XY recorder. In this way the potential difference between the probe and the peak anode voltage may be found. An oscilloscope photograph of the anode voltage oscillations together with the peak anode voltage gives the instantaneous anode voltage.

A typical probe characteristic is shown in fig. A3.2. For probe voltages sufficiently below the space potential the current increases only very slowly with voltage. The current drawn by the

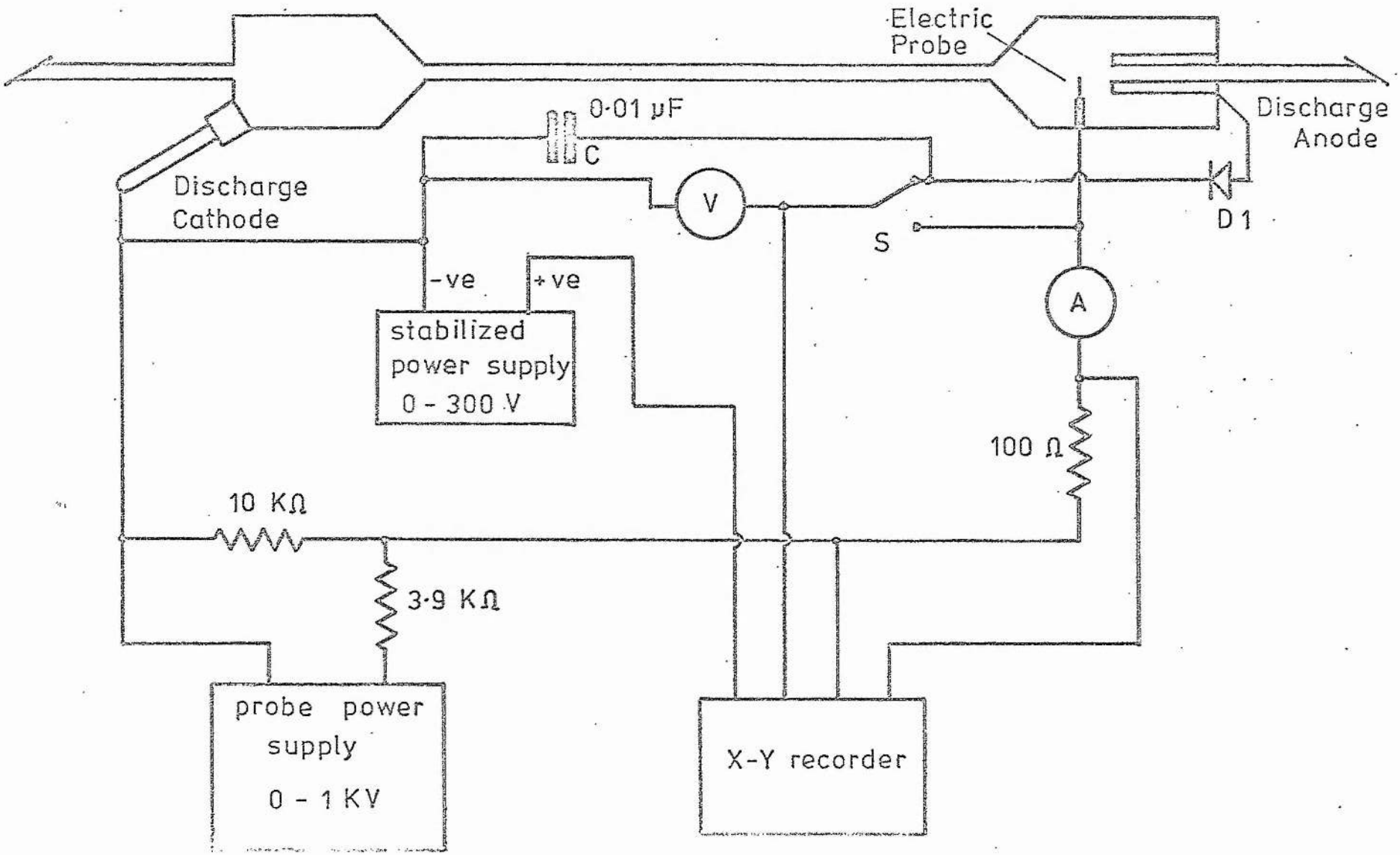

fig A 3.1 Circuit for Electric Probe Measurement

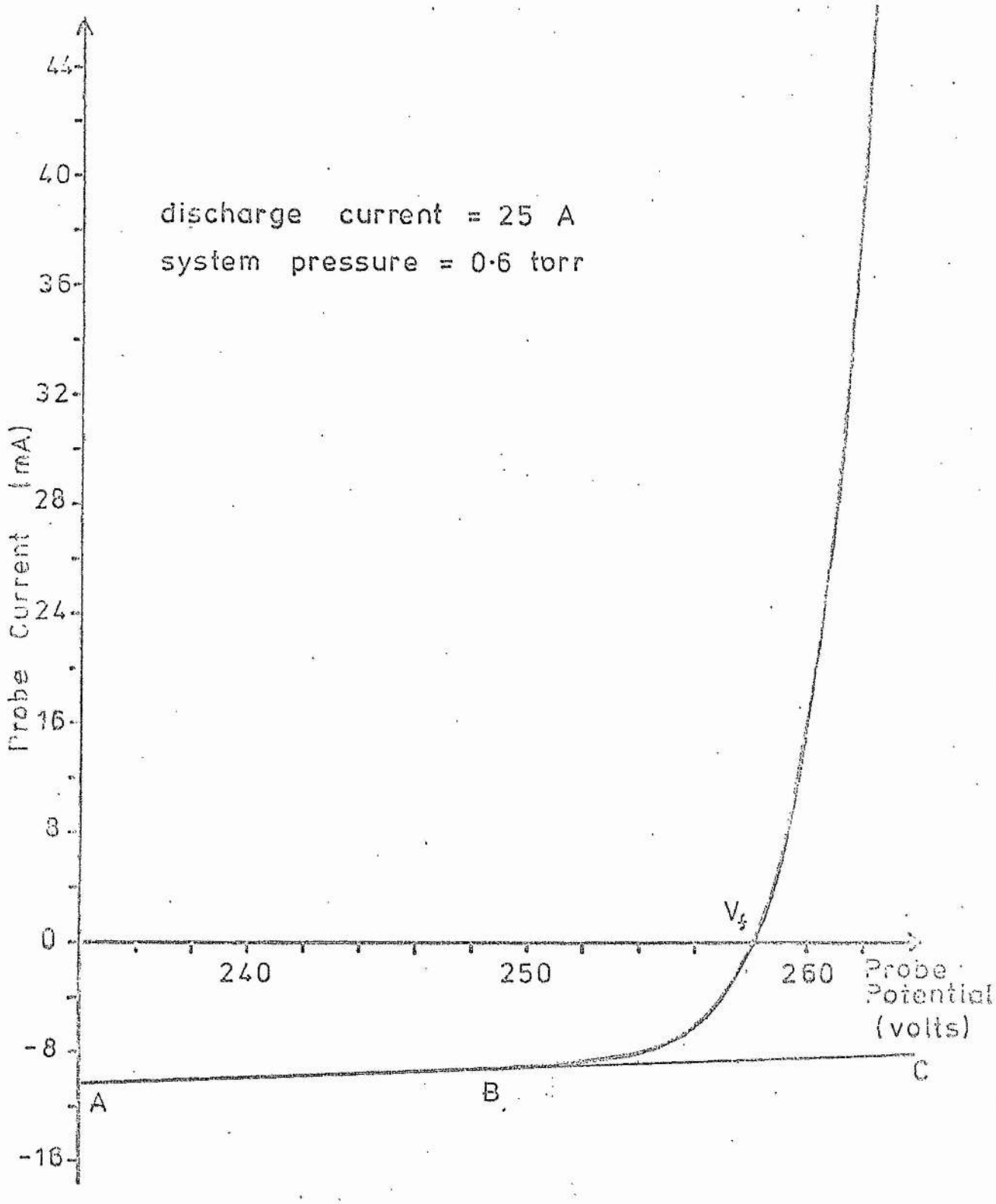

fig A3.2 Typical Probe Characteristic

probe in this region is the ion saturation current I_+. As the probe potential approaches the space potential an electron current I_e is collected by the probe and the total probe current changes sign and increases rapidly with voltage. The potential at which the current drawn by the probe is zero is the floating potential V_f.

The total probe current I_p is given by

$$I_p = I_e - I_+$$

where I_e and I_+ are the magnitudes of the electron and ion currents. The electron current is separated from the ion current by assuming that the ion current varies linearly with voltage and that the saturation ion current may be extrapolated as a straight line ABC (fig. A3.2). The electron current is the difference between the total probe current and this extrapolated ion current. Any errors introduced by this procedure will be small provided $I_e >> I_+$.

The following assumptions are made in order to interpret the probe characteristic (the validity of these assumptions will be examined below)

(1) The net space charge is zero.

(2) The electron mean free path λ_e and the ion mean free path λ_+ are much greater than the probe radius r_p.

(3) The electron temperature T_e is much greater than the positive ion temperature T_+.

(4) The probe radius r_p is much greater than the Debye length λ_D.

(5) The energy distribution of the electrons is Maxwellian.

Subject to these conditions the electron current is given by (40 p.13)

$$I_e = n_e\, e\, A_p \left(\frac{kT_e}{2\pi m_e}\right)^{\frac{1}{2}} \exp\left\{\frac{e(V-V_s)}{kT_e}\right\} \quad \text{if } V < V_s \qquad \text{(A6)}$$

where

n_e = electron density A_p = probe area

e = electronic charge V_s = space potential

m_e = mass of electron V = probe potential

The ion current is more difficult to treat theoretically. Many theories of ion collection have been proposed (see 40 chapter 6, and 41) some of which are very difficult to apply. An approximate expression for the ion current, subject to the conditions (1) to (5) is, (40, p.12 and p.115, and 41 p.150)

$$I_+ \simeq \kappa A_p n_e e \left(\frac{kT_e}{M}\right)^{\frac{1}{2}} , \qquad (A7)$$

where κ is a constant between 0.5 and 0.6 and M is the ion mass.

The constant κ varies according to the ion temperature (40 p.115). The value used here was 0.5. The derivation of (A7) is far from rigorous so great precision is not justified and only order of magnitude agreement can be expected. This simple expression for I_+ does not predict any variation of ion current with voltage, there is therefore some ambiguity in deciding at what potential (A7) may be considered to apply. For convenience it was decided to apply (A7) at the floating potential V_f.

The electron temperature is found from the probe characteristic by plotting the logarithm of the electron current I_e found as described above against the probe voltage. This usually gives a good straight line indicating that the electron energy distribution is Maxwellian (fig A3.3). The gradient of the line is proportional to T_e^{-1}. When the electron temperature has been found, the electron density may be calculated from the ion saturation current using (A7).

It is usual to determine the space potential by increasing the probe current until the electron current saturates; the potential at which this occurs is the space potential. This method could not be used as a current of over 1 A could be drawn from the probe without any sign of saturation. Currents as large as this will tend to

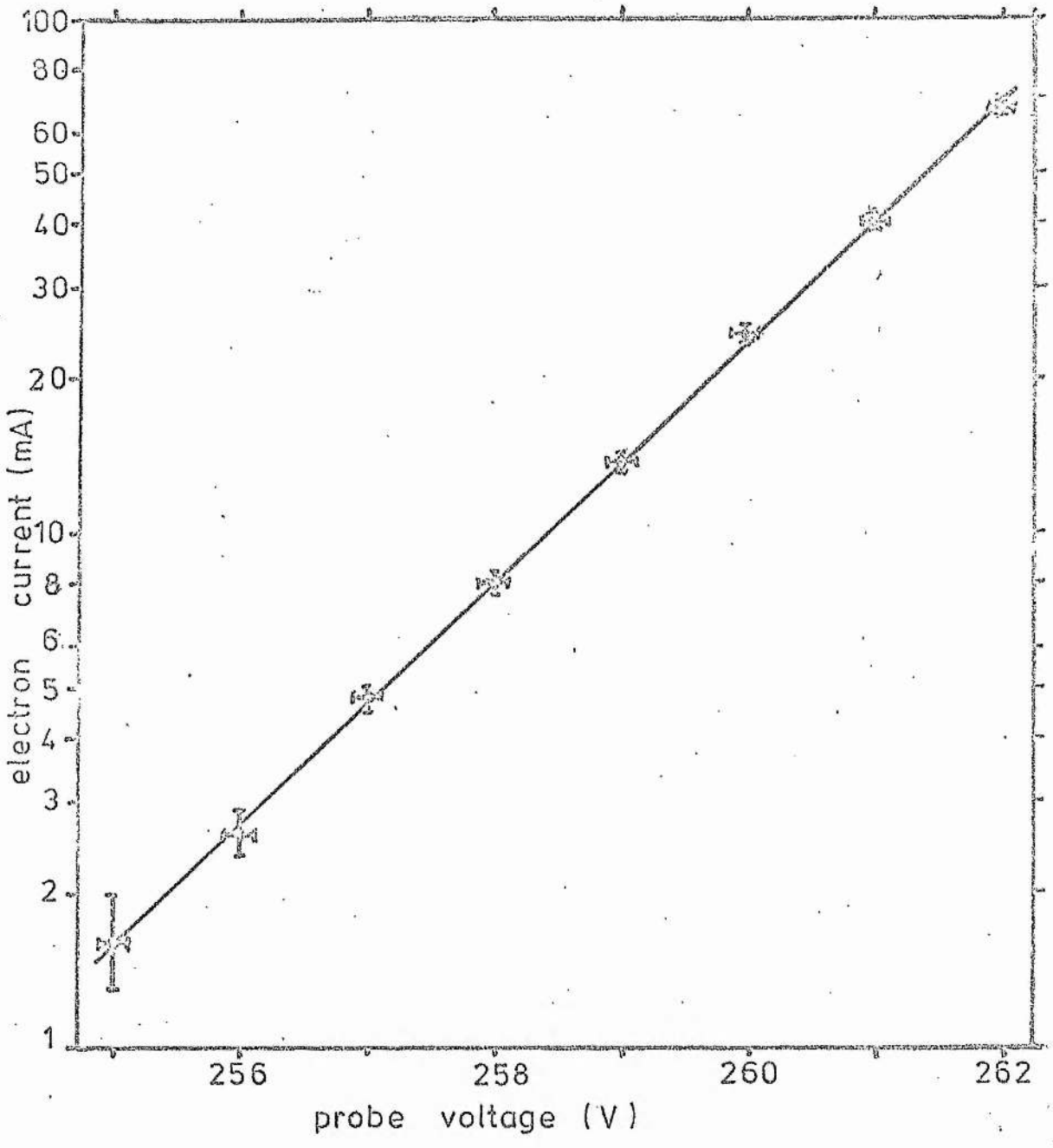

fig A 3.3 Semi-log Plot of Probe-Electron Current against Probe Voltage from the Probe Characteristic shown in fig. A 3.2

overheat the probe and probably seriously perturb the sheath around the probe by thermionic emission. The space potential was found, therefore, using (A6) and (A7) and the floating potential V_f. At V_f, I_e is equal to I_+ so that equating I_e and I_+ eventually gives

$$V_s = V_f + \frac{kT_e}{2e} \ln \left(\frac{M}{\kappa^2 \pi m_e}\right) \qquad (A8)$$

Experimentally T_e is found to lie within the range 17,000 - 24,000 K and n_e is of the order 1-2 x 10^{13} cm^{-3} for a laser current of between 20 and 40 A and a pressure of the order of 0.5 torr. The gas temperature has been found to be about 1800 K by measuring the Doppler broadening of the spectral lines (chapter 4.4). The validity of assumptions (1) - (5) may now be examined.

Assumption (1) is believed to be justified as spectroscopic examination suggests the probe is well outside the anode fall region (chapter 4.2). The gas pressure reduced to 273 K ranges from about 0.05 to 0.08 torr. At this pressure the electron mean free path will be about 13 mm (40 p.18) and the ion mean free path will be about 1/4 of this value. Thus condition (2) is satisfied. The experimental values of T_e are about an order of magnitude greater than T_+ so (3) is also satisfied. The Debye length λ_D is given by

$$\lambda_D = \left[\frac{\epsilon_o kT_e}{e^2 n_e}\right]^{\frac{1}{2}}$$

Taking T_e = 23,200 K and n_e = 10^{13} cm^{-3} gives λ_D = 3.3 x 10^{-4} cm therefore (4) is also satisfied. It has already been noted that a Maxwellian distribution appears to be appropriate for the electrons, so that all 5 conditions are satisfied, and equations (A6) and (A7) should be appropriate.

If the oscillations modulate the plasma parameters near the probe, the interpretation of the probe characteristics is complicated (42, 43). It has been found, however, that provided the discharge current is not modulated by the oscillations, the probe voltage is not modulated. The probe must therefore be placed outside the region in which the oscillations are produced.

APPENDIX A4

THE TEMPERATURE OF ATOMIC HYDROGEN IN AN ARGON PLASMA

It has been observed that the temperature of hydrogen atoms in the anode region of the discharge is much higher than that of the argon atoms (section 4.4). This may be expected since a hydrogen atom being lighter gains more energy from each collision with an electron than does an argon atom. This process will be examined in more detail using elementary kinetic theory.

Only elastic collisions are considered, and the electrons and atoms are treated as smooth, hard spheres. The plasma is assumed to consist of 5 components: heavy atoms (argon) mass m_1, light atoms (hydrogen) mass m_2, electrons mass m_3, heavy ions mass m_1 and light ions mass m_2. Heavy particles will be designated type (1) and light particles by type (2). The concentration of light atoms is much less than that of the heavy atoms and the fractional ionization is assumed to be small (< 1%). The concentration of light ions is assumed to be very small and will be ignored.

The energy gained by a particle of mass m_1 colliding with a particle of mass m_2 is given by

$$\Delta E_{12} = \frac{2\, m_1 m_2}{(m_1+m_2)^2} \{m_2 u_2^2 - m_1 u_1^2 + m_1 u_1 u_2 - m_2 u_1 u_2\} \qquad (A9)$$

where u_1 and u_2 are the components of the velocities of particles (1) and (2) along the line of centres.

Although the system is not in thermodynamic equilibrium, it is convenient to assume a Maxwell Boltzmann distribution of energy. The Langmuir probe measurements (appendix A3) indicate that this is quite a good approximation for the electron energy distribution. In principle it is possible to deduce the velocity distribution of the atoms from the Doppler broadened profile of the spectral lines, although in practice this method is likely to be rather inaccurate due to noise on the measured line profile.

Using a Maxwell Boltzmann distribution (A9) can be averaged over the velocities of particles type (1) and (2). The average energy transferred from (2) to (1) per collision is given by

$$\overline{\Delta E_{12}} = \frac{2\, m_1 m_2\, k}{(m_1+m_2)^2}\,(T_2 - T_1)\,, \tag{A10}$$

where T_1 and T_2 are the respective temperatures and k is Boltzmann's constant.

For the chosen model of the plasma, the rate at which energy is gained by type (2) particles from the electrons must be equal to the rate at which it is lost to the type (1) particles. (The electrons are treated as an infinite heat source and the heavy particles as an infinite heat sink). Equating the rates of gain and loss of energy gives,

$$\frac{2\, m_2 m_3\, k}{(m_2+m_3)^2}\,(T_3 - T_2)\nu_{23} = \frac{2\, m_1 m_2\, k}{(m_1+m_2)^2}\,(T_2 - T_1)\nu_{12} + \frac{2\, m_1 m_2}{(m_1+m_2)^2}\,(T_2 - T_4)\nu_{24} \tag{A11}$$

where ν_{12} is the collision rate between light and heavy atoms

ν_{23} is the collision rate between electrons and light atoms

ν_{24} is the collision rate between light atoms and heavy ions.

T_1, T_2, T_3 and T_4 are the temperatures of the heavy atoms, light atoms electrons, and heavy ions respectively.

Since $m_1 >> m_2 >> m_3$ (A11) may be simplified to give,

$$T_2\left(1 + \frac{m_1 m_3}{m_2^2}\,\frac{\nu_{23}}{\nu_{12}} + \frac{\nu_{24}}{\nu_{12}}\right) = T_1 + \frac{m_1 m_3}{m_2^2}\,\frac{\nu_{23}}{\nu_{12}}\,T_3 + \frac{\nu_{24}}{\nu_{12}}\,T_4 \tag{A12}$$

Experimentally it is found T_4 is close to T_1 (T_4 = 2,400 K, T_1 = 2000 K) and since the fractional ionization is small we have $\nu_{24} << \nu_{12}$, and so (A12) may be simplified to give

$$T_2\left(1 + \frac{m_1 m_3}{m_2^2}\,\frac{\nu_{23}}{\nu_{12}}\right) = T_1 + \frac{m_1 m_3}{m_2^2}\,\frac{\nu_{23}}{\nu_{12}}\,T_3 \tag{A13}$$

The collision rate between heavy atoms and light atoms may be written

$$\nu_{12} = N_1 N_2 \sigma_{12} \bar{u}_2 \quad \text{collisions cm}^{-3}\ \text{sec}^{-1} \tag{A14}$$

where N_1 and N_2 are the number densities of the heavy and light atoms, σ_{12} is the collision cross section and $\bar{u}_2$ is the average velocity of the light atoms. (The heavy atoms move much more slowly than the light atoms so $\bar{u}_2$ must be used).

Similarly the collision rate between the light atoms and the electrons is given by

$$\nu_{23} = N_2 N_3 \sigma_{23} \bar{u}_3 , \tag{A15}$$

where N_3 is the electron number density, σ_{23} is the cross section for the collision, and $\bar{u}_3$ is the average velocity of the electrons.

From (A14) and (A15) the ratio of the collision rates is given by

$$\frac{\nu_{23}}{\nu_{12}} = \frac{N_3}{N_1} \frac{\sigma_{23}}{\sigma_{12}} \left(\frac{T_3 m_2}{T_2 m_3} \right)^{\frac{1}{2}} . \tag{A16}$$

The easiest way to compare this theory with experimental results is to use the measured values of T_1, T_2, and T_3 to calculate ν_{23}/ν_{12} from (A13) and then compare this with the value calculated from (A16).

From (A13) the ratio ν_{23}/ν_{12} is given by

$$\frac{\nu_{23}}{\nu_{12}} = \frac{T_2 - T_1}{T_3 - T_2} \frac{m_2^2}{m_1 m_3} . \tag{A17}$$

If the light atoms are hydrogen and the heavy atoms argon $m_1 = 40\ m_2$ and $m_2 = 1840\ m_3$. Typical values of T_1, T_2 and T_3 are 2000 K, 5,500 K, and 20,000 K. Thus ν_{23}/ν_{12} is equal to 90.

To calculate ν_{23}/ν_{12} from (A16) requires a knowledge of σ_{23}/σ_{12}. If the atoms and electrons are treated as hard spheres with the electrons much smaller than the other particles which are assumed to have the same diameter, then $\sigma_{23}/\sigma_{12} = 1/4$. Typical values of N_3 and N_1 are 10^{13} cm^{-3} and 2×10^{15} cm^{-3}. Substituting these values in (A16) gives $\nu_{23}/\nu_{12} \approx 1/10$, very much less than the value (90) calculated from (A17).

It is clear therefore that this theory is totally inadequate to explain the large difference between the temperature of the argon and the temperature of the hydrogen. Using this model the expected difference in temperature is only 70 K.

To explain the observed temperatures, we now consider the effects of inelastic collisions. These collisions generally transfer less translational energy from the electrons to the atoms than elastic collisions, however there is an important exception. A hydrogen molecule may be dissociated by an electron collision if the molecule is excited to the $1^3\Sigma_u$ state. This state is repulsive and the atoms fly apart, each carrying off 2.1 eV of kinetic energy (44). This process provides a source of high energy hydrogen atoms which only lose their energy to the heavier argon atoms after many collisions. The threshold for excitation of the $1^3\Sigma_u$ state by electron collision is 8.8 eV.

The high temperature of the hydrogen atoms is probably due to the energy gained by the hydrogen atoms in the dissociation of a hydrogen molecule. The average energy of the hydrogen will be determined by the rate at which energy is lost by the atoms to the heavier argon atoms and by the dissociation rate. Recombination of hydrogen atoms (probably at the walls) will provide a continuous source of hydrogen molecules to sustain the dissociation rate. This process is difficult to analyse since recombination rates and diffusion times to and from the walls are not known.

APPENDIX A5

THE STABILITY CRITERION FOR THE ANODE FALL

It has been shown in section 5.1 that the stability criterion for the anode fall is that the roots of the equation

$$p + \frac{da}{\varepsilon_o} \left.\frac{dZ}{dV_a}\right|_{V_o} e^{-p\tau} = 0 \qquad \text{(A18)}$$

should have negative real parts.

It is convenient to introduce a function g(q) where

$$g(q) = q + ce^{-q} \qquad \text{(A19)}$$

with $q = x+iy = p\tau$, and $c = \frac{da\tau}{\varepsilon_o} \left.\frac{dZ}{dV_a}\right|_{V_o}$.

The real and imaginary parts of g are given by

$$\begin{aligned} R\{g\} &= x + ce^{-x} \cos y \qquad \text{(a)} \\ I\{g\} &= y - ce^{-x} \sin y \qquad \text{(b)} \end{aligned} \qquad \text{(A20)}$$

In order to examine the behaviour of this function g and locate the zeros in the q-plane, the function is plotted in the g-plane with x as a fixed parameter and y as a variable parameter. The locus of (R{g}, I{g}) as y is varied is a cycloid (fig. A5.1), which may be either prolate (b) or curtate (a) and (c). The centre of the circle tracing out the cycloid moves along the line $x = x_o$ (x_o is the fixed value of the parameter x) and the radius of the circle is ce^{-x}.

The roots of (A18) are found from the zeros of (A19). If g(q) has a zero with the real part of q equal to x_o then the locus of $g(x_o+iy)$ must pass through the origin as y is varied. The values of x_o and y at which this occurs give the roots of (A18). The condition for stability is that the locus must not pass through the origin for x_o greater than or equal to zero.

Consider first the locus with c = 1.2 and x = o (fig. A5.1 (a)). In this case the cycloid is curtate but the central loop does not

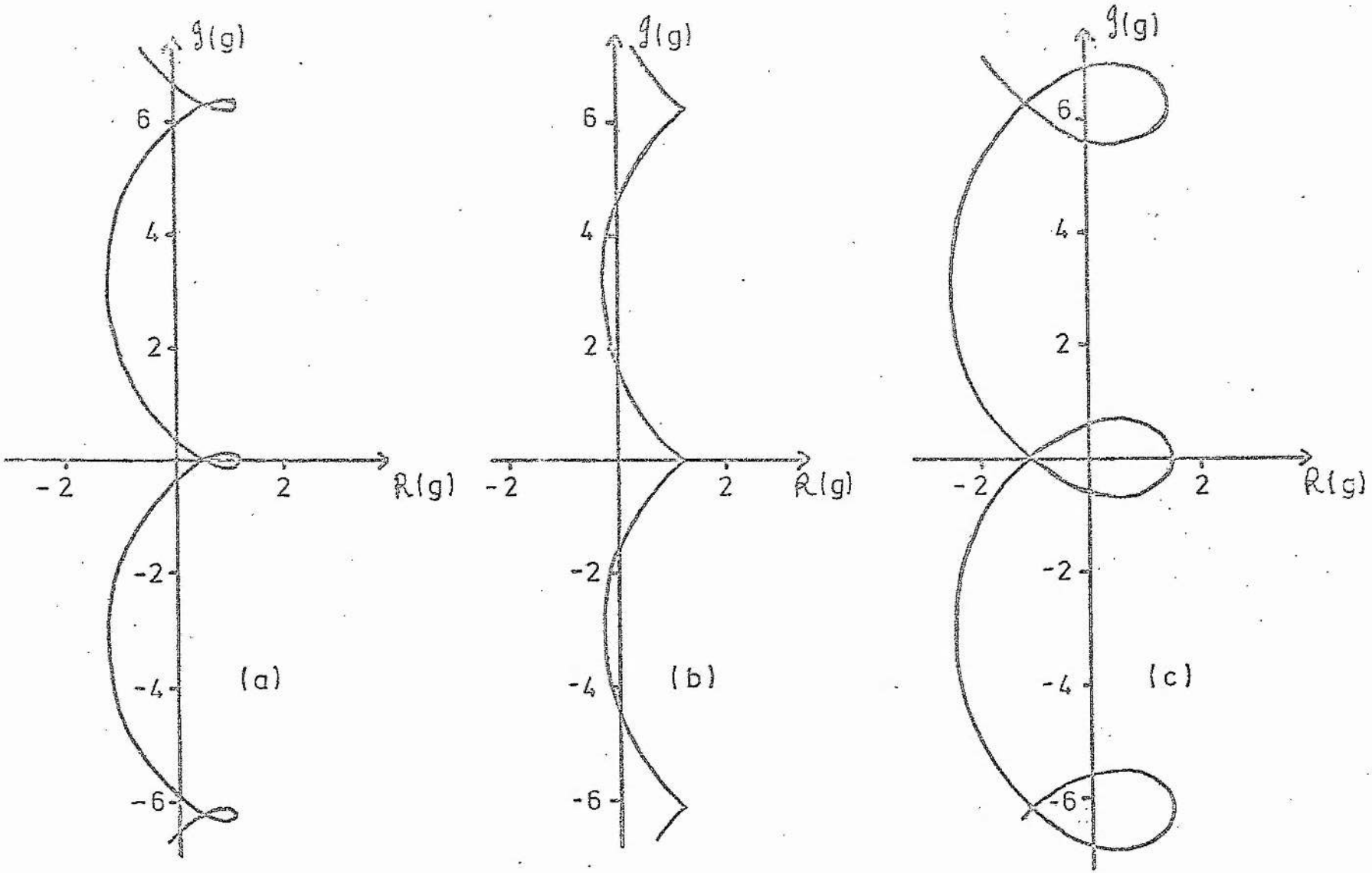

fig A5.1 The Locus of $g(x_0+iy)$ as y is varied, (a) $x_0=0$; (b) $x_0=0{\cdot}5$; (c) $x_0=-0{\cdot}5$; with $c=1{\cdot}2$

enclose the origin, the locus passes to the right of the origin. Increasing the value of x_o decreases the radius of the circle tracing out the cycloid and shifts its centre to the right, so that the locus can not pass through the origin for positive x_o (fig. A5.1 (b)). Reducing the value of x_o below zero enlarges the radius of the circle tracing out the cycloid and shifts its centre to the left. In fig. 5.1 (c), with $x_o = -0.5$ the central loop encloses the origin so that between $x_o = -0.5$ and $x_o = 0$ there is a value of x_o for which the locus passes through the origin. In this case therefore there are roots with negative real parts but no roots with positive real parts.

With a larger value of c, ($c=2$) the loops of the cycloid enclose the origin for $x_o = 0$ (fig. A5.2 (a)). Increasing the value of x_o once again reduces the radius of the circle tracing out the cycloid and shifts its centre to the right (fig. A5.2 (b)). However in this case between the values of $x_o = 0$ and $x_o = 1$ there is a value of x_o for which the locus passes through the origin. Therefore there are at least two positive roots of (A18). (There are at least two roots since if p is a root of (A18) then its complex conjugate p^* is also a root).

If the locus of g(iy) does not encircle the origin then all the zeros of g occur for values of q with negative real parts. The critical value of c for which g(iy) passes through the origin is readily found from (A20) and is $c = \pi/2$. If c is less than $\pi/2$ the cycloid g(iy) does not enclose the origin, if c is greater than $\pi/2$ then it does. The criterion required therefore for (A18) to have all its roots with negative real parts is

$$\frac{da\tau}{\varepsilon_o} \left.\frac{dZ}{dV_a}\right|_{V_o} < \pi/2 \ .$$

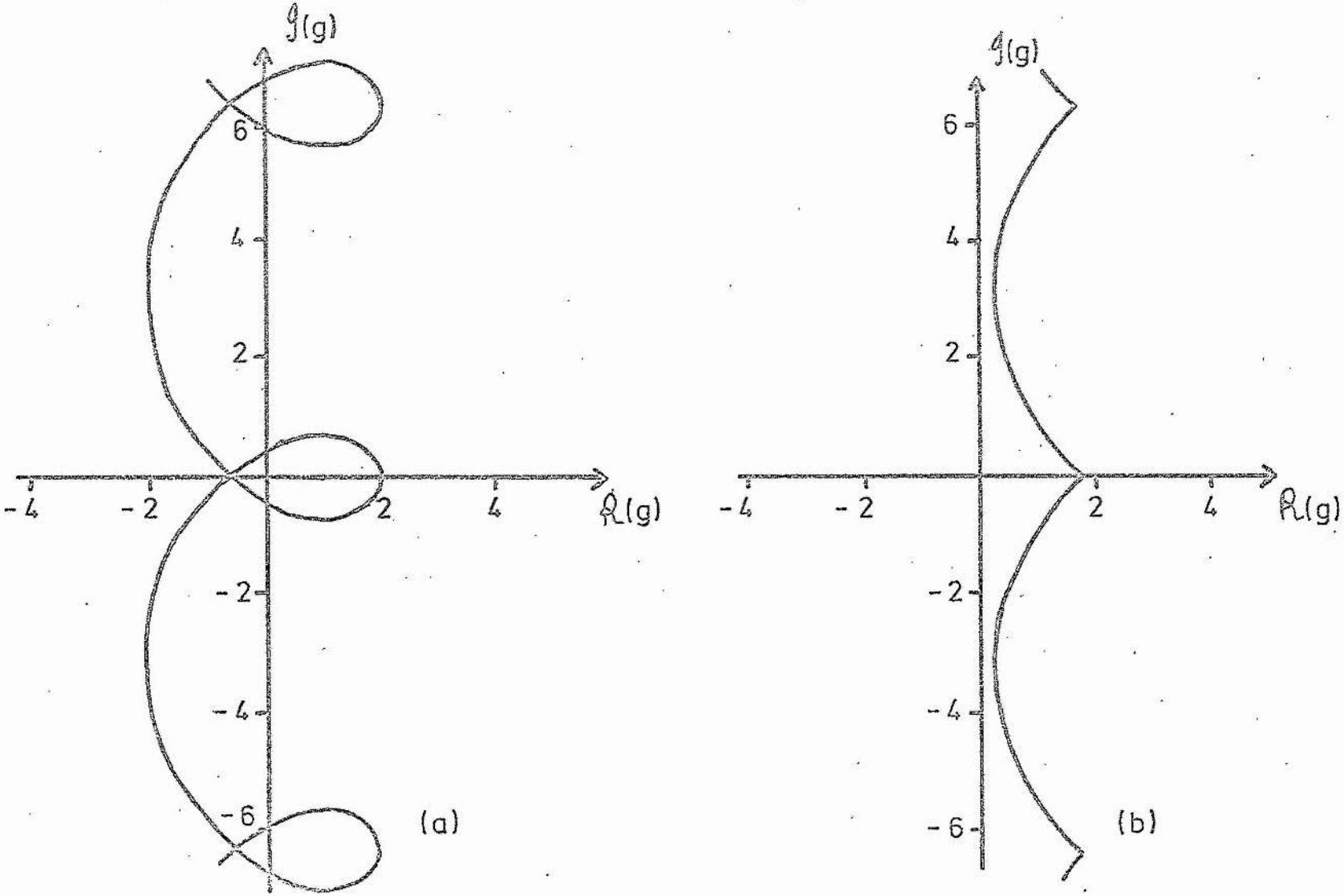

fig. A5.2 The Locus of $g(x_o+iy)$ as y is varied with c = 2 (a) $x_o=0$, (b) $x_o=1$

APPENDIX A6

J. Phys. D: Appl. Phys., 1971, Vol. 4. Printed in Great Britain

Phase modulated axial modes in a passive cavity

J. N. ROSS†

Laser Associates, 697 Stirling Road, Slough, Bucks

MS. received 9th March 1971

Abstract. The fm laser consists of a laser with a phase modulator in the cavity, driven at a frequency of approximately the axial mode spacing. A passive two-mirror cavity and a passive ring cavity containing such a modulator are analysed using travelling plane waves. The axial modes of the cavities are shown to be phase modulated and their centre frequencies and peak phase deviation are determined in each case.

1. Introduction

A method of stabilizing a multimode laser is to lock the modes together in phase. One method of doing this is to include in the cavity a phase modulator driven at a frequency of approximately the mode spacing. The nature of the resulting laser output depends on how close the modulation frequency is to the mode spacing frequency. If the frequencies are exactly the same then the output of the laser is a train of narrow pulses repeated at the modulation frequency. However, if the modulation frequency is slightly detuned from the mode spacing, under certain circumstances the laser radiation may be frequency modulated and the amplitude noise due to beating of the modes may be suppressed. This was first demonstrated by Harris and Targ (1964) and has been analysed in considerable detail by Harris and McDuff (1965) using Lamb's (1964) semi-classical theory.

Here we present a different way of analysing the frequency modulated laser which is applicable to both travelling and standing waves. We solve the wave equation for a one-dimensional passive cavity containing a phase modulator. The electric field is represented by a sinusoidal travelling wave with an arbitrary phase term which is permitted to be a function of time and space. We show that when the wave equation is solved for this cavity the solutions have the same centre frequency as the modes of a simple cavity but that the arbitrary phase term takes on the character of a sinusoidal phase modulation. The value of the peak phase deviation is the same for all modes and in a special case reduces to that derived by Harris and McDuff.

The modes of the cavity are now no longer of constant phase but are phase modulated. For a two-mirror cavity the electric field cannot now be reduced to standing waves as is the case in the absence of a modulator. The method is also applied to a ring laser cavity and it is shown that, in contrast to the two-mirror cavity, the peak phase deviation does not depend on the position of the modulator in the cavity.

2. The passage of a wave through a medium with time-varying susceptibility

In this section we consider electromagnetic waves in a medium with a polarization $P(z, t)$. To simplify the problem we consider only a polarized plane wave travelling in the positive z direction, thereby reducing the problem to one dimension. The appropriate one-dimensional wave equation for the electric field may readily be derived from Maxwell's

† Present address: Physics Department, School of Physical Sciences, St Andrews University, St Andrews, Scotland.

equations and is

$$\frac{\partial^2 E}{\partial z^2}+\mu_0\epsilon_0\frac{\partial^2 E}{\partial t^2}+\mu_0\sigma\frac{\partial E}{\partial t}=-\mu_0\frac{\partial^2 P}{\partial t^2} \tag{1}$$

where σ is the conductivity of the medium.

In the linear approximation P is proportional to E and we write

$$P=\epsilon_0(\chi'+i\chi'')\,E \tag{2}$$

where χ' and χ'' are the in-phase and quadrature susceptibilities. We only consider a passive cavity, therefore both σ and χ'' are zero. For this case, and letting χ' be time dependent, equation (1) becomes

$$-\frac{\partial^2 E}{\partial z^2}+\mu_0\epsilon_0\frac{\partial^2}{\partial t^2}\{(1+\chi')\,E\}=0. \tag{3}$$

We assume that χ' is of the form

$$\chi'=\chi_0'+\Delta\chi'\cos\nu t \tag{4}$$

where $\Delta\chi'\ll\chi_0'$.

When the susceptibility varies, the optical path length varies and so we expect the time-varying susceptibility to modulate the phase of the wave. Therefore we look for a solution of the form

$$E=E_0\exp i(\omega t+\phi(z,t)-\kappa z) \tag{5}$$

where ω and κ are constants and ϕ is a slowly varying phase term. The condition that ϕ is slowly varying may be written $\partial\phi/\partial z\ll\kappa$, $\partial\phi/\partial t\ll\omega$.

We now assume $E\,\partial\chi'/\partial t\ll\chi'\,\partial E/\partial t$ so that equation (3) becomes

$$-\frac{\partial^2 E}{\partial z^2}+\mu_0\epsilon_0(1+\chi_0'+\Delta\chi'\cos\nu t)\frac{\partial^2 E}{\partial t^2}=0. \tag{6}$$

From equations (5) and (6) we finally obtain

$$\{\kappa^2-\mu_0\epsilon_0(1+\chi_0')\,\omega^2\}-2\kappa\frac{\partial\phi}{\partial z}-2\omega\frac{\partial\phi}{\partial t}\mu_0\epsilon_0(1+\chi_0')-\mu_0\epsilon_0\Delta\chi'\omega^2\cos\nu t=0 \tag{7}$$

where we have neglected terms of order $\partial^2\phi/\partial z^2$, $\partial^2\phi/\partial t^2$, $(\partial\phi/\partial z)^2$, $(\partial\phi/\partial t)^2$ and $\Delta\chi'\,\partial\phi/\partial t$.

Introducing the refractive index n_0 and the speed of light c, defined respectively by

$$n_0^2=1+\chi_0', \qquad c^2=1/\mu_0\epsilon_0$$

and defining κ so that $\kappa=n_0\omega/c$, we then obtain

$$\frac{c}{n_0}\frac{\partial\phi}{\partial z}+\frac{\partial\phi}{\partial t}+\frac{\Delta\chi'\omega}{2n_0^2}\cos\nu t=0. \tag{8}$$

If we can find an acceptable solution to equation (8), then equation (5) is a solution of the wave equation (3). In the case of a constant χ', that is $\Delta\chi'=0$, then solving equation (8) shows ϕ to be a function of $t-n_0z/c$. This tells us that in a non-dispersive medium the phase modulation is transmitted at the phase velocity of the wave and that there is no distortion.

3. The phase modulator

Phase modulation is achieved by passing light through a medium of time-varying susceptibility. The variation in susceptibility is brought about by applying an electric field of the required frequency in a direction which depends on the non-linear crystal used as a modulator. In designing modulators, one of two courses is usually adopted. In the first, the modulator is made short so that the transit time of the light through the crystal is much less than the

period of the modulation. Alternatively, at high frequencies, the electric field producing the susceptibility variations is in the form of a travelling wave with the same direction and phase velocity as the light wave. (This is the principle of phase matching familiar in the theory of second harmonic generation of light.)

We consider a plane wave incident upon a modulator in which the phase of the time-varying susceptibility is the same throughout the modulator. We shall investigate an incident wave with an arbitrary phase modulation and how it is modified in passing through the modulator. The treatment to follow adopts the first course without the restriction on the length of the modulator. The problem is to solve the wave equation in three regions of space:

Region A	$z<l$	where $\chi'=0$
Region B	$l\leqslant z\leqslant l+d$	where $\chi_0'\neq 0$, $\Delta\chi'\neq 0$
Region C	$z>l+d$	where $\chi'=0$.

In region A we have a plane wave and we note that it must be of the form (5) in which ϕ is a function of $t-n_0z/c$; with $n_0=1$ we get

$$E=E_0\exp \mathrm{i}(\omega t+\phi_A(t-z/c)-\omega z/c) \tag{9}$$

where ϕ_A is an arbitrary phase modulation. To obtain the field E in region B we must first solve equation (8). If $\Delta\chi'$ were zero, ϕ_B would be a function of $t-n_0z/c$, where n_0 is given by $n_0=(1+\chi_0')^{1/2}$. Therefore we try as a solution

$$\phi_B(z,t)=B(t-n_0z/c)+A(t)$$

and obtain

$$\frac{\mathrm{d}A}{\mathrm{d}t}+\frac{\Delta\chi'\omega}{2n_0^2}\cos\nu t=0$$

which gives

$$A=-\frac{\Delta\chi'\omega}{2n_0^2\nu}\sin\nu t+\text{constant}.$$

We may absorb the constant into the function B to obtain

$$\phi_0(z,t)=B(t-n_0z/c)-\eta\sin\nu t \tag{10}$$

where

$$\eta=\frac{\Delta\chi'\omega}{2n_0^2\nu}. \tag{10a}$$

From equation (5), the electric field in region B may be written

$$E=E_0\exp \mathrm{i}(\omega t+\phi_B(z,t)-\omega n_0z/c) \tag{11}$$

with $\phi_B(z,t)$ given by (10). In region C we have $\chi'=0$ so the electric field is of the form

$$E=E_0\exp \mathrm{i}(\omega t+\phi_C(z,t)-\omega z/c). \tag{12}$$

The boundary conditions are that at $z=l$ and $z=l+d$ the amplitude and phase of the waves in each region must be the same.

Equating the phases at the first boundary $z=l$ we get

$$B(t-n_0l/c)=\phi_A(t-l/c)+(n_0-1)\,l/c+\eta\sin\nu t.$$

If we replace t by $t-n_0z/c+n_0l/c$ in this equation we can find $B(t-n_0z/c)$ and hence obtain $\phi_B(z,t)$ from (10); we get

$$\phi_B(z,t)=\phi_A\{t+(n_0-1)\,l/c-n_0z/c\}+(n_0-1)\,\omega l/c+\eta\{\sin\nu(t-n_0z/c+n_0l/c)-\sin\nu t\}. \tag{13}$$

Similarly, by equating the phases at the second boundary, we obtain

$$\phi_C(t-z/c)=\phi_A\{t-(n_0-1)\,d/c-z/c\}-(n_0-1)\,\omega d/c + \eta\,[\sin \nu\{t-n_0 d/c+(l+d)/c-z/c\}-\sin \nu\{t+(l+d)/c-z/c\}]. \quad (14)$$

We have found the phase modulation term for the wave emerging from the modulator. The time-independent term in equation (14) just represents a constant phase shift term and ϕ_A is the original phase modulation of the wave entering the modulator, also with an appropriate phase shift. The remaining term describes the phase modulation introduced by the medium of the phase modulator.

A case of special interest occurs when the transit time is much less than the period of modulation. This condition is given by $n_0 d/c \ll 1/\nu$. Expanding equation (14) and imposing this condition we obtain

$$\phi_C(t-z/c)=-(n_0-1)\,\omega d/c+\phi_A\{t-(n_0-1)\,d/c-z/c\} -\frac{\Delta\chi'\omega d}{2n_0 c}\cos \nu\{t+(l+d)/c-z/c\}.$$

To show that this is in agreement with the value obtained by simple arguments, assuming that the thickness of the modulator is small, we write

$$n^2=(n_0+\Delta n\cos \nu t)^2=1+\chi_0'+\Delta\chi'\cos \nu t$$

which gives $2n_0\Delta n=\Delta\chi'$. Therefore the peak phase deviation is $\Delta n\omega d/c$, which is just the value obtained by elementary considerations in which it is assumed that the modulation frequency is very small.

Two special cases of the general solution (14) are worth noting; these occur for $\nu n_0 d/c=\pi$ and $\nu n_0 d/c=2\pi$. In the first case, in which we have $\nu n_0 d/c=\pi$, the modulation is a maximum. In the second case the modulation is zero. For the constant phase type of modulator, the optimum length is therefore $d=\pi c/\nu n_0$, provided the modulator is not required to operate at a wide range of frequencies. The particular range depends upon the frequency distortion which can be tolerated.

4. Phase modulator in a passive cavity

We consider a passive cavity with two infinite plane mirrors M_1 and M_2 separated by a distance L. Inside the cavity is a phase modulator region of variable susceptibility, as in figure 1. The region of the phase modulator is defined by $l \leqslant z \leqslant l+d$ and its susceptibility is $\chi'=\chi_0'+\Delta\chi'\cos \nu t$. The other two regions of the cavity are defined by $0<z<l$ and $l+d<z<L$ and have $\chi'=0$.

In such a cavity we have two travelling waves, one travelling left to right and the other right to left. To simplify the mathematics the cavity is replaced by the 'real' cavity plus its

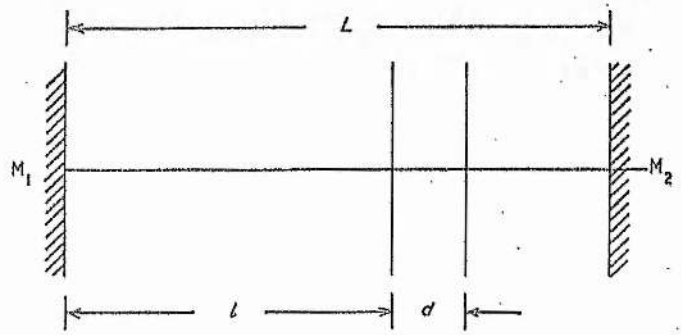

Figure 1. The passive cavity and modulator.

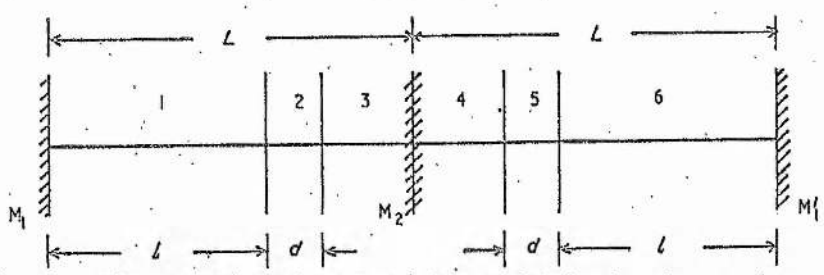

Figure 2. The cavity and modulator with their mirror image.

reflection in M_2 the 'image' cavity, as shown in figure 2. The wave travelling left to right starts at M_1 and travels to M_2. It is then reflected in real space by M_2 and becomes a wave travelling right to left, but in this representation it travels through the mirror image cavity from M_2 to M_1'. The constant phase shift at M_2 can be absorbed in the cavity length. In figure 2 the 'real' cavity is represented by regions 1, 2, 3 and the 'image' cavity by regions 4, 5, 6; the modulator is represented by region 2 and its image by 5. Self consistency requires that the electric field at M_1 is the same as at M_1', that is $E'(0)=E'(2L)$; this gives the modes of the cavity. To find the field $E(z)$ in the real cavity of figure 1, we must add the fields in the two appropriate parts of the cavity of figure 2 giving

$$E(z)=E'(z)+E'(2L-z)$$

where E is the field in the real cavity and E' the field in our representation of the cavity.

We start with a wave in the region $0<z<l$

$$E'=E_0' \exp \mathrm{i}(\omega t+\phi_1(z,t)-z/c)$$

where ϕ_1 is an unknown phase term. Using (14) we obtain the phase term in regions 3 and 4

$$\phi_3(z,t)=\phi_4(z,t)=\phi_1\{t-(n_0-1)\,d/c-z/c\}-\omega(n_0-1)\,d/c$$
$$+\eta[\sin\nu\{t+(l+d)/c-n_0d/c-z/c\}-\sin\nu\{t+(l+d)/c-z/c\}].$$

Similarly, the phase in region 6 is given by

$$\begin{aligned}\phi_6(z,t)=\phi_1\{&t-2(n_0-1)\,d/c-z/c\}-2\omega(n_0-1)\,d/c\\&+\eta[\sin\nu\{t-2(n_0-1)\,d/c+l/c-z/c\}\\&-\sin\nu\{t-(n_0-1)\,d/c+(l+d)/c-z/c\}\\&+\sin\nu\{t-n_0d/c+(2L-l)/c-z/c\}\\&-\sin\nu\{t+(2L-l)/c-z/c\}].\end{aligned}$$

The condition that the wave is a mode of the cavity is that $E'(0)=E'(2L)$, where we have ignored any phase shift at M_1. This condition implies that

$$\phi_1(0,t)=\phi_6(2L,t)+2\pi p-2L\omega/c$$

where p is an integer. Substituting for ϕ_6 and equating the time-independent terms we obtain

$$\omega=\frac{\pi pc}{L+(n_0-1)\,d}. \tag{15}$$

Equation (15) gives the centre frequencies of the modes of the cavity and the mode spacing. Equating the time-dependent terms we get, with

$$\phi_1\{t-2L+2(n_0-1)\,d/c\}-\phi_1(t-0)=\Phi \quad \text{(say)}$$
$$\begin{aligned}\Phi=-\eta[&\sin\nu\{t-2(n_0-1)\,d/c+l/c-2L/c\}\\&-\sin\nu\{t-(n_0-1)\,d/c+(l+d)/c-2L/c\}\\&+\sin\nu\{t-n_0d/c-l/c\}\\&-\sin\nu\{t-l/c\}].\end{aligned} \tag{16}$$

The frequency of modulation is ν. We shall consider the case when ν is almost equal to the mode spacing. We define the detuning frequency $\Delta\nu$ by

$$\Delta\nu=\frac{\pi c}{L+(n_0-1)\,d}-\nu, \tag{17}$$

assuming that $\phi_1(t)$ has the same frequency as the modulator (ie linear response).

By expanding equation (17) we obtain

$$L+(n_0-1)\,d=(\pi c/\nu)\,(1-\Delta\nu/\nu). \tag{18}$$

Substituting (18) into (16) we obtain

$$\Phi=\phi_1(t-2\pi/\nu+2\pi\Delta\nu/\nu^2)-\phi_1(t-0).$$

Assuming that $\phi_1(t)$ is periodic in t with period $1/\nu$, that is $\phi_1(t-2\pi/\nu)=\phi_1(t)$, we obtain

$$\Phi=\left(\frac{\partial\phi_1}{\partial t}\right)_{z=0}\frac{2\pi\Delta\nu}{\nu^2}. \tag{19}$$

Using (19) and (16) we get

$$\left(\frac{\partial\phi_1}{\partial t}\right)_{z=0}=-\frac{\nu^2}{\pi n_0^2\Delta\nu}\,(\delta_c\sin\nu t+\delta_s\cos\nu t) \tag{20}$$

where

$$\delta_c=\frac{\omega\Delta\chi'}{4\nu}\,[\cos(\nu/c)\,\{2(n_0-1)\,d+2L-l\}-\cos(\nu/c)\,\{(n_0-1)\,d-(l+d)+2L\}+\cos(\nu/c)\,(n_0d+l)-\cos\nu l/c]$$

and

$$\delta_s=\frac{\omega\Delta\chi'}{4\nu}\,[\sin(\nu/c)\,\{(n_0-1)\,d-(l+d)+2L\}-\sin(\nu/c)\,\{2(n_0-1)\,d-l+2L\}-\sin(\nu/c)\,(n_0d+l)+\sin\nu l/c].$$

Since ϕ_1 is a function of $t-z/c$ we can integrate (20) to obtain

$$\phi_1(t-z/c)=\frac{\nu}{\pi n_0^2\Delta\nu}\,\{\delta_c\cos\nu(t-z/c)-\delta_s\sin\nu(t-z/c)\}. \tag{21}$$

Equation (21) gives the phase modulation in region 1. The phase modulation in any other region can be readily found. The measurable quantity is the peak phase deviation which is given by

$$\Gamma=\frac{\nu}{\pi n_0^2\Delta\nu}\,(\delta_c^2+\delta_s^2)^{1/2}. \tag{22}$$

Neglecting $\Delta\nu$ in (17) we can simplify δ_c and δ_s to get

$$\delta_c=0$$

$$\delta_s=\frac{\omega\Delta\chi'}{2\nu}\,\{\sin\nu l/c-\sin\nu(n_0d+l)/c\}.$$

In this case (22) reduces to

$$\Gamma=\frac{\nu}{\pi n_0^2\Delta\nu}\,|\delta_s|. \tag{23}$$

For the special case $n_0=1$ we have $\nu/c\simeq\pi/L$. Now by introducing a function defined by

$$\Delta\chi'(z)=\begin{cases}\Delta\chi', & l\leqslant z\leqslant l+d\\ 0, & \text{otherwise}\end{cases}$$

we get

$$\delta_s = -\frac{\omega}{2c}\int_0^L \Delta\chi'(z)\cos(\pi z/L)\,dz. \tag{24}$$

This is just the coupling coefficient introduced by Harris and McDuff (1965), so that equation (23) reduces to the same form as their equation for Γ in the linear theory.

5. A phase modulator in a ring laser cavity

This travelling wave theory may readily be applied to the ring cavity shown in figure 3. We shall restrict our attention to the wave travelling in an anticlockwise direction, but we could equally well consider the wave travelling in the clockwise direction. The analysis proceeds as before.

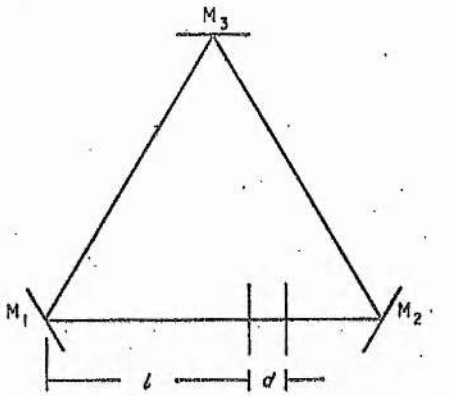

Figure 3. The ring cavity and modulator.

The total length of the cavity, that is for one round trip, is L and we measure z in the anticlockwise direction, z being the distance travelled round the cavity from the origin at M_1. The modulator is in the region $l \leqslant z \leqslant l+d$ and in this case during one round trip the wave passes through the modulator only once. The cavity is divided into three regions $0<z<l$, $l \leqslant z \leqslant l+d$ and $l+d<z<L$ denoted by regions 1, 2 and 3. Treating the problem as above with the modified boundary condition $E(0, t)=E(L, t)$, we obtain the centre frequency ω of the modes and the phase modulation term ϕ_1:

$$\omega = \frac{2\pi pc}{L+(n_0-1)\,d} \tag{25}$$

$$\phi_1(t-z/c) = \frac{\nu}{\pi n_0^2 \Delta\nu}\{\Delta_c \cos\nu(t-z/c) - \Delta_s \sin\nu(t-z/c)\} \tag{26}$$

where

$$\Delta_c = \frac{\omega\Delta\chi'}{4\nu}\,[\cos\nu\{l/c-(n_0-1)\,d/c-L/c\}-\cos\nu\{(l+d)/c-L/c\}]$$

and

$$\Delta_s = \frac{\omega\Delta\chi'}{4\nu}\,[\sin\nu\{l/c-(n_0-1)\,d/c-L/c\}-\sin\nu\{(l+d)/c-L/c\}].$$

The peak phase deviation Γ is given by

$$\Gamma=\frac{\nu}{\pi n_0^2\Delta\nu}(\Delta_0^2+\Delta_s^2)^{1/2}$$

$$=\frac{\omega\Delta\chi'}{4\pi n_0^2\Delta\nu}\{2-2\cos(\nu n_0 d/c)\}^{1/2}. \tag{27}$$

Notice that for a two-mirror cavity Γ depends on l and d, while for a ring cavity Γ depends only on d. The difference arises because in a two-mirror cavity the wave passes through the modulator twice in completing one round trip of the cavity. For one round trip the modulator must have no net effect if the travelling wave is to be a mode. The effective modulation due to the two regions of modulation depends on their separation, and, since the separation depends on l, the phase deviation of the modes depends on l.

6. Conclusion

We have shown that for both two-mirror and ring cavities containing a phase modulator the axial modes of the cavity are phase modulated. Standing wave modes cannot exist in either cavity and the above approach emphasizes the travelling wave nature of the electric field. The modes form a family of phase-modulated travelling waves whose centre frequencies are equally spaced. The peak phase deviation Γ is the same for every mode and may vary over quite a wide range provided that the conditions imposed in obtaining the solution are not violated. The value of Γ obtained reduces to that of Harris and McDuff as a special case.

Acknowledgments

The author wishes to thank Mr A. Maitland for his assistance and encouragement in producing this paper, and Professor J. F. Allen of the School of Physical Sciences at the University of St Andrews where this work was undertaken.

References

HARRIS, S. E., and TARG, T. R., 1964, *Appl. Phys. Lett.*, 5, 202–4.
HARRIS, S. E., and MCDUFF, O. P., 1965, *IEEE J. Quant. Electron.*, 1, 245–62.
LAMB, W. E., Jr, 1964, *Phys. Rev.*, 134, A1429–50.

APPENDIX A7

THE MEASUREMENT OF SPECTRAL LINE WIDTHS USING A SCANNING FABRY-PEROT INTERFEROMETER

A7.1 Theory

The Fabry-Perot interferometer is a multiple reflection interferometer with two parallel plane mirrors. For parallel light at normal incidence it has a transmission maximum when the wavelength of the light satisfies the condition

$$\lambda = \frac{2L}{m},$$

where λ is the wavelength, L is the separation of the mirrors, and m is an integer. The separation between successive maxima is most readily expressed in terms of frequency and is given by,

$$\Delta\nu = \frac{c}{2L},$$

where $\Delta\nu$ is the frequency between successive maxima (the free spectral range) and c is the velocity of light.

In the scanning interferometer one of the mirrors is translated along the axis through one or more half wavelengths so that the frequencies of the transmission maxima are scanned through one or more free spectral ranges. The widths of the transmission maxima are determined by the reflectivity, the flatness, and the parallelism of the mirrors. Flatness and parallelism usually become important when the mirrors have reflectivities greater than about 95% (multilayer dielectric mirrors). Alignment of the mirrors requires care to ensure that the greatest finesse is obtained (the finesse is the ratio of the free spectral range to the half width of the transmission maxima).

To measure the widths of spectral lines of a complex spectrum using a Fabry-Perot interferometer the instrument is used with a monochromator, to separate the spectral lines. The optical

arrangement used in the present experiments is shown in fig. A7.1. The separation of the mirrors is chosen to ensure that the free spectral range is about three times the half width of the gas-discharge line to be measured (to prevent excessive overlap of the fringes and still ensure that the measured fringe width is much larger than the instrumental width). The intensity of the transmitted light is measured with a photomultiplier.

A7.2 Experimental Details

The widths of H_α and H_β lines have been measured using an interferometer with silvered plates. The separation of the plates used for these measurements was 1.58 n.m. giving a free spectral range of 95 GH_z. The finesse obtained using this interferometer was low (about 6.3) but silvered mirrors were necessary to enable the H_α (656.3 n.m.) and H_β (486.1 n.m.) lines to be measured.

The interferometer was scanned through about 1.5 free spectral ranges by applying a sawtooth waveform with an amplitude of 150 V (peak-to-peak) to the piezo-ceramic stack on which one mirror was mounted. The sawtooth waveform was obtained from an oscilloscope. The output of the photomultiplier was either observed on the oscilloscope or recorded with a pen recorder. The scan time was determined by the time constant of the recording apparatus. With the pen recorder a resistance capacity filter was used to give a time constant of about 1 sec and the scan time was between 1 and 5 minutes.

The light level is rather low so that the shot noise is quite large even with a time constant of 1 second. The scan of the H_α line in fig. A7.2 is typical of the results obtained at a discharge current of 40 A and a system pressure of around 0.3 torr. At lower discharge currents the light intensity is less and the shot noise greater.

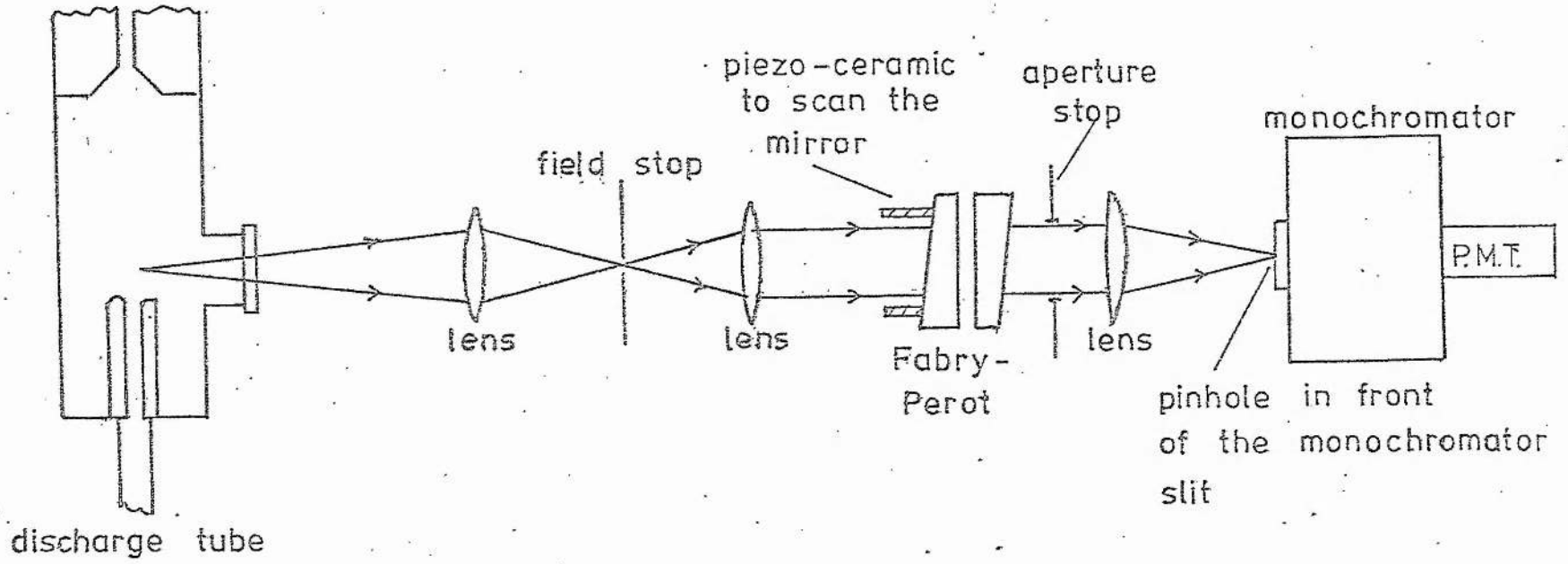

fig A 7.1 Optical Arrangement of the Fabry-Perot Interferometer

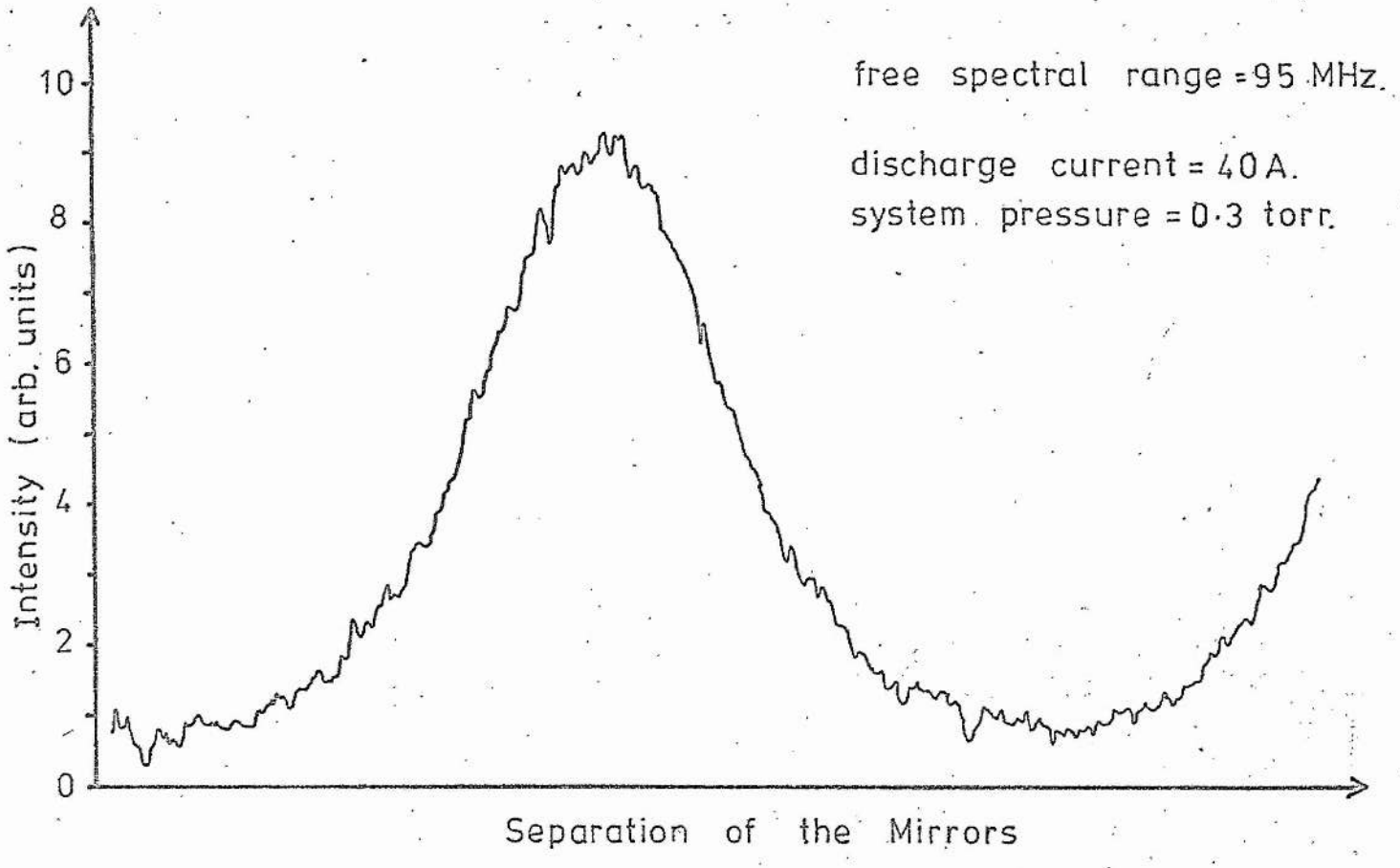

fig. A7.2 Profile of H_α Line as measured with the Fabry-Perot Interferometer

In order to obtain the spectral line width it is necessary to allow for the instrumental width (which is about half the fringe width). To do this it was assumed that the instrumental profile is Lorentzian and the spectral line profile is Gaussian. The assumption of a Gaussian profile should be valid for the H_α line and will be a fair approximation for the H_β line if the Stark broadening is small (as the results indicate). The instrumental line profile is compared with a Lorentzian profile in fig. A7.3. There is good agreement in the central region but in the wings the Lorentzian profile is greater than the measured profile. The slight asymmetry is probably due to misalignment of the Fabry-Perot. A computer program (due to M.H. Dunn) was available for calculating the convolution of a Gaussian profile and a Lorentzian profile.

The instrumental width was measured by scanning an argon line at a wavelength close to the hydrogen line to be measured. The argon lines have a width 10 times less than the hydrogen lines so that, for our instrument, the resulting line profile is a good approximation to the instrumental line profile. The measured fringe width and the instrumental line width are normalized so that the instrumental width is unity. The Gaussian width is then found using the graph of fig. A7.4 which is a plot of the half width of the convolution of a Gaussian profile and a Lorentzian profile against the Gaussian half width, with a Lorentz half width of unity.

The measured half widths of the H_α line ranged from 22 to 24.5 GHz (0.032 to 0.035 n.m.) and the widths of the H_β line from 30 to 33 GHz (0.023 to 0.026 n.m.) at a discharge current of 40 A and a pressure of 0.3 torr. No significant difference in line widths was observed when the current was reduced to 25 A or the pressure increased to 0.6 torr. (The values still lay within the ranges given above).

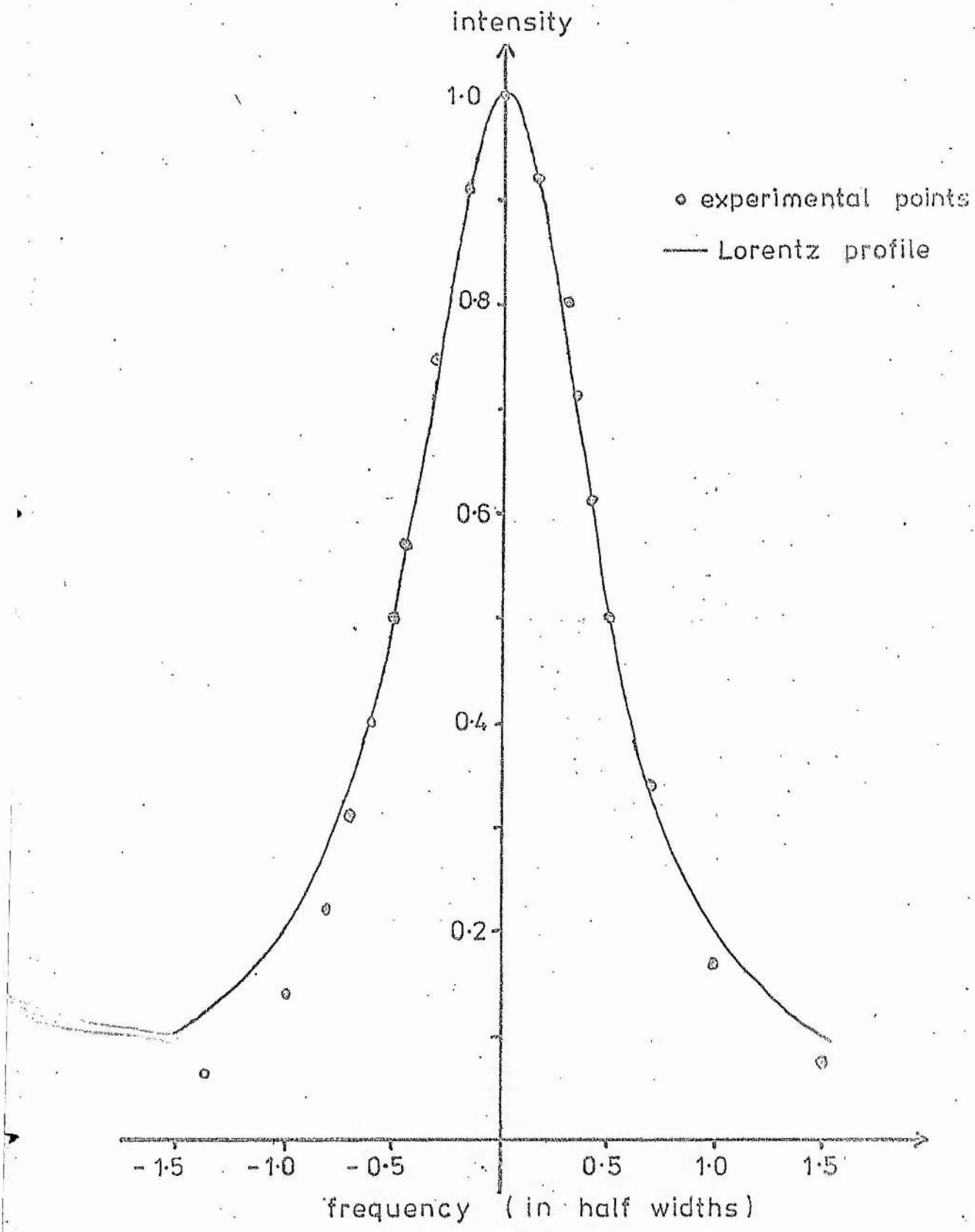

fig A 7.3 A Comparison of the Instrumental Pass Band of the Fabry-Perot Interferometer with a Lorentz Profile with the same Half-Width

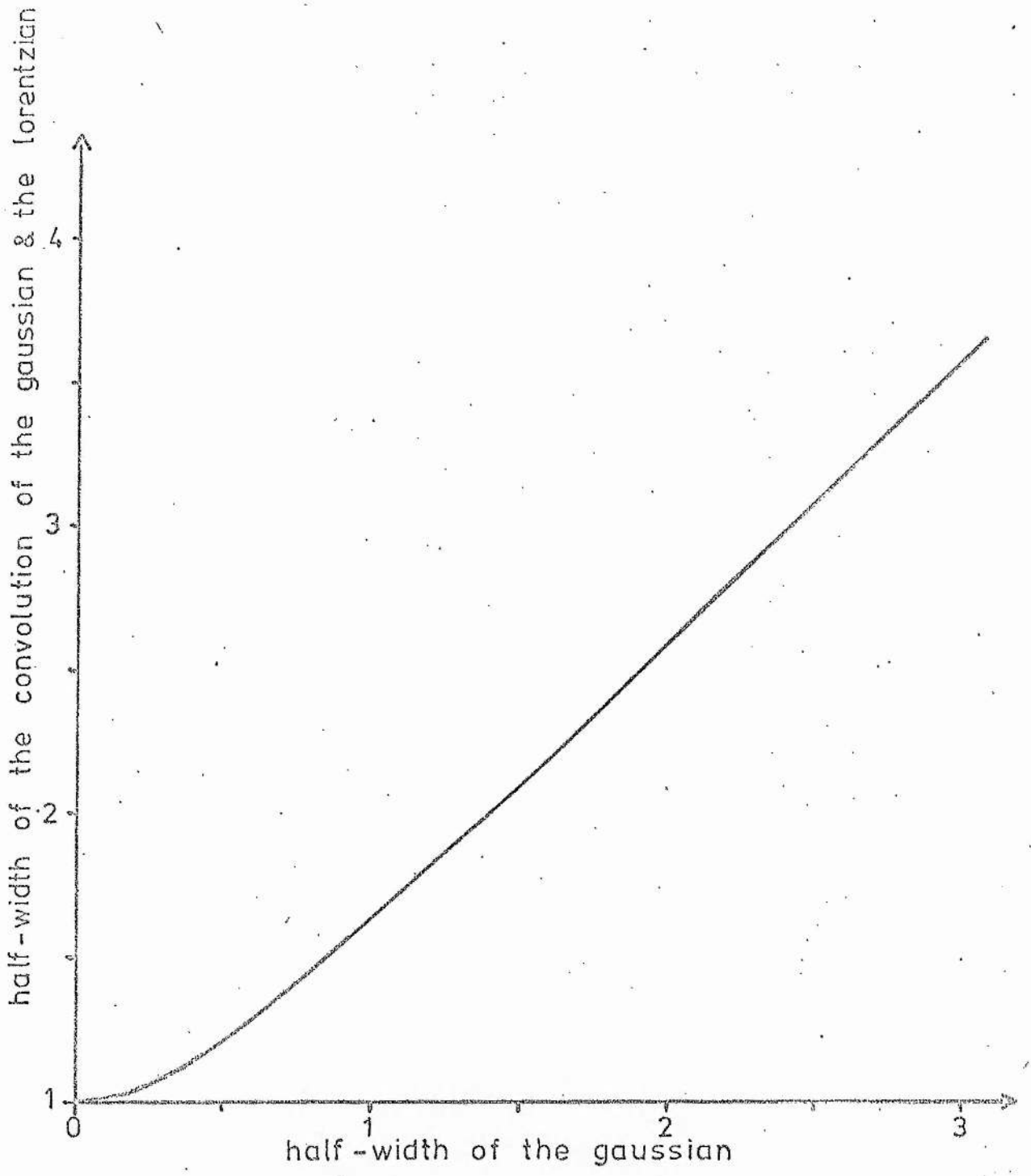

fig A 7.4 The Half-Width of the Convolution of a Gaussian Profile with a Lorentz Profile of Unit Half-Width

The widths of the 470.2 n.m. and 518.8 n.m. lines of AI and the 480.6 n.m. line of AII have been measured using a Fabry-Perot interferometer with multi-layer dielectric mirrors, but otherwise similar to the interferometer used to measure the H_α and H_β lines. The finesse of this instrument is about 20 over the range 470 - 515 n.m. and rather less at 518.8 n.m. With such a high finesse the instrumental broadening of the fringes is small and was ignored. (The fringes have a width of about one-third of a free spectral range).

The widths of the 470.2 n.m. and 518.8 n.m. lines were 3.32 GHz and 3.16 GHz at a discharge current of 40 A and a pressure of 0.3 torr, with an uncertainty of ± 5%. This is consistent with the assumption that the broadening is due only to the thermal motion of the atoms. The width of the 470.2 n.m. line increases with discharge current from 3 GHz to 3.32 GHz as the current is increased from 25 to 40 A (at a pressure of 0.3 torr). The half width of the 480.6 n.m. line is about 3.5 GHz at 40 A but the line is too weak to be measured at 25 A.

REFERENCES

(1) Jackson, D.A. and Paul, D.M., J. Sci. Inst. (J. Phys. E) 2, pp.1077-1080 1969.

(2) Kitaeva, V.F., Odintsov, A.N. and Sobolev, N.N., Sov. Phys. Usp. 12, pp.699-730 1970.

(3) Sze, R.C. and Bennett, W.R., Phys. Rev. A 5, pp.837-853 1972.

(4) Hernqvist, K.G. and Fendley, J.R., I.E.E.E. J. Quant. Elect. 3, pp.66-72 1967.

(5) Cornish, J.C.L. and Maitland, A., J. Phys. E Sci. Inst. 6, pp.880-884 1973.

(6) Maitland, A. and Dunn, M.H., Laser Physics (North-Holland, 1969).

(7) Prescott, L.J. and Van der Ziel, A., J. Quant. Elect. 2, pp.173-177 1966.

(8) Freed, C. and Hauss, A.H., Appl. Phys. Letts. 6, pp.85-87 1965.

(9) Garscadden, A., Bletzinger, P. and Friar, E.M., J. Appl. Phys. 35, pp.3432-3433 1964.

(10) Zakharenko, Yu G. and Privalov, V.E., Opt. and Spectrosc. 29, pp.124-127 1970.

(11) Galehouse, D.C., Ingard, U., Ryan, T.J. and Ezekiel, S., Appl. Phys. Letts. 18, pp.13-15 1971.

(12) Suzuki, T., Jap. J. Appl. Phys. 10, pp.1419-1424 1971.

(13) Pupp, W., Physik Z. 34, pp.756-761 1933.

(14) Yosimoto, H., J. Phys. Soc. Jap. 8, pp.59-68 1953.

(15) Ogwa, K., J. Phys. Soc. Jap. 14, pp.1746-1751 1959.

(16) Ross, J.N., J. Phys. D : Appl. Phys. 6, pp.1917-1928 1973.

(17) Coulter, J.R.M., Armstrong, N.H.K. and Emeleus, K.G., Proc. Phys. Soc. 77, pp.476-482 1961.

(18) Jackson, A.T., J. Phys. D : Appl. Phys. 4, pp.1963-1964 1971.

(19) Pupp, W., Physik Z. 33, pp.844-847 1932.

(20) Oleson, N.L. and Cooper, A.W., Advances in Electronics and Electron Physics 24, pp.153-278 1968.

(21) Grossu, D., Rev. Roum. Phys. 16, pp.1035-1037 1971.

(22) Maitland, A., Brit. J. Appl. Phys. (J. Phys. D) 2, pp.535-539 1969.

(23) Targ, R. and Yarborough, J.M., Appl. Phys. Letts. 12, pp.3-4 1968.

(24) Smith, P.W., Proc. I.E.E.E. 58, pp.1342-1357 1970.

(25) Hodara, H. and George, N., I.E.E.E. J. Quant. Elect. 2, pp.337-340 1966.

(26) Uchida, T. and Ueki, A., I.E.E.E. J. Quant. Elect. 3, pp.17-30 1967.

(27) Bridges, T.J. and Rigrod, W.W., I.E.E.E. J. Quant. Elect. 1, pp.303-308 1965.

(28) Harris, S.E. and Targ, R., Appl. Phys. Letts. 5, pp.202-204 1964.

(29) Harris, S.E. and McDuff, O.P., I.E.E.E, J. Quant. Elect. 1, pp.245-262 1965.

(30) Lamb, W.E. Jr., Phys. Rev. A 134, pp.1429-1450 1964.

(31) Ross, J.N., J. Phys. D : Appl. Phys. 4, pp.1092-1099 1971.

(32) Maitland, A. and Cornish, J.C.L., J. Phys. D : Appl. Phys. 5, pp.1807-1814 1972.

(33) Von Engel, A., Phil. Mag. 32, pp.417-426 1941.

(34) Günterschulze, A., Bär, W. and Betz, H., Z. für Phys. 109, pp.293-309 1938.

(35) Griem, H.R., Plasma Spectroscopy (McGraw-Hill Book Company, New York, San Francisco, Toronto, London 1964).

(36) Rapp, D. and Englander-Golden, P., J. Chem. Phys. 43, pp.1464-1479 1965.

(37) Vriens, L., Phys. Letts. 8, pp.260-261 1964.

(38) Herziger, G. and Seelig, W., Z. Phys. 215, pp.437-465 1968.

(39) De Mars, G., Seiden, M. and Horrigan, F.A., J. Quant. Elect. 4, pp.631-637 1968.

(40) Swift, J.D. and Schwar, M.J.R., 'Electric Probes for Plasma Diagnostics' (Illife Books Ltd. 1970).

(41) Chen, F.F., 'Electric Probes' in 'Plasma Diagnostic Techniques' Ed. Huddlestone, R.H. and Leonard, S.L. (Academic Press, New York, London, 1965).

(42) Crawford, F.W., J. Appl. Phys. 34, pp.1897-1902 1963.

(43) Boschi, A. and Magistrelli, F., Il Nuovo Cimento 29, pp.488-499 1963.

(44) Von Engel, A., 'Ionized Gases' (second edition) p.51 (Oxford University Press, 1965).

(45) El-Kareh, A.B. and El-Kareh, J.C.J., Electron Beams, Lenses and Optics, Vol. 1 (New York: Academic Press 1970).